Graduate School of
Systemic Neurosciences

LMU Munich

In vivo analysis of calcium-initiated axon degeneration in an animal model of MS

Submitted by

Marta Malgorzate Wesolowski

24.05.2018

Dissertation der

Graduate School of Systemic Neurosciences

der Ludwig-Maximilians-Universität

München

In vivo analysis of calcium-initiated axon degeneration in an animal model of MS

Submitted by

Marta Malgorzate Wesolowski

24.05.2018

Dissertation der Graduate School of Systemic Neurosciences der Ludwig-Maximilians-Universität München

Graduate School of
Systemic Neurosciences
LMU Munich

Examination committee:

1st reviewer and supervisor: Prof. Dr. Martin Kerschensteiner

2nd reviewer: Prof. Dr. Thomas Misgeld

External reviewer: Dr. Don Mahad

Date of the oral examination: 14. October.2018

To szivem Zotyó and my beloved family

“Knowing is not enough; we must apply.
Willing is not enough; we must do.”

“Es ist nicht genug zu wissen, man muss es auch anwenden;
Es ist nicht genug zu wollen, man muss auch tun”

Wilhelm Meisters Wanderjahre
Goethe

Table of Contents

List of Abbrevations

2PM	2-photon microscopy
Å	Ångström, 10^{-10} m
AAD	Acute axonal degeneration
Abcc8	ATP-binding cassette transporter sub-family C member 8
aCSF	Artificial cerebrospinal fluid
Axed	Axundead
BBB	Blood brain barrier
BF	Bleed through
C57BL/6	Common inbred strain of laboratory mouse, C57 black 6
CerTNL15	CerTNL15 calcium sensor protein
CFA	Complete Freud's Adjuvant
CFP	Cyan fluorescent protein
CIS	Clinically-isolated syndrome
CSF	Cerebrospinal fluid
DLK	Delta like non-canonical Notch ligand1
DMSO	Dimethylsulfoxide
DMT	Disease modifying treatment
DNA	deoxyribonucleic acid
dSarm	*Drosophila* sterile alpha and Armadillo motif
EAE	Experimental acute encephemyelitis
EBV	Epstain barr virus
EDSS	Expanded disability status scale
FAD	Focal axonal degeneration
FRET	Förster resonance energy transfer
GECI	Genetically encoded Ca^{2+} indicator
GFP	Green fluorescent protein
Hiw	Highwire
i.p.	Intraperitoneal
iNOS	Inducible nitric oxide synthetase
JNK	c-Jun N-terminal Kinase
LSM	Laser scanning microscope
LTP	Long term potentiation
MAP	Microtubule-associated protein
MBP	Myelin basic protein
MHC	Major histocompability complex
MMF	Medetomidine-midazolam-fentanyl
MOG	Myelin oligodendrocyte glycoprotein
MRI	Magnetic resonance imaging
MRS	Magnetic resonance spectroscopy
MS	Multiple sclerosis
MyD88-5	myeloid differentiation primary response 88-5
N.A.	Numberical aperture
NAA	N-acetyl aspartate
NAWM	Normal-appearing white matter
NfL	Neurofilament light chain
NMO	Neuromyelitis optica

ON	Optic neuritis
Phr1	PAM/Highwire/Rpm1
PLP	Proteolipid protein
PPMS	Primary progressive MS
PTX	Pertussis toxin
RIS	Radiologically isolated syndrome
RNS	Reactive nitrogen species
ROS	Reactive oxygen species
RRMS	Relapse-remitting MS
s.c.	Subcutan
S/N	Signal-to-noise ratio
Sarm1	Sterile alpha and TIR motif-containing protein 1
SCG10	stathmin 2, STMN2
SD	Standard deviation
SEM	Standard error of the mean
sNfL	serum Neurofilament light chain
SPMS	Secondary progressive MS
Sur1	sulfonylurea receptor 1
TMEV	Theiler’s murine encephalomyelitis virus
TNFalpha	Tumor necrosis factor alpha
TrpM4	Transient receptor potential cation channel subfamily M4
Ube4b	Ubequitin conjugation factor E4 b
WD	Wallerian degeneration
Wlds	Wallerian degeneration-like phenotype
WLDs	Wallerian degeneration slow protein
WT	Wildtype
YFP	Yellow fluorescent protein
ΔNLS	Deficient in nuclear localization sequence

List of Figures

List of Tables

Abstract

Multiple sclerosis (MS) is a chronic inflammatory disease of the central nervous system and a major cause of neurological disability in young adults. There is robust evidence showing that immune-mediated axon damage is a major cause for progression of permanent neurological deficits. Previously our lab used in vivo imaging in a mouse model of MS to identify focal axonal degeneration as a correlate of inflammatory axon loss. It is characterized as a sequential process, beginning with focal swellings and progressing to multi-focal axon fragmentation. This process is observed in axons with intact myelin sheaths and its early stages can recover spontaneously. We were able to show that elevated calcium levels influence the axonal fate to degenerate in EAE lesions, however the degenerative process triggered via elevated calcium is not understood. In my thesis work, I now investigated how cytoplasmic calcium accumulations mediate neurodegeneration in experimental autoimmune encephalomyelitis (EAE), an animal model of MS. We assessed the effect of delayed Wallerian degeneration genotypes (ΔNLS-Wlds and Sarm1 knock-out), which did not result in a reduction of clinical disability or reduction of axonal fragmentation in acute or chronic lesions in vivo. The inhibition of Calpain, a calcium-activated protease, however reduced axonal fragmentation in acute lesions in vivo. These results indicate that the degeneration of axons in neuroinflammatory lesions is distinct from Wallerian degeneration and opens up possibilities for neuroprotective therapies targeting the calcium-calpain axis.

Zusammenfassung

Die Multiple Sklerose (MS) ist eine chronische Entzündung des zentralen Nervensystems und ein Hauptauslöser neurologischer Behinderung bei jungen Menschen. Wissenschaftliche Studien zeigen, dass die immunvermittelte Nervenschädigung eine der Ursachen für das Voranschreiten unwiederbringlicher neurologischer Funktionausfälle ist.

Unser Labor hat in vorherigen intravitalen Mikroskopiestudien in einem Mausmodel der Multiplen Sklerose die Fokale Axondegeneration (FAD) als Korrelat von entzündungsbedingtem Axonverlust erkannt. FAD ist ein sequenzieller Prozess, der mit fokalen Schwellungen beginnt und bis zur multifokalen Axonfragmentierung fortschreitet. Dieser Prozess wird auch in Axonen mit intakten Myelinschichten beobachtet und die frühen FAD Stadien haben das Potential, sich spontan zu erholen. Wir konnten zeigen, dass erhöhtes intrazelluläres Kalzium die anschließende Fragmentation der Axone begünstigt. Jedoch wird der degenerative Prozess, der durch den pathologischen Anstieg an intrazellulärem Kalzium in den betroffenen Axonen ausgelöst wird, bislang noch nicht vollständig verstanden.

In meiner Arbeit beschäftige ich mich mit den Mechanismen der Axondegeneration ausgelöst durch zytoplasmatischen Kalziumanstieg in Experimenteller Autoimmuner Enzephalomyelitis (EAE), einem Tiermodell der Multiplen Sklerose. Zunächst haben wir die Wirkung von genetischen Mutationen (ΔNLS-Wlds and Sarm1 knock-out) untersucht, die die Wallersche Degeneration nach einer traumatischen Nervenverletzung verzögern. Wir konnten jedoch keine Verminderung der klinischen Beeinträchtigung oder axonaler Fragmentation in akuten oder chronischen EAE Läsionen feststellen. Die Inhibierung von Calpain, einer durch Kalzium aktivierten Protease, zeigte eine Veringerung der axonalen Fragmentation in akuten Läsionen *in vivo*. Diese Ergebnisse weisen darauf hin, dass die Degeneration der Axone in neuroinflammatorischen Läsionen sich von Wallerscher Degeneration unterscheidet. Darüber hinaus eröffnet die erfolgreiche pharmakologische Reduzierung der Fragmentation neue Möglichkeiten für neuroprotektive Therapien, die an der Kalcium-Calpain-Achse ansetzen.

1 Introduction

1.1 Multiple Sclerosis (MS)

1.1.1 Epidemiology and etiology

"We all look very good and we look healthy, but it's the symptoms we deal with on a daily basis that people don't get".

Carol Cooke. 2016

Multiple sclerosis is an unpredictable disease; every patient experiences different symptoms. This inspired Paralympian Carol Cooke, who was diagnosed with multiple sclerosis (MS) 20 years ago, to sit together with neurologists, physiotherapists, bike mechanics and other MS patients to develop a special racing bike for the MS Melbourne Cycle that mirrors common MS symptoms. For example, the wheels were weighed down to resemble fatigue, the design of the handlebars lead to a pin and needle sensation while riding or the gears were designed to slip unpredictably. In that way, the rider is not able to control the speed, direction or momentum of its bike, in analogy to a MS patient, who has to battle loss of motor control. Since it is not obvious to outsiders, the bike became a perfect metaphor for what MS patients have to go through every day. With fundraising campaigns like this, which are organized by charity organization and MS associations around the world, awareness has risen significantly in the past years.

MS is a chronic inflammatory disease of the central nervous system (CNS) with a presumed autoimmune etiology. The mean age of onset is 30 years, but MS can be also diagnosed in childhood or after the age of 60. It affects women three times more than men (Ribbons et al., 2017) and is considered to be one of the major causes of neurological disability and premature retirement among young adults (Flachenecker et al., 2008, 2017). Since there is no curative treatment available, MS causes a considerable healthcare, social and family burden (Kobelt et al., 2017). With campaigns like the above-mentioned, awareness and therefore funding is being raised for research in order to get a better understanding of the underlying causes and to develop more effective possibilities of treatment.

Until this very day, MS remains a disease with a not entirely known etiology. It has been suggested that the disease is triggered in people having a genetic predisposition by certain still unknown environmental factors. This assumption is supported by migration studies. The prevalence rate of immigrants tends to be similar to that of the indigenous population, especially when the migration occurred before puberty (Gale and Martyn, 1995). With the introduction of Next Generation Sequencing and bioinformatics it was possible to identify that approximately

1/3 of the genetic susceptibilities to MS are localized to the major histocompatibility complex (MHC) class II (Hollenbach and Oksenberg, 2015) which would explain the autoimmune character of the disease. Twin and sibling studies confirmed the finding that genes are responsible for 30 % of the total disease risk.

Several environmental factors are found to contribute to the risk of developing MS. In studies, a connection between MS and vitamin D deficiency has been found as well as to reduced exposure to sunlight and ultraviolet radiation (DeLuca and Plum, 2017), smoking (Degelman and Herman, 2017) and obesity (Novo and Batista, 2017). An infection with EBV appears to be closely associated with MS and it has been proposed that MS development might be a result of failed viral clearance (Burnard et al., 2017). This complexity in disease etiology leads to a diagnostic challenge, despite the huge progress in diagnostic methods.

1.1.2 MS Pathology

MS is a chronic disease with a thousand faces. Every patient has a unique set of clinical manifestations, regarding type of symptom during a relapse and the duration and frequency of such relapses. The disease course of MS is for a single patient not predictable. A patient, who presents with optic neuritis (ON) might have only this Clinically Isolated Syndrome (CIS). However, if symptoms reappear in another functional system and at a different time point, the CIS becomes the onset of MS. Therefore, the diagnosis of MS remains a challenge.

Although the first recorded description of MS dates already back to 1421 (Medaer, 1979), it was still not identified as a separate disease by the German pathologist Friedrich von Frerichs until 1849. The “father of neurology” Jean Martin Charcot was the first one, who collected several cases and demonstrated in a lecture series at the La Salpétrière hospital the connection between the diverse symptoms and the underlying pathological changes that lead to the development of the first diagnostic criteria for MS: nystagmus, ataxia and dysarthria (Charcot triad) (Milo and Miller, 2014). The diagnostic criteria were since then revised several times and adapted to the continuously improvements of diagnostic methods and knowledge about the disease in general. Nowadays the 2017 revision of the McDonald diagnostic criteria (Thompson et al., 2017) is used, which incorporate the use of MRI imaging and cerebrospinal fluid analysis as diagnostic tools. In short, for a MS diagnosis it needs to be demonstrated that inflammatory lesions are disseminating in space and in time, along with exclusion of an alternative diagnosis.

The histopathological hallmarks of MS are the presence of scattered demyelinated plaques that consist of inflammatory mononuclear cells, damaged axons and gliosis. This pathological activity translates to a wide variety of possible neurological symptoms that affect different parts of the CNS. Common symptoms are paresthesia or numbness, motor weakness, monocular visual disturbance, diplopia, incoordination, gait disturbances, dizziness and vertigo. This can be accompanied by symptoms like fatigue, spasticity, ataxia, nystagmus, sensory loss, neuropathic pain, urinary urgency or retention, sexual dysfunction, depression or other emotional changes, heat intolerance, Lhermitte`s phenomenon, cognitive dysfunction and more (Milo and Miller, 2014). A relapse is defined as a clinical symptom that is present for at least 24 hours and is not explainable due to an infection or change of body temperature (Uhthoff-phenomenon). The interval between two relapses should be at least 30 days to classify them as independent (Gold, 2014).

1.1.3 Clinical Course of MS

Although every patient experiences a different clinical course, based on the relapse frequency and grade of recovery four major disease types are recognized:

- Clinically isolated syndrome (CIS):

In a CIS, a patient presents for the first time with a - for a demyelinating event typical - clinical symptom without evidence for previous episodes of demyelination (Gold, 2014; Miller et al., 2012). After the CIS the disability may still persist, or the patient has a complete remission of clinical symptoms (see *Figure 1A*). Initially CIS was not included in the MS clinical descriptions. Depending on in which part of the CNS the CIS occurs, the conversion to clinically definite MS is reported to happen in 65 % of patients (in case of ON), 60 % of patients (in case of CIS in brain stem) or 61 % of patient (in case of CIS in spinal cord) (Fisniku et al., 2008; Miller et al., 2012). CIS patients that are treated with MS disease-modifying agents show reduced MRI activity and develop less frequently a second exacerbation which would be the fulfilling criteria to MS diagnosis (Comi et al., 2009).

In some cases, patients are presented with unusual MRI activity with absence of clinical signs or symptoms. This radiologically isolated syndrome (RIS) is not considered a distinct MS phenotype since there is no clinical evidence of demyelinating disease (Okuda et al., 2009).

- Relapsing-remitting MS (RRMS):

Clinically MS starts in 80 – 85 % of patients as RRMS (Healy and Liguori, 2012). Relapsing-onset patients are more likely to be female (gender ratio 2-3 females to 1 male) and the mean age at onset is 25 – 35 years (Confavreux and Vukusic, 2006). During RRMS, clearly defined attacks of new or recurrent neurological symptoms and signs with full or partial recovery are observable. There is a lack of disease progression between disease relapses. At different points in time, the clinical course may be characterized as either active (increased MRI activity or relapses) or inactive. Following relapse, the clinical symptoms may disappear completely, or the patients exhibits a worsening of disability level (see *Figure 1B*). Relapsing forms of MS are defined by inflammatory attacks. Relapsing MS patients tend to develop more brain lesions with a high density of inflammatory cells (plaque or scars) that can be visualized in MRI scans. These findings explain the nature of the episodic bouts of deficits like visual problems, spasticity, cognitive and memory problems.

- Secondary-progressive MS (SPMS):

After a period of 10 years, in 50% of patients that were initially diagnosed with RRMS the symptoms worsen gradually over time with or without relapses. Therefore, this form is called secondary-progressive MS (SPMS). The transition between RRMS and SPMS is unpredictable and the diagnosis of SPMS is made retrospectively. To be defined as a chronic progressive course the neurological deficits are continuously worsening and accumulating over a period of at least 6 months (Trojano et al., 2003). In *Figure 1C* a representative course is shown.

- Primary-progressive MS (PPMS):

In 10 – 15 % of MS patients the disease course is predominantly degenerative from onset on. Their neurological symptoms worsen progressively with time. There are no early relapses or remissions observable (for a representative course see *Figure 1D*). Therefore, this type is defined as primary-progressive MS (PPMS). During their clinical course PPMS patients can show occasional relapses and/or increased MRI activity. They may experience stable not active phases, but also active and not active progressive phases that result in a gradual accumulation of disability. The numbers of female and male PPMS patients are approximately equal (1-1.5 female to 1 male). The mean age at first diagnosis is 10 years higher than in relapsing MS forms. In contrast to relapsing forms of MS, progressive MS patients develop more spinal cord lesions that contain fewer inflammatory cells. The predominance of motor symptoms in progressive MS patients is consistent with the increased spinal cord atrophy found in this patient group (Healy and Liguori, 2012).

Manifestation of MS is more complex than these 4 classifications suggest. Patients suffering from a progressive form of MS might still experience relapses (progressive relapsing MS). This is indicated in Figure 1 by superimposed relapses on the progressive course (Figure 1 C and D). Based on the MRI activity a progressive disease course can be characterized as active (contrast-enhancing lesions or new and unequivocally enlarging T2 lesions) or inactive (no sign of MRI activity). Therefore, progression as measured by clinical evaluation and activity assessed using MRI are important disease modifiers (Lublin et al., 2013).

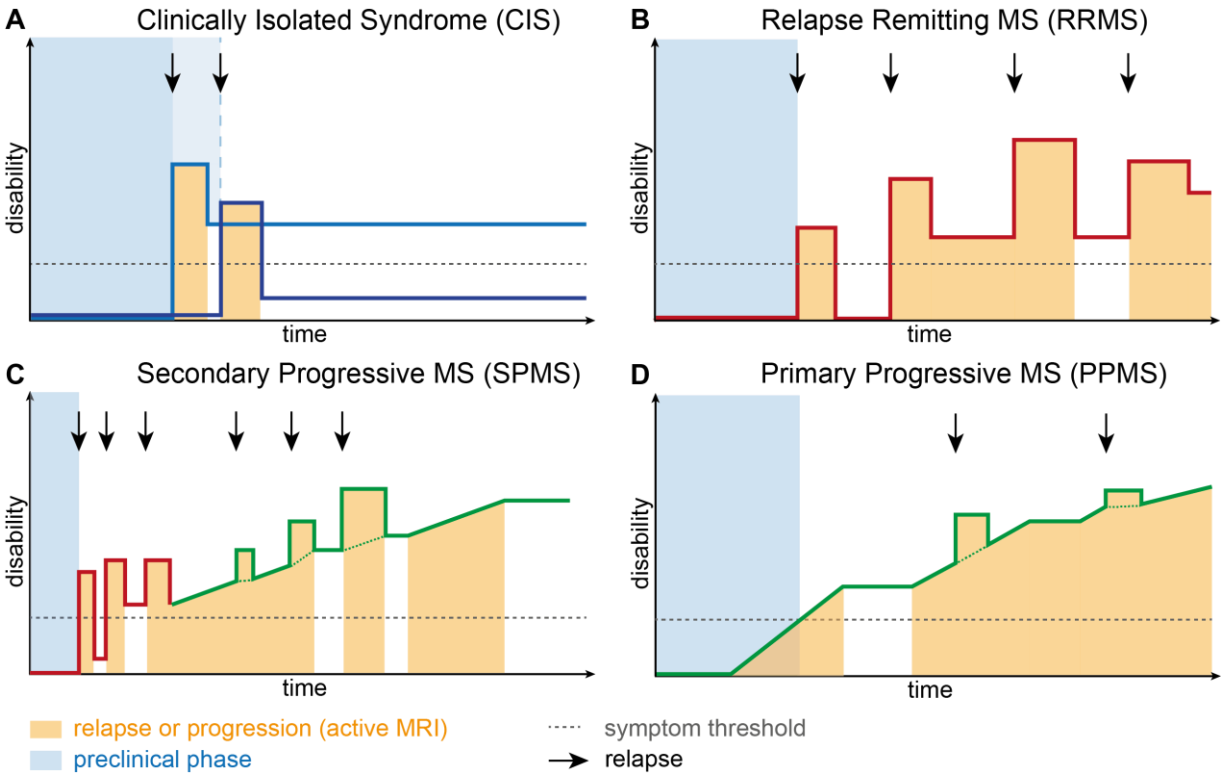

Figure 1. Representation of possible MS disease courses

A) Two representative disease courses for CIS. The remission of clinical deficits can be complete (dark blue) or incomplete (light blue). B) A representative clinical course for RRMS (red curves): Following a relapse, new symptoms may disappear without any increase in neurological disability, or recovery after a relapse may be incomplete, thereby worsening the disability level. C) Following RRMS, many patients show a constantly increasing disability over time (SPMS: progressive course in green). The progressive course can have brief stable periods, may show active lesions (relapses, increased MRI activity) followed either by complete or incomplete disability remission. D) Patients may show a continuous worsening of neurological function from the onset of symptoms, without earlier signs of relapses or remissions (PPMS: primary progressive MS). Inspired by MS disease course overview on My-MS.org (https://my-ms.org/images/chart_ms_course_2013_665.jpg**), based on (Thomson et al. 2017).**

1.1.3.1 Inflammation

Already early in the disease, there are signs of both neuroinflammation and neurodegeneration present. Two competing models exist that debate whether axonal damage is a consequence of severe inflammation that results from abnormalities in immune processes outside the CNS (outside-in model) or an axonal dysfunction initiates chronic inflammation in the CNS (inside-out model). Due to some still unclear initiation mechanism, it is thought that sensitized lymphocytes migrate across the damaged BBB (Viglietta et al., 2004), because regulatory T cells fail to suppress these effector cells, and/or the overexpression of survival factors overcome the apoptosis of autoreactive cells (Shi et al., 2007).

The complexity of the immune system is then reflected in the high diversity of infiltrating effector cells found in MS and EAE lesions. It is thought that the autoimmune pathology seen in MS and EAE (Billiau and Matthys, 2001) is mostly driven by auto-reactive T-cells (Fletcher et al., 2010). However, there is evidence accumulating that B cells are involved in the disease process as well (Lehmann-Horn et al., 2017). They are found in the brain parenchyma and are thought to contribute to the compartmentalization of humoral immune response with intrathecal antibody production (Romanelli et al., 2016). In a recent study, it was found that the meningeal inflammation is preceding parenchymal inflammation at all levels of the spinal cord of MOG_{35-55}-induced EAE mice, thereby identifying the meninges to be significantly involved in the development and propagation of CNS inflammation associated with EAE (Shrestha et al., 2017). Further research is necessary to fully understand the interaction of CNS and immune system during neuroinflammatory, demyelinating diseases.

1.1.3.2 Myelin damage

Active demyelination is a central event in MS. In a detailed immunopathological study, four different patterns of demyelination have been recognized in MS (Lassmann et al., 2001). In pattern I (macrophage-associated demyelination) the destruction of myelin is induced by toxic products of activated macrophages such as reactive species. Pattern II of demyelination is characterized by complement mediated lysis of antibody-targeted myelin. This antibody-mediated demyelination pattern can be found in EAE models that result from sensitization with MOG. If demyelinated regions are accompanied by distal oligodendrogliopathy and apoptosis it is categorized as pattern III. Lesions with prominent oligodendrocyte degeneration in a small rim of periplaque white matter are defined as pattern IV.

In EAE models it was demonstrated that the immune cells attack myelin, which is first deformed on the myelin sheath surface to bulb-like structures, called myelinosomes. The damage then further progresses to the oligodendrocyte soma. Myelinosome formation is found in active demyelinating MS lesions as well and can be initiated by anti-myelin antibodies and inhibited by complement depletion in EAE model (Romanelli et al., 2016).

1.1.3.3 Axon degeneration

Neuroaxonal damage was already described in early studies of MS but generally thought to be a secondary process to the immune-mediated demyelinating attacks. More refined studies of MS pathology suggest that axonal damage starts early in MS (Trapp et al., 1998). Diffuse histopathological abnormalities, as one example, are present already in early disease stages as well in normal-appearing white matter (NAWM) and cortical grey matter, as shown through reduction of the axonal integrity marker N-acetyl aspartate (NAA) in proton magnetic spectroscopy (Bjartmar et al., 2001; Dutta and Trapp, 2007; Filippi et al., 2003). With immunohistochemical stainings against amyloid precursor protein or SMI-32 in biopsies of MS patients a correlation of axonal injury and inflammation in MS lesion is detectable (Bitsch et al., 2000). In non-active, “burned-out” lesions axonal damage is present as well (Kornek et al., 2000; Lassmann, 2003).

There are not many reliable tools available that can monitor non-invasively neuronal damage. With MRI imaging, lesions with pronounced axonal damage are detected as hypointense T1 weighed black holes and atrophy in CNS can be observed as well early in disease course (Barkhof et al., 2009). In a recent study, serum levels of neurofilament light chains (NFL) are proposed to be sensitive and clinically meaningful, non-invasive biomarkers for neuronal damage in MS patients (Disanto et al., 2017). NFL are scaffolding proteins unique to neuronal cells and serum levels of NFL (sNFL) are increased in patients suffering from acute brain and spinal cord injury, but as well in patients with MS, ALS and other neurodegenerative disorders. In spinal cord samples of patients with SPMS a significant reduction of axonal density as measured with immunohistochemical staining against neurofilament is found in both, chronic inactive, completely demyelinated plaques and the NAWM, compared to control samples from anatomically identical regions (Lovas et al., 2000). Both, acute inflammatory damage and chronic diffuse neuronal loss, can contribute to the increase in sNFL levels, which correlate highly with relapse and disability state as measured by the expanded disability status scale (EDSS). This supports further the possible use of sNFL levels to monitor treatment effects in patients. Disanto et al. observed a significant decrease of sNFL in patients under DMT.

Increasing evidence indicates that axonal loss correlates best with irreversible neurological disability in MS patients. This is even more evident in progressive MS.

The cause of axon dismantling in MS lesions is still unclear. Several possible mechanisms have been recognized to be involved in other disease settings. CNS injury, genetic defects, toxins and metabolic disturbances can all lead to axon degeneration. The axon degeneration mechanism most discussed is the Wallerian degeneration-like (WD) pathway and the neurodegeneration pathway induced via excitotoxicity that will be further discussed below (1.2.1. and 1.2.2., respectively). Using in vivo imaging in EAE lesions a novel process of axonal degeneration was identified (Nikić et al., 2011): Focal axonal degeneration (FAD) is characterized by stable swellings at one or more distinct sites (often at nodes of Ranvier) that can disrupt almost simultaneously at several sites along the axons. Morphologically it is very similar to other axonal loss pathways like WD, but it has some distinct features: fragmentation spreads in both directions, it is even observed in absence of demyelination and its initial phase – the swelling of axons – is still able to recover. Axonal abnormalities suggestive of FAD and mitochondrial damage were observed within lesion area in MS biopsies as well (Nikić et al., 2011).

The mechanism by which immune cells induce axon degeneration is still not fully understood. In general, it is assumed that activated T cells migrate into the CNS (Kawakami et al., 2012), where they recognize self-antigens in genetically susceptible individuals. During such an attack inflammatory cytokine like tumor-necrosis factor alpha (TNF alpha) is secreted by the T cells. Resident microglia are activated as well and release chemo- and cytokines into their surroundings (Amor et al., 2014; van Noort et al., 2012). Additionally, microglia produce excessively reactive nitrogen species (RNS) like NO (Dheen et al., 2007; Witte et al., 2010) which can catalyze many degenerative processes in the axons, e.g. the modification of the cytoskeleton via nitrosylation of microtubule-associated protein (MAP) 1B (Kapoor et al., 2003; Stroissnigg et al., 2007). In MS models, these deficits in axonal transport occur before any structural changes to organelles or alterations to microtubule network are observable (Sorbara et al., 2014). Microtubule disintegration promotes further axonal transport failure that is coupled with NAD and ATP depletion and accumulation of organelles like mitochondria, which become a source of reactive oxygen species (ROS). ROS are mediators of oxidative stress and affect even further the axonal transport. Application of H_2O_2 or NO donors is sufficient to induce the same mitochondrial changes as observed in EAE lesions and recovery can be achieved by neutralization of ROS and RNS in the majority of axons by anti-inflammatory treatment or redox scavengers (Nikić et al., 2011; Sorbara et al., 2014). The exact mechanisms are still unknown, but all these observations suggest that ROS, RNS and mitochondrial failure play a crucial role in triggering downstream axonal disintegration. These impairments of mitochondrial function and

axonal transport are observed within axons in MS patients as well (Dutta et al., 2006; Mahad et al., 2009).

1.1.4 Treatment options for MS

Traditionally, MS is considered to be an autoimmune inflammatory disorder of the CNS, in which CNS structures, in particular myelin, are attacked by infiltrating immune cells. Consistent with this classification of MS as primary autoimmune disease, most of the MS patients present with a relapsing-remitting form of MS, in which the inflammatory component dominates the disease pathology. Waves of inflammation entering the brain driven by systemic immune reaction induce focal demyelinating lesions primarily in white matter. It is assumed that the observed atrophy in MS patients is a result of secondary degeneration initiated by an inflammatory burden which has become somewhat independent from the initial inflammatory assaults. Patients suffering in the first 2 years of frequent, severe relapses are more likely to present with a more aggressive form of progressive MS (Scalfari et al., 2010). Therefore, major effort was put in revealing the immunological causes and developing pharmacological agents that modulate the immune system in order to reduce relapses and disease progression. In the past few decades, clinical research made great progress in developing efficient treatment options. The currently approved disease-modifying treatments (DMT) are immunomodulatory or immunosuppressive therapies that significantly, although not completely reduce the relapse frequency and severity (Finkelsztejn, 2014). However, these DMT have limited efficacy in preventing the conversion of relapsing MS to the progressive form and show no effect once progression has started. Although, a new study introduces Ocrelizumab, a humanized monoclonal antibody that selectively depletes CD20-expressing B cells, as an immunomodulatory drug in treatment of PPMS (Montalban et al., 2017), its clinical benefit is only modest and limited to a selected population of patients (young patients with shorter disease duration and a high probability of disease activity). Despite DMT, around 80 % of initially RRMS patients convert to SPMS (Kremenchutzky et al., 2006), indicating that these treatments fail to halt disease progression. Progressive MS is characterized by prominent cortical demyelination and diffuse pathology in NAWM. New active lesions are rare and pre-existing lesions surrounded by a rim of activated mircoglia expand slowly (Lassmann et al., 2007). After immunomodulation, it appears that there is a dissociation of relapse suppression and disability accumulation, as if the reduction of inflammatory insult unmasks the ongoing, steadily progressive neurodegeneration. Besides this, the prognosis in MS is not substantially affected by the initial course type (RRMS vs PRMS), but rather the age at disease onset correlates with disability progression. The earlier the disease onset, the younger the age at reaching disability milestones (Confavreux and Vukusic, 2006). There are several more clinical

abnormalities that can not be explained by a solely autoimmune cause of MS. Inflammation might by secondary to an underlying neurodegenerative process (inside-out hypothesis). Regardless of this chicken or egg situation, it is a fact that disability progression is due to neuronal damage and axonal loss, which is in turn a correlate of clinical disability. There is a great need for neuroprotective strategies that besides DMT can improve disease management and ideally halt the disability progression.

1.1.5 Animal models of MS

Experimental autoimmune encephalomyelitis (EAE) is the most commonly used model for studying autoimmune-mediated damage to the CNS. The model is based on the attempts of Rivers and his colleagues to reproduce acute disseminated encephalomyelitis in rhesus monkeys via intramuscular injections of adult rabbit brain extracts (Rivers et al., 1933) that lead to pathological changes accompanied by myelin destruction. The induction protocol was further optimized by adding adjuvants composed of mineral oil and heat-killed tuberculosis bacteria to the brain emulsions (Kabat et al., 1947). Usually complete Freud's adjuvant (CFA) and pertussis toxin (PTX) is used, that facilitates the development of immune response and the breakdown of blood-brain barrier (BBB). Although EAE can be induced in many different species, rodents are the species of choice. Different EAE induction protocols were developed, all resulting in different disease characteristics regarding immunology and pathology. For instance, in rodents not only brain or spinal cord homogenate is used for immunization, but also purified myelin proteins like myelin basic protein (MBP), proteolipid protein (PLP) and myelin oligodendrocyte glycoprotein (MOG) or peptides of these proteins representing the significant epitopes.

EAE reflects the autoimmune origin of MS and shares with the human disease many pathological features: Similar to MS, EAE animals develop a demyelinating disease that is characterized by scattered lesions throughout the CNS and perivascular localization of immune cell infiltrations. In these lesions, both in the animal model and the human disease, damage to myelin sheaths and axons can be observed. However, unlike MS, EAE can only mimic parts of the MS disease course, but not the full disease spectrum, depending on which mode of induction is used.

In the active sensitization models, the disease is induced by immunization with myelin proteins. However, in recent studies, also non-myelin derived antigens are used for induction of CNS inflammation. (Krishnamoorthy et al., 2009; Mathey et al., 2007) This process results in the direct priming of myelin epitope-specific CD4+ T cells in vivo, which migrate to the CNS and mediate autoimmune responses. In the passive adoptive EAE model, the capability of activated

T-cell subtypes to induce CNS inflammation is deployed. Activated CD4+ T cells are isolated from draining lymph nodes of immunized animals, restimulated with the initiating antigen in vitro and then reinjected into naïve recipients.

The rodent's genetic background has an influence on the induced disease course (Terry et al., 2016). For the RR-model type SJL/J mice are immunized with MBP-derived peptides, MBP-reactive T cell clones (Zamvil et al., 1985) or synthetic myelin PLP139-151 peptide. To induce a chronic model, C57BL/J mice are immunized with MOG or PLP peptide. For a chronic-relapsing disease course Biozzi ABH mice are used (Terry et al., 2016).

As both the active and passive EAE models are induced by the experimentator, they tend to be not suited to study the immunological mechanisms that initiate the disease process, thereby reflecting the spontaneous manifestation in MS patients. Therefore, a genetic, "spontaneous" EAE model was developed, in which T-cell receptor of encephalitogenic T-cells is transgenically expressed that recognizes a CNS antigen, like MOG (Bettelli et al., 2003). These mice develop an autoimmune inflammatory demyelinating disease several months after birth that resembles conventional EAE models in many ways. Furthermore, a neurotrophic viral injection model for MS was developed. Theiler's murine encephalomyelitis virus injected in rodents induces an immune-mediated attack on CNS. Despite the difference of demyelination pattern in mice compared to MS patients (Dal et al., 1996), this model still is used for testing new therapies since it shows similar clinical manifestation and pathology that is induced by activation of immune system.

Although thanks to this large spectrum of different models, useful insights into the mechanisms involved in EAE could be gained and in some cases treatments options for MS could be successfully evaluated, it needs to be highlighted that the results gained from EAE are not necessarily transferable to MS. Many therapies that showed success in EAE model were either inefficient or caused harmful side effects when used in MS patients. This discrepancy can result from the different genetic nature and temporal differences of immune reactivity and response to therapy between rodents and human. EAE displays more limitations: Compared to MS, EAE animals show less brain infiltrates and limited demyelination (Lovett-Racke, 2017). EAE mainly affects the spinal cord WM whereas in MS prominent demyelination of cerebral and cerebellar cortex is found. Since the basis for EAE is the injection of a self-peptide, the pathological changes found in EAE originate rather from a CD4+ cell activation. It was found that in MS the pathological changes are likely mainly CD8+ cell mediated, and B cell make an important contribution (Bettelli et al., 2003; Hauser et al., 2008). In many EAE models, however, the B cell contribution is missing which points out one of the deficiencies of EAE as an animal model for MS.

1.2 Mechanisms of axon degeneration

As mentioned above, there are several mechanisms considered to be involved in axon degeneration in MS and EAE lesions. As already described FAD is a degenerative process characterized by focal swelling with subsequent fragmentation. It was also observed in axons with intact myelin sheaths in both EAE and acute MS lesions (Nikić et al., 2011). Wallerian degeneration, originally described in 1850, has been considered to be a prototypical axon degeneration process that mediates axonal demise not only after transection. Therefore, it has been proposed that some mechanism of Wallerian-like degeneration might be involved in axonal degeneration in EAE lesions as well. Other mediators, partly proposed as part of these degeneration cascades, e.g. high intra-axonal calcium levels, other molecules that are activated by increased calcium levels or ion channels are potential candidates as well. In the following sections, the possible molecular pathways of axonal loss will be discussed.

1.2.1 Wallerian degeneration

1.2.1.1 Introduction and pathogenesis

It was long thought that the dying of axons is a passive process that results from deprivation of survival factors. About 170 years ago, August Waller observed that the peripheral axon distal from the transection injury degenerates, whereas the cell body remains intact (Waller, 1850). Such an anterograde degeneration is seen in neurodegenerative diseases as well, therefore this mechanism is known as “Wallerian-like degeneration” (WD). After a certain latent phase of around 24 - 48 hours the axonal cytoskeleton disintegrates, resulting in the breakdown of axonal membrane, disruption of myelin sheaths and attraction of macrophages. During this process axons exhibit focal swellings that are many times wider than a normal axon several hours before the actual fragmentation (Beirowski et al. 2010). These observations underline that WD is a sequential process (Simon et al., 1969). Following acute axonal degeneration (AAD) after a stab lesion the distal end begins rapidly to fragment after a heterogeneous latent phase (around 30 h) and spread in a proximal to distal direction, whereas the proximal axon bulb remained stable or even showed signs of early outgrowth (Kerschensteiner et al., 2005). Surprisingly, the distal ends of axons in C57BL/Wld^{S} mice survive up to several weeks after nerve transection or crush in the PNS and CNS (Perry et al., 1991), suggesting that this kind of axonal dying back pathways are active processes.

1.2.1.2 Animal models with delayed Wallerian degeneration

The discovery of Wallerian degeneration slow protein (Wld^S) and its neuroprotective effect was a coincidence, but it ignited the quest for further insights into this retrograde degeneration mechanism. C57Bl/6 mice developed this mutation at a single locus spontaneous at Harlan Olac. Wld^S is a dose-dependent, semi-dominant phenotype that appears to be intrinsic to axons and does not interfere with other death pathways like apoptosis. Further research on molecular interactions involved in axonal degeneration delayed by Wld^S expression revealed that mice lacking Sarm1 exhibit a similar neuroprotective phenotype like Wld^S mice. On this way two popular rodent models to study the mechanisms of rapid Wallerian degeneration emerged: C57Bl/Wld^S and Sarm1-/-.

Further examination of the C57BL/Wld^S revealed that compared to other lines these mice express an in-frame fusion protein that is a result of a spontaneous 85-kb tandem triplication within the distal chromosome 4 (Coleman et al., 1998). This chimeric gene is a fusion of the 5' end of the ubiquitin conjugation factor E4 B (Ube4b) and the complete NMNAT1, a key enzyme involved in nicotinamide adenine dinucleotide (NAD^+) biosynthesis (Mack et al., 2001). Mutating the nuclear localization sequence (ΔNLS) of Wld^S retargeted the fusion protein from the nuclei to the cytosol that lead to a more robust protective effect of Wld^S (Beirowski et al., 2009). Transgenic mice expressing Wld^S or the stronger mutant ΔNLS-Wld^S are widely used to examine neuron, axon or synapse protection in WD and in neurodegeneration models (Sajadi et al., 2004; Wang et al., 2012; Wright et al., 2010).

A F2 forward screen in *Drosophila* uncovered that loss of function of dSarm (Drosophila sterile alpha and Armadillo motif) provides axonal preservation that rivals that of Wld^S in Drosophila. Endogenous dSarm therefore is required to drive WD in the nervous system and its discovery further supports the hypothesis that this degeneration pathway is an active program. Based on these results a transgenic mouse line with a null mutation for the mouse orthologue of dSarm, Sarm1 (or in mammals general known as MyD88-5) was created. After axotomy *in vivo* the synaptic integrity was preserved, and the cut distal axons remained intact several weeks after axotomy (rather than 2 days), indicating that the absence of Sarm1 protects as robustly as Wld^S. Furthermore, these findings indicate that the axon destruction pathway is an ancient, evolutionary conserved mechanism (c.elegans, fruit fly, zebrafish, and mouse) (Osterloh et al., 2012). A direct comparison of the protection capabilities in a non-injury, severe axonopathy model of NMNAT2 deficiency revealed that Sarm1 deletion rescues into old age, whereas mice rescued by $Wld^{S/S}$ developed hindlimb muscle denervation from 3 months and severe hindlimb paraparesis by 10 months (Gilley et al., 2017). This suggests that Sarm1 deficiency might be stronger protectant that Wld^S.

As Wld^S and Sarm1-/- mice robustly protect against WD in injury models these transgenic mice are the model of choice to investigate the involvement of Wallerian-like mechanisms in neurodegeneration models, like EAE.

1.2.1.3 Molecular pathways of Wallerian degeneration

The exact molecular mechanisms of WD are still not fully understood and at times controversial. With the discovery of the Wld^S, which exhibits Nmnat1 activity, the NAD^+ scavenging pathway was identified as a potential key mechanism in WD. Furthermore, this is supported with expression of enzymatically dead versions of Wld^S that fail to delay WD in flies (Avery et al., 2009) or mice (Conforti et al., 2009). Expression of different modified constructs were used to dissect the function of different Wld^S domains in *Drosophila* in vivo. This showed that relocalization of NMNAT enzymatic activity away from the nucleus showed maximal protection of severed axons. Interestingly, overexpression of Nmnat1 and Nmnat3, but not the nuclear Nmnat2, could mirror the neuroprotection of Wld^S. Nmnat3 is known to be localized to mitochondria. This might indicate that the axon protection is exerted via Wld^S/Nmnat activity in mitochondria (Avery et al., 2009). On the other hand, there is evidence that indicate that WD and NMNAT/$Wlds^S$-mediated axon protection is a mitochondria-independent mechanism (Kitay et al., 2013). In other words, the exact site of action of Wld^S-sensitive protection remains elusive. It is as well not clear, if NAD^+ is the protective Wld^S product. Several studies interfering with NAD^+ salvage pathway could not conclude that NAD^+ is the sole key actor in Wld^S protection (Conforti et al., 2009; Sasaki et al., 2009; Yahata et al., 2009). In summary, the mechanism of Wld^S is more complex than simple overexpression of Nmnat1. The Ube4b domain of Wld^S is certainly important for its function as well. Studies showed that an N-terminal 16 amino acid sequence of the chimeric protein binds to valosin-containing protein (VCP), thereby probably driving the relocalization of Wld^S to sites outside of the nucleus. This is supported as well by the more potent Wld^S mutant lacking the nuclear localization sequence: ΔNLS (Beirowski et al., 2009).

Since the chimeric gain of function Wld^S protein is normally absent in wild-type organisms, the involvement of dSarm/Sarm1 in Wallerian-like degeneration (Osterloh et al., 2012) was an important finding towards understanding the endogenous axon destruction pathway, that is distinct from developmental axonal pruning and apoptotic cell death. Sarm1 belongs to the TIR domain containing family of proteins that act as scaffolding molecules downstream of Toll receptors in immune functions; but in contrast to the other family members, Sarm1 deletion does not impair TLR signaling (Kim et al., 2007). Additionally, Sarm1 contains SAM and Armadillo domains that mediate or modulate protein-protein interactions, respectively, that are

both important in initiation of Sarm1-mediated axon degeneration (Gerdts et al., 2013). Sarm1 is suggested to be activated by an injury-induced or dysfunction-induced Ca^{2+} signaling pathway (Rosenberg et al., 2012). The site of action of Sarm1 is still debated; antibodies developed against Sarm1 identified its localization to neurites (Chen et al., 2011) or mitochondria (Gerdts et al., 2013; Kim et al., 2007). For support of the latter, the Sarm1 sequence contains mitochondrial localization sequences (Panneerselvam et al., 2012). However, deletion of these

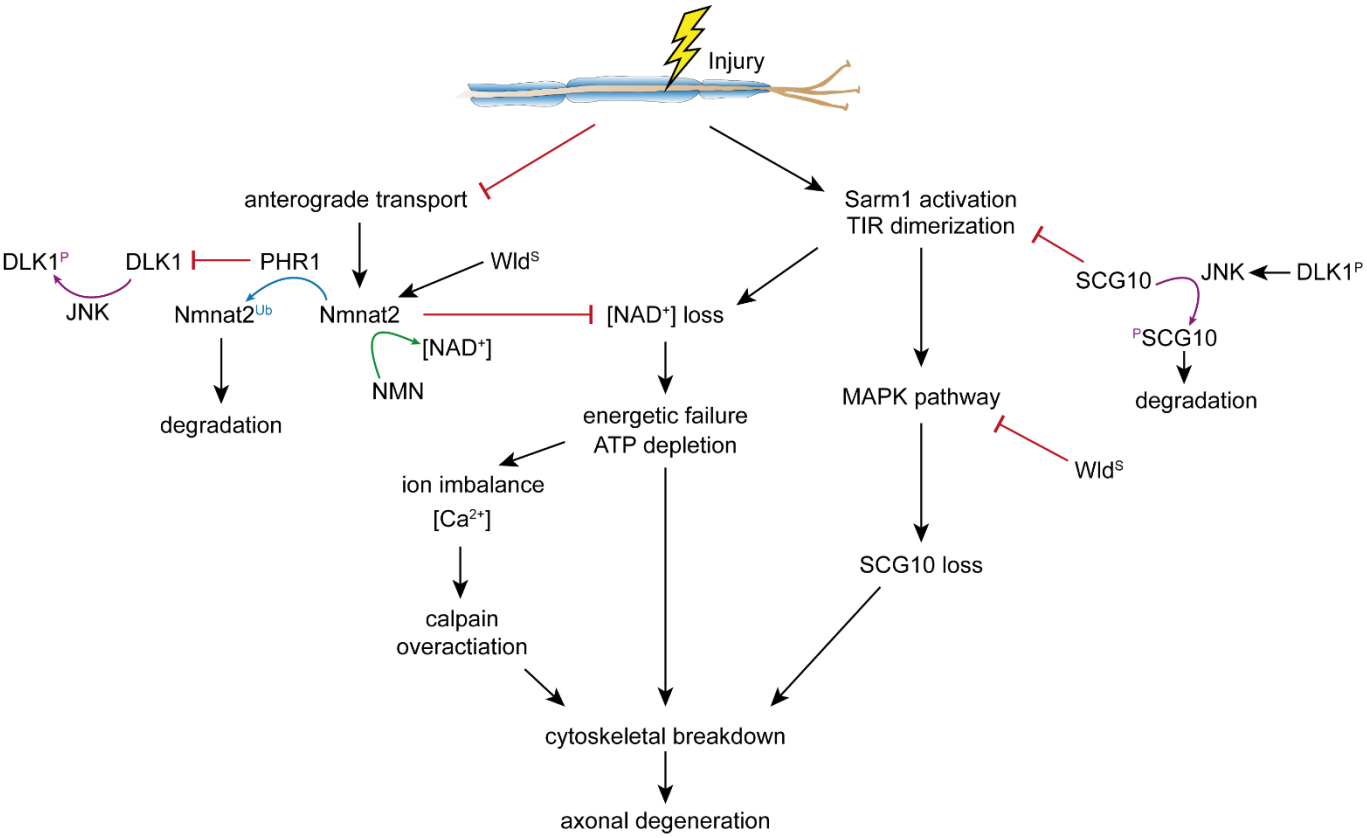

has no positive effect on axon survival in vitro after axotomy (Gerdts et al., 2013).

Although Sarm1 has no known enzymatic activity itself, its molecular structure indicates that Sarm1 probably forms multimers via SAM domain (Gerdts et al., 2013) and usually is auto-inhibited probably via ARM in its N-terminal domain (Chuang and Bargmann, 2005). Upon injury, the conformation of Sarm1 might change, leading to exposure of the active TIR domains, which initiate the destructive pathway. Forced dimerization of the TIR domains is sufficient to

Figure 2. Possible interaction of key players involved in Wallerian-like degeneration

An injury of the axon leads to impaired anterograde transport that results in decrease of Nmnat2 which catalyzes the production of NAD^+. PHR1 activation leads to degradation of Nmnat2. [NAD^+] loss can also be a result of TIR dimerization upon Sarm1 activation. Either way [NAD^+] loss is associated with ATP depletion and energetic failure which finally results in axonal degeneration.

Another consequence of Sarm1 activation is the activation of MAPK pathway and the consequent SCG10 loss which can be inhibited through Wld^S. SCG10 regulates microtubule dynamic and is associated with axon regeneration. Presence of SCG10 interferes with Sarm1 dimerization and its loss leads to cytoskeletal breakdown. DLK/JNK are part of the MAPK pathway and have their role in promoting degeneration, e.g. JNK facilitates the SCG10 degradation.

This overview scheme is a composition of (Gerdts et al., 2015)**,** (Inman and Harun-Or-Rashid, 2017) **and** (Walker et al., 2017)**.**

induce rapid axon fragmentation (Gerdts et al., 2013; Yang et al., 2015), by acting as an activating scaffold for further downstream effectors. The E3 ubiquitin ligase Highwire (Hiw) and its murine orthologue PAM/Highwire/Rpm1 (Phr1) are identified to be essential for WD, although their loss of function acts not as strong as Sarm1-/- (Babetto et al., 2013; Xiong et al., 2012). *Figure 2* gives an overview of possible interactions that play a role in Wallerian-like degeneration.

In summary, three key players have been identified for the execution of injury-induced axonal degeneration. First the pro-survival factor NMNAT2, whose depletion within the axon after injury is a trigger for WD. It is supposed that Wld^S acts by regulating NMNAT2 levels within the axon. Dual leucine zipper kinases and associated MAP kinases are promoting axonal degradation and regeneration. Finally, Sarm1 plays the role as the central executioner.

1.2.1.4 Wallerian degeneration-like pathways and MS

Patterns of axonal loss that are consistent with classic Wallerian Degeneration were observed in MS patients from the early stages of the disease (Simon et al., 2000). It is assumed that Wallerian degeneration contributes significantly to axonal injury and loss in lesions (Dziedzic et al., 2010), but diffuse axonopathy was found in regions distant from the focal lesions, often independent of inflammatory demyelination (Haines et al., 2011).

A few studies contribute further support to the hypothesis that Wallerian degeneration is at least partly contributing to the axonal loss seen in EAE lesions (Chitnis et al., 2007; Kaneko et al., 2006). Mice expressing Wld^S show an ameliorated disease course with modest protection against demyelination and neurodegeneration. Administration of Nicotinamide (NAm) improves axonal pathology and behavioral deficits, suggesting that Wld^S and the NAD biosynthesis precursor nicotinamide (NAm) act through limiting the NAD decline that is seen in EAE lesions (Kaneko et al., 2006). Other studies, however, fail to reproduce the protective effect of Wld^S expression in EAE (Singh et al., 2017). Since neurodegeneration in EAE and MS lesions has no clear onset, the neuronal damage observed is a combination of acute degenerative damage that might be Wld^S-insensitive and secondary degeneration that resembles classical WD.

1.2.2 Excitotoxic neurodegeneration

Another suggested mechanism how neurons and their axons undergo death is excitotoxicity due to uncontrolled glutamate release-induced persistent depolarization and calcium influx. This kind of cell death program is called accidental necrosis due to the absence of death receptor signaling. Glutamate is the primary excitatory neurotransmitter in the peripheral and central nervous system and it is involved in several essential activities, like cognition, learning, memory, but also it contributes to the development of the CNS. Glutamate modulates the connection of the CNS with peripheral organs and therefore contributes to cardiorespiratory, endocrine and reproductive functions. Since glutamate affects so many vital functions but is also a basic amino acid and nutrition factor, it is essential that glutamate signaling is tightly controlled, especially in the CNS. Oxidative stress, Ca^{2+} overload, mitochondrial dysfunction and energy deficiency can lead rapidly to abnormalities of excess glutamate (Levite, 2017). MS patients were found to have a disturbed glutamate homeostasis. Either their glutamate levels in the CSF (Sarchielli et al., 2003) or brain (Cianfoni et al., 2007) are elevated, or the expression of actors of the glutamate homeostasis like glutaminase and glutamate transporters are found to be highly expressed in active MS lesions (Werner et al., 2001). Furthermore, there is evidence that glutamate activates its receptors in autoimmune T cells that lead to cytotoxicity and neuroinflammation. Glutamate-activated T cells produce more glutamate that contributes further to the excitotoxicity and further autoimmunity (Levite, 2017). Other immune and glial cells are also known to have the capabilities to expel and take up the neurotransmitter.

The uncontrolled release of glutamate leads to overactivation of glutamatergic receptors. The resulting persistent depolarization damages the neuron. The duration of depolarization should usually be self-limited and end with the depletion of glutamate vesicles. However, the neuron remains in a depolarized state long after the initial injury, finally leading to the neuron's death. This suggest that excitotoxicity has two parts: a glutamate-dependent and a glutamate-independent step.

1.2.2.1 Molecular pathways of axon fragmentation

There is increasing evidence that the transient receptor potential M4 (TrpM4) channel is involved in the glutamate-independent step of excitotoxicity. TrpM4 is a non-selective cation channel of the TRP superfamily, permeable to monovalent cations, especially sodium and potassium that is activated by intracellular Ca^{2+} and low ATP concentration (Guo et al., 2017). Overactivation of TrpM4 might be a possible explanation for the depolarization despite

glutamate depletion (Simard and Gerzanich, 2017). By pharmacologically blocking or silencing TrpM4, the depolarization could be reduced in a cerebral ischemia-reperfusion model (Leiva-Salcedo et al., 2017). More evidence for the involvement of TrpM4 is the nature of the channel itself. Under physiological conditions TrpM4 is blocked by intracellular ATP. The necessary ATP concentration of the TrpM4 blockage is very low (Ullrich et al., 2005). Such low ATP concentration is usually associated with a severe metabolic depletion bordering on cell death. If the challenging condition persist, this can lead to an unchecked channel opening, Na^+ overload leading to membrane disruption and even rupture (Simard et al., 2012). Schattling et al. could show that the lack of Trpm4 saves neurons from glutamate-induced depolarization and cell body swelling (Schattling et al., 2012).

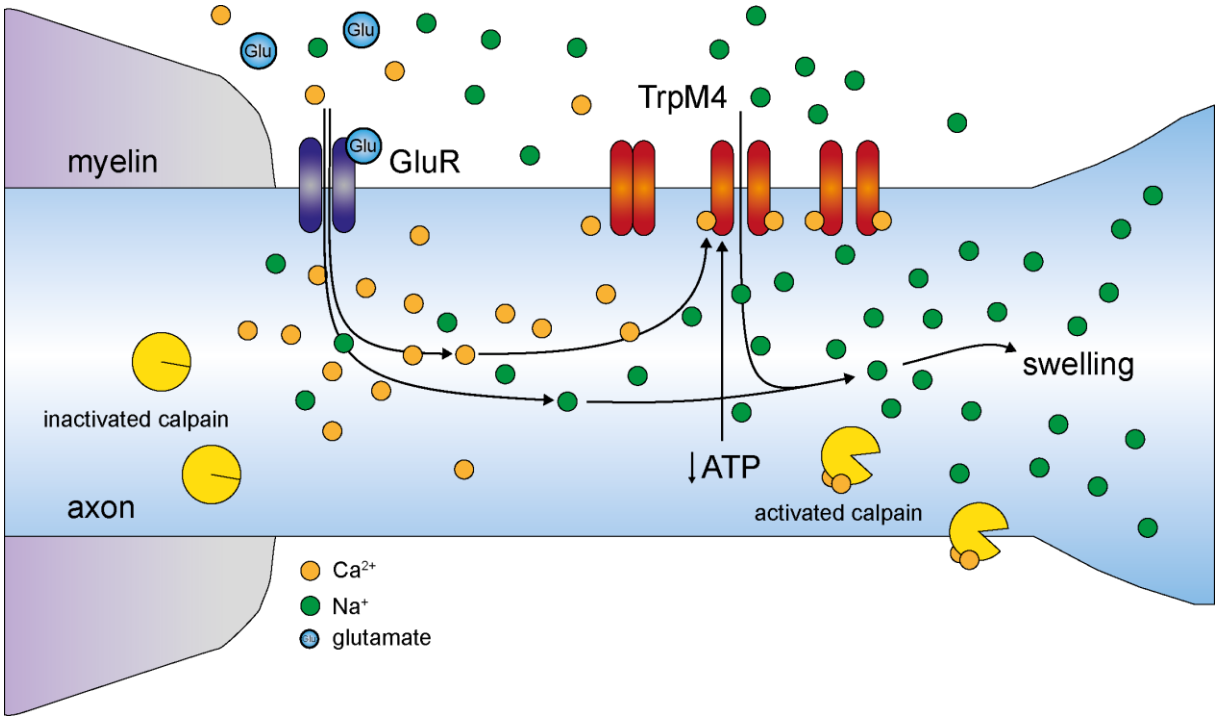

Figure 3. Molecular mechanism of axonal swelling induced by activated TrpM4

Glutamate Receptors GluR are activated by excess extracellular glutamate (Glu) which results in a channel opening and a rise in intraaxonal calcium (Ca) and sodium (Na). Increased intraaxonal Calcium and ATP depletion activate TrpM4 channel that potentiate sodium influx which is associated with oncotic axonal swelling and subsequent degeneration. Figure inspired by Friese et al. 2014.

TrpM4 is ubiquitously expressed in different cell types. Its exact physiological role is still unclear. It was found that TrpM4 is *de novo* expressed in capillaries after traumatic impact, thereby initiating secondary hemorrhage (Gerzanich et al., 2009). Isolated cardiac conduction disease is linked to a gain-of-function mutation in the TRPM4 gene (Liu et al., 2010). Physiologically, TrpM4 is likely associated with regulation of Ca^{2+} oscillations and therefore influences Ca^{2+} signaling in different cells (Launay et al., 2004). For instance, TrpM4 expression is identified to drive NFATc1 localization in T cells to the nucleus (Weber et al., 2010), where it

has a different effect on various T cell subsets. The inhibition of TrpM4 expression in Th1 cells lead to a decrease in Ca^{2+} levels and nuclear NFATc1, resulting in less motile Th1 cells with increased cytokine expression. In Th2 cells inhibition of TrpM4 expression had an opposite effect. *Figure 3* shows an overview of the molecular mechanisms that are possibly involved in TrpM4-dependent axonal swelling.

Taken all together, TrpM4 is a good candidate for a common converging downstream mechanisms of neuronal cell death as response to energy failure and Ca^{2+} influx, which are seen in several neurodegenerative diseases like in MS, Alzheimer's disease and stroke.

1.2.2.2 Involvement of TrpM4 in MS

TrpM4 is expressed in motor neurons of human spinal cord and cerebral cortex. In active demyelinating MS lesions, the proportion of TrpM4 expressing axons is significantly higher compared to healthy individuals (Schattling et al., 2012). This increase in immunoreactivity is only seen in active demyelinating lesions, whereas in inactive lesions or non-inflamed periplaque white matter only a small proportion of TrpM4+ axons was detected. These findings could be reproduced in EAE mice (Schattling et al., 2012). Although, it was discovered that TrpM4 modulates immune cell function, the deletion of TrpM4 in mice was not modifying the EAE autoimmune responses (Schattling et al., 2012). Nevertheless, mice deficient in TrpM4 showed reduced disease severity compared to WT littermates (Schattling et al., 2012). With the inhibition of TrpM4 currents via glibenclamide in WT mice this amelioration could be reproduced. Glibenclamide does not only block TrpM4 currents, it is rather associated to inhibit sulfonylurea receptor 1 (Sur1). TrpM4 and Sur1 were found to form *de novo* heterodimeric channels upon CNS injury (Tosun et al., 2013; Woo et al., 2013) and Sur1-TrpM4 is upregulated in astrocytes in EAE lesions (Makar et al., 2015). Inflammatory burden, demyelination, axonal damage and the overall clinical disease scores are reduced in mice deficient in Abcc8, which encodes for the Sur1 channel (Makar et al., 2015). A recent study further supported that inhibition of Sur1-TrpM4 via glibenclamide is beneficial during the chronic phase of EAE. Moreover, they found that Sur1 is upregulated in demyelinating, active lesions of MS patients (Gerzanich et al., 2017).

Global gene silencing of either Trpm4 or Abcc8 (encoding for Sur1) are found to exert similar beneficial effects on inflammation, myelin preservation and neurological function. Therefore, TrpM4 might be a potential target to ameliorate EAE progression.

1.2.3 Calpains

1.2.3.1 Molecular pathways (Calpain-Calpastatin system)

The calpain system consists of calpain and its endogenous highly specific inhibitor calpastatin. Calpain is a Ca^{2+}-dependent cysteine protease with papain-like activity that is activated upon increased Ca^{2+} concentration. There are two isoforms of calpain that differ in Ca^{2+} sensitivity (Cong et al., 1989). µ-calpain or calpain I is located in the cytosol or near the membrane and senses small changes in the Ca^{2+} concentrations. Physiological Ca^{2+} concentration ranges from 100 – 1000 nM, whereas under excitotoxic condition it can rise up to 5 – 10 µM (Campbell, 2014). On the other hand, m-calpain or calpain II is found at the membrane and requires mM concentrations of Ca^{2+} for activation. It is more likely that m-calpain is activated through an intracellular signaling pathway that involves its phosphorylation by PKA (protein kinase A) (Goll et al., 2003) or translocation to plasma membrane (Leloup et al., 2010). Both calpains autoproteolyze in the presence of Ca^{2+}, thereby reducing the Ca^{2+} concentration required for half-maximal proteolytic activity without affecting the specific activity (Goll et al., 2003).

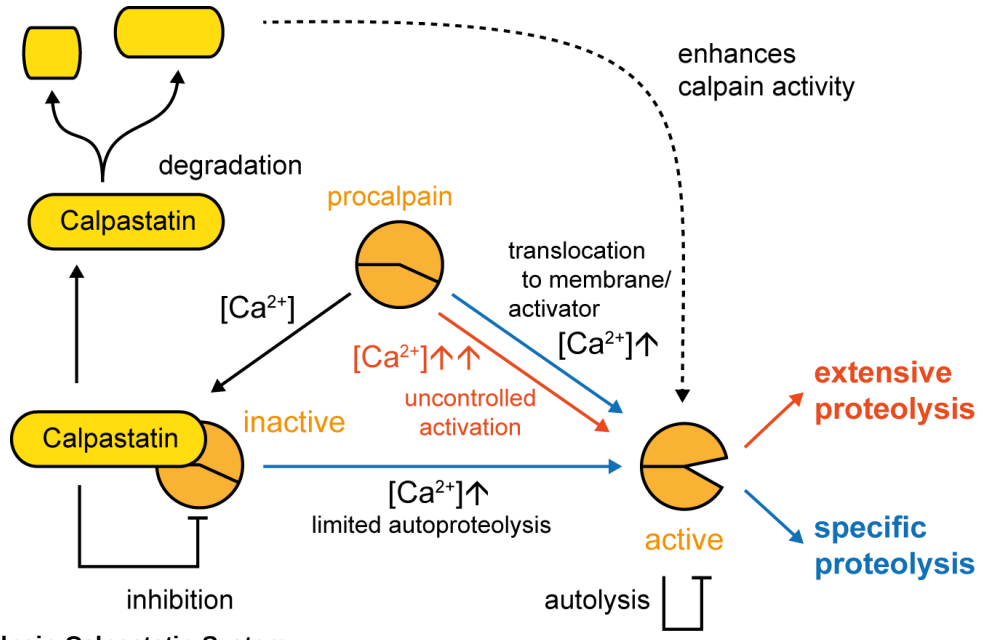

Figure 4. Calpain-Calpastatin-System

Under physiological conditions it is proposed that procalpain translocates to the membrane or binds to an activator molecule, in both ways activating calpain that then, in turn, regulates cell processes through specific proteolysis. For activation the procalpain molecule proteolyzes itself. In injury or disease, the intracelluar calcicum rises to pathological levels, which leads to an uncontrolled activation of calpain and an extensive proteolysis. There are several control mechanisms: calpastatin interacts in an inhibitory way with calpain under increase of intracellular calcium. Furthermore, calpain has a build-in self-regulation: further autolysis leads to deactivation of calpain. It was reported that caspase-3 and activated calpain can degrade calpastatin. The calpastatin fragments can enhance the calpain activity.

Calpastatin is an endogenous inhibitor that specifically inhibits calpain and no other protease (Cottin et al., 1981). It derives from one single gene and exists in different splicing variants depending on tissue localization and physiological states (Goll et al., 2003; Tullio et al., 2007). The physiological significance of these different variants remains still a mystery. It is required that Ca^{2+} binds to calpain for inhibitory interaction with calpastatin (Otsuka and Goll, 1987). The necessary concentration for binding is dependent on the calpain isoform and inhibition can be reversed via chelating calcium with EDTA. Immunolocalization reveals that calpain and calpastatin are frequently colocalized in the cell. Based on the required calcium concentrations in vitro calpain is rather found to be bound to calpastatin before its proteolytic activity is initiated. This is supported by the frequent colocalization of calpain and its specific inhibitor in the cell (Goll et al., 2003). There are a few proposed mechanisms that allow calpain activity in the cell despite calpastatin presence. Either the required calcium concentration for proteolytic activity is decreased in certain conditions (Goll et al., 1992) or calpain is separated through translocation away from calpastatin to be able to act (Goll et al., 2003).

Calpains recognize only a limited number of cleavage sites and the cleavage leads mostly to large, catalytically active fragments. This and the nature of the substrates indicates that calpains have rather a regulatory and signaling function than solely a digestive function. It is involved in cell motility by cleaving cytoskeleton substrates like cadherin, myosin, neurofilament and alpha-II-spectrin. Calpain substrates are e.g. kinases and phosphatases like PKC that modulate gene expression, signal transduction and long-term potentiation (Goll et al., 2003; Liu et al., 2008). Knockout mice lines have shown calpain is essential for embryonal development (Zimmerman et al., 2000). The role of calpain in apoptosis is not clear. There is evidence that calpain inhibits apoptosis by inactivating upstream caspases, but as well that calpain acts as positive regulator of apoptosis, being aligned with the direct degradation of cytoskeletal proteins by calpain (Momeni, 2011; Squier et al., 1994). However, calpain was found to play a role as well in other cell death mechanisms as necroptosis, autophagy and others (Orrenius et al., 2015).

Figure 2 illustrates a summary of the complex calpain-calpastatin-system. Under physiological cytosolic calcium concentration, the proenzyme procalpain gets activated by translocalization to the plasma membrane where it interacts with PIP2 (Leloup et al., 2010) or by binding of activator molecules (Pontremoli et al., 1990). In this way calpain can act modulatory by specific proteolysis of limited substrates. The activation of calpain is controlled by binding of calpastatin to calpain. If the cytosolic calcium levels increase extensively, calpain gets activated and proteolyzes in an uncontrolled manner that results in i.a. cytoskeletal breakdown. The latter is proposed to be involved in neurodegeneration.

1.2.3.2 Calpain involvement in MS and MS models

Under physiological conditions only a few calpain molecules are activated in a controlled way, allowing reorganization of the cellular scaffold - in process of synapses remodeling and memory formation (Liu et al., 2008). However, sustained increase in calcium concentration, as it is found in pathological conditions, activates all calpains present in the cell. In traumatic brain injury, the calcium rises with severe cellular damage, thereby initiating calpain mediated neuronal death and axonal disintegration (Schoch et al., 2012; Huh et al., 2006). Indeed, viral overexpression of calpastatin restored the deficits in axonal transport after optic nerve stretch injury (Ma et al., 2012). Likewise, inhibiting calpain in a spinal cord contusion injury saved the axons from fragmentation (Williams et al., 2014).

Since myelin proteins are substrates of activated calpain (Sloane et al., 2003), it seems likely that calpain also plays a role in myelin degradation. In spinal cords of Lewis rats with EAE the transcriptional expression of the calpain system was not altered. On translational level, however, expression of calpain was highly increased in combination with myelin loss. A correlative study in Lewis rats showed that increased calpain activity correlates with clinical symptoms and cell infiltration (Schaecher et al., 2002). In PBMC cells from MS patients calpain activity is increased as well. Treatment with calpeptin decreased the Th1 cytokines and myelin degradation (Imam et al., 2007). During relapses, infiltrating immune cell are suggested to secrete calpain that initiates myelin breakdown. Further, calpain overactivation has been implicated in neurodegeneration in MS and EAE lesions (Das et al., 2008). With double-immunofluorescence labeling an overexpression of m-calpain was found to be localized to NeuN positive cells. Axonal damage was not evident until the onset of clinical symptoms and it correlated with increased calpain expression. However, neuronal death occurs later in the course of disease (Das et al., 2008; Guyton et al., 2005). Axonal injury can be prevented in acute and chronic EAE using calpain inhibitors, reducing inflammation, demyelination as well as markers of axonal injury like APP (Hassen et al., 2006; 2008).

Taken all together, calpain is another promising candidate mediator of axonal degeneration in MS and EAE. It is activated in presence of high intracellular calcium levels and cytoskeletal proteins like spectrin are among its various substrates.

1.3 In vivo visualization of neuronal calcium levels

1.3.1 Principles of 2-photon excitation microscopy

The biggest challenge in high-resolution imaging of biological tissue is the limitation of light scattering that results in blurred, suboptimal resolution. Due to scattering, emitted photons cannot be addressed to their origin. Therefore, the tissue penetration in conventional (linear) one photon microscopy is limited to less than 100 µm (near the tissue surface).

In the last decades, non-linear microscopy was developed that reduced the limitations of surface and tissue light scattering. 1990 Denk combined the principle of laser scanner microscopy with the principle of 2-photon excitation, which is a higher order light-matter interaction and is therefore not linearly dependent on the incident light intensity.

In fluorescence microscopy a single electron of the fluorophore is usually excited by a photon, whose energy matches the energy difference between the electronic ground state S_0 and excited state S_1. The relaxation and falling back to S_0 results in an emission of a photon from the excited fluorophore. The wavelength of the emitted photon depends on the energy difference between the excited and ground state (see *Figure 5*).

This excitation can be achieved as well by 2 photons in the near-infrared wavelength range that simultaneously (within 0.5 fs) arrive at the molecule (*see Figure 5*). The generated emission photons have higher energies than the excitation light, the emission occurs in the visible spectral range. To achieve a higher excitation efficiency, the incident light source needs to be highly concentrated in photons in time (short pulse laser) and space (higher N.A. for high spatial intensities). As the laser beam is focused, the probability of two photons interacting simultaneously with a single fluorophore is increased. These properties explain the difference in excitation volume:

In case of single photon microscopy, the excitation is not limited to a focal point. Fluorophores can be stimulated above and below the focal plane. Confocal microscopy achieves a better z-resolution and optical sectioning via introducing a pinhole in the detection light pathway that excludes light that does not originate from the focal plane. This detection pinhole filters the depth of focus and blocks signals not originating from the focal plane. Although the pinhole enhances Z-resolution, absorption outside the focal plane is not inhibited. This can lead to photobleaching and phototoxicity in the cone-shape excitation volume. Furthermore, the insertion of the pinhole reduces the intensity of the detected signal and therefore the signal-to noise ratio.

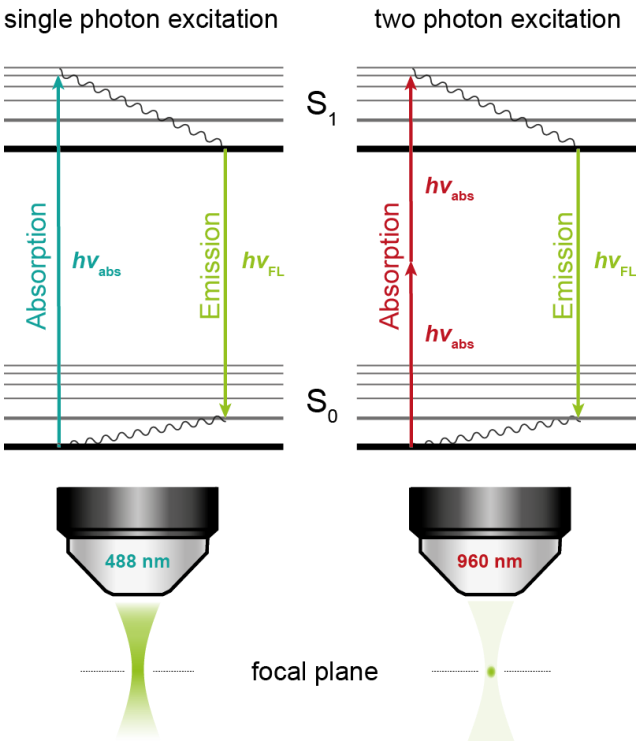

Figure 5. Overview of confocal and 2 photon principles.

(A) Jablonski diagram illustrating one and two-photon excitation of a fluorophore from the ground state S_0 to the excited state S_1. (B) In the case of single-photon microscopy laser light with lower wavelength is used and the excitation results in a cone-shaped excitation volume. For 2-photon microscopy near infra-red light is used for excitation and there is no out-of-focus signal. Inspired by, Helmchen and Denk, 2005.

For 2-photon excitation, on the other hand, the high spatial and temporal photon density needed is only reached in the focus point of the excitation laser. Above and below this focus point the photon density is not sufficient. This provides an inherent three-dimensional resolution without the usage of a pinhole that reduces signal intensity (see *Figure 5*, lower part). Additionally, photobleaching and phototoxicity occur only in close proximity to the focal point (Denk et al., 1990). However, the usage of highly dense photons in near-infrared spectrum for excitation can harm the tissue by photothermal damage or optical breakdown (Hopt and Neher, 2001; König, 2006).

In summary, 2-photon excitation microscopy is a strong tool for *in vivo* imaging. It provides the same optical sectioning capability combined with a better tissue penetration (up to 800 µm), stronger in-focus signal with minimal photobleaching and phototoxic effects.

1.3.2 Genetically encoded calcium indicators

As Ca^{2+} is a universal secondary messenger and is involved in many essential regulatory and signaling pathways, the need of developing an appropriate indicator for studying the involvement of Ca^{2+} is high. In mammalian neurons the intracellular calcium concentration is around 50 – 100 nM and can increase transiently during electrical activity up to levels 100 times higher. This broad concentration range and the mode of dye delivery are challenges for calcium sensor design. Furthermore, the commonly used delivery approaches like bulk or intracellular loadings of synthetic Ca^{2+} sensors are not cell type or population specific. Since the invasive application of these indicators causes tissue damage, they are not suitable for chronic repetitive *in vivo* imaging.

Genetically encoded Ca^{2+} indicators (GECI) are more suitable for *in vivo* imaging. Their delivery is minimal invasive and since they are expressed robustly a stable baseline can be measured. Ideally, GECI show a decent signal for Ca^{2+} transients without interfering with intracellular processes and ion homeostasis. For quantitative imaging, a sensor is needed that changes its emission and/or excitation behavior according to the Ca^{2+} concentration. Miyawaki and colleagues designed the first version of a FRET based GECI that is composed of two fluorophores connected by a peptide that induces conformational changes upon Ca^{2+} binding (Miyawaki et al., 1997). The two fluorophores are chosen in such a manner that Förster resonance energy transfer (FRET) can occur. The emission spectrum of one fluorophore, the donor, overlaps partially with the excitation spectrum of the higher wavelength fluorophore, the acceptor. If donor and acceptor are less than 100 Å apart a non-radiative energy transfer occurs if the donor is excited (Jares-Erijman and Jovin, 2003). Over the last years GECI were optimized with brighter fluorophore variants and different Ca^{2+} binding domains that have an influence on the Ca^{2+} binding affinity and kinetics (Rose et al., 2014).

By injecting purified linear DNA fragments of the engineered sensor into pronuclei of mouse oocytes, transgenic mouse lines were produced that stably express the GECI variant CerTNL15 under the Thy1 promotor that drives expression in neurons (Heim et al., 2007). CerTNL15 is composed of the fluorophore duo Cerulean and YFP and a chicken variant of the skeletal muscle Troponin C which shows improved Ca^{2+} sensitivity and sensor brightness compared to previous biosensor variants. This transgenic mouse line allows the investigation of Ca^{2+} levels in distinct neurons and their dendrites in the healthy and the diseased nervous system.

1.3.3 Intra-vital 2-Photon microscopy of the healthy and diseased nervous system

In vivo imaging has been a powerful analytical approach to resolve cell biological processes in healthy and diseased context, including axonal degeneration and regeneration. With conventional *in vitro* methods, immunohistochemistry or postmortem analysis a clear discrimination of different degeneration mechanisms is difficult. Only limited conclusions can be drawn from *in vitro* studies about the mechanisms in the intact organism. Before introduction of 2-photon excitation microscopy, imaging in tissue was challenging. Wide-field and confocal microscopy usually have compromised resolution and a low signal-to-noise ratio due to higher light scattering. 2-photon excitation microscopy allows the visualization of dynamics and time resolution of processes in their natural physiological environment in living animals. Although mechanisms are preferably first studied in a simplified manner that is easier to manipulate, like cell culture and *ex vivo* brain slice culture, it is difficult to recreate axons and their exact native context. 2-photon excitation microscopy and development of various calcium sensors enabled the investigation of the mammalian CNS *in vivo* (Helmchen and Waters, 2002). The spine dynamics in a healthy rodent brain can be observed and manipulated, thereby increasing our understanding of long-term potentiation and memory formation. With the *in vivo* approach, axonal disintegration in EAE lesions could be observed *in vivo*. Furthermore, it could be shown that this axonal degeneration is in some degree reversible, thereby revealing a therapeutic potential for intervention (Nikić et al., 2011). Utilizing intra-vital dyes it is possible to investigate other cellular signaling molecule in neurons or other cells and organelles within a cell (Romanelli et al., 2013). In the past years other genetically encoded biosensors were developed that detect changes in membrane potential (Storace et al., 2015), mitochondrial redox signals (Breckwoldt et al., 2014) or NADPH metabolism (Tao et al., 2017). The microtubule dynamics within different neuronal compartments could be visualized using a transgenic mouse line that expresses EB3 fused to yellow fluorescent protein (YFP) (Kleele et al., 2014). With the development of another transgenic mouse line that labeled all neuronal mitochondria with a fluorophore (Thy1-mitoCFP and nse-mitoYFP) in vivo imaging of mitochondrial transport and its changes in pathology in vivo was possible (Misgeld et al., 2007; Sorbara et al., 2014).

Thus, a diverse biosensor toolset emerged over the years that allows together with the constantly improving in vivo imaging techniques to get better insights in the complex pathogenesis of nervous system disease including the mechanisms that mediate the degeneration of axons in inflammatory lesions.

2 Objectives

Previous work in our lab could identify that axons in acute EAE lesions undergo focal axonal degeneration which is an active sequential process that still has potential to recover in the early phases (Nikić et al., 2011). Using a transgenic mouse line that expresses a FRET based calcium sensor in neurons our group could further show that intra-axonal calcium levels can predict the probability of axons to degenerate within an acute EAE lesion. The overall aim of my PhD project was to investigate how this axonal degeneration is initiated through pathologically increased intra-axonal calcium concentrations in EAE lesions.

There are several molecular candidates that are known to be involved in axonal degeneration in other contexts. In particular, I focused my investigation on three candidate mechanisms that might be triggered in acute EAE lesions: Wallerian-like degeneration, TrpM4 induced axonal damage and calpain-initiated axonal fragmentation. This work aims to answer the following specific questions:

- Do genetic mutations that inhibit Wallerian-like degeneration such as Sarm1 loss or the presence of the fusion protein Wld^S affect Ca^{2+}-mediated inflammatory axon degeneration *in vivo* and do they have any effect on the lesion pathology or axonal morphology within acute or chronic EAE lesions?
- Does lack of TrpM4 alter the intra-axonal calcium concentration and degeneration sequence *in vivo* within acute EAE lesions?
- Can pharmacological inhibition of calpain *in vivo* change the fate of axons with increased calcium levels and can a long-term treatment influence the disease outcome?

3 Materials and Methods

3.1 Material list

3.1.1 Surgery procedures

3.1.1.1 Surgery reagents

Description	Source
Ketamine hydrochloride 10% (Ketamine)	*Bremer Pharma GmbH, Warburg, Germany*
Xylariem 20 mg (Xylazine)	*Riemser Arzneimittel AG, Greifswald-Insel Riems, Germany*
Forene (Isoflurane)	*Abbott AG, Baar, Switzerland*
Sterile artificial mouse cerebrospinal fluid (aCSF)	*Solution A:* *8,66 g NaCl (Merck)* *0,224 g KCl (Merck)* *0,206 g CaCl2 · 2H2O (Sigma-Aldrich)* *0,163 g MgCl2 · 6H2O (Sigma-Aldrich)* *Solution B:* *0,214 g Na2HPO4 · 7H2O (Merck)* *0,027 g NaH2PO4 · H2O (Merck)* *dH20 ad 500 ml* *Mixture of solutions A and B in a 1:1 ratio*
Bepanthen Augen- und Nasensalbe 5 g (eye ointment)	*Bayer Vital GmbH, Leverkusen, Germany*
Ringerlösung Fresenius KabiPac (Ringer's solution)	*Fresenius KaBI Dtl., Bad Homburg, Deutschland*
Cutasept F Lösung 250 ml (disinfectant spray)	*Bode Chemie GmbH & Co, Hamburg, Germany*
Agarose	*Sigma-Aldrich® Chemie GmbH, 82024 Taufkirchen, Germany*
Ethanol 70 %	*CLN GmbH, 85416 Niederhummel, Germany*

3.1.1.2 Surgical tools and materials

Description	Source
Wella contura W7807 (Hair clipper)	*Wella, Darmstadt, Germany*
Syringe 3pc 5 ml OmnifixTM luer slip (syringe for injection of Ringer's solution)	*B. Braun Melsungen AG, Melsungen, Germany*
BD Plastipak Hypodermic luer slip syringe 1 ml (syringe for Ketamine/Xylazine and Ptx injection)	*Becton, Dickinson and Company, Franklin Lakes (New Jersey), USA*
Feather stainless steel blade (surgical blade)	*pfm medical ag, Cologne, Germany*
Noyes Spring Scissors (Large spring scissors)	*Fine Science Tools GmbH, Heidelberg, Germany*
Vannas-Tübingen Spring Scissors (Small angled spring scissors)	*Fine Science Tools GmbH, Heidelberg, Germany*
Dumont Mini Forceps – Inox Style 3 (Small forceps)	*Fine Science Tools GmbH, Heidelberg, Germany*
Dumont Mini Forceps – Inox Style 5 (Small forceps, smaller tip than Inox style 3)	*Fine Science Tools GmbH, Heidelberg, Germany*
Hypodermic Needles BD Microlance 3 30 Gauge (0,3 mm, yellow) for subcutaneous injection of Ringer's solution and anesthesia	*Becton, Dickinson and Company, Franklin Lakes (New Jersey), USA*
Ethicon Ethilon monofil 6-0 size, 667H (skin suture)	*Johnson & Johnson Medical GmbH, Norderstedt, Germany*
Ethicon Vicryl 4-0 size, MIC101H (intracorporal suture)	*Johnson & Johnson Medical GmbH, Norderstedt, Germany*
Sugi (absorbent triangles)	*Kettenbach GmbH & Co. KG, Eschenburg, Germany*
Metal plate	*Custom-made*
Cast Alnico Button Magnets	*Eclipse Magnetics Ltd, Sheffield, UK*
Rubber band	
Support cushion	*Custom-made*
Osmotic minipump (Model 1007B)	*Alzet, Cupertino (California), USA*
Intrathecal catheter (Model 7743)	*Alzet, Cupertino (California), USA*

3.1.1.3 Devices

Description	Source
Olympus KL 1500 LCD (cold light source for stereomicroscopy)	*Olympus Deutschland GmbH, Hamburg, Germany*
Olympus Stereo Microscope SZ51	*Olympus Deutschland GmbH, Hamburg, Germany*
FST 250 Hot Bead Sterilizer (sterilizer for surgical instruments)	*Fine Science Tools GmbH, Heidelberg, Germany*
T/Pump (Heating pad)	*Gaymar Industries, Orchard Park (New York), USA*
MouseOx Plus® Rat & Mouse Pulse Oximeter	*Starr Life Sciences Corp., 333 Allegheny Ave, Oakmont, PA 15139, United States*
Mouse Thigh Sensor	*Starr Life Sciences Corp., 333 Allegheny Ave, Oakmont, PA 15139, United States*
Mouse Temperature Sensor	*Starr Life Sciences Corp., 333 Allegheny Ave, Oakmont, PA 15139, United States*

3.1.2 Perfusion and immunohistochemistry

3.1.2.1 Reagents

Description	Source
PFA (paraformaldehyde) 4%	*8% PFA (Sigma-Aldrich) in dH2O, heated up to 55 ° filtrated and mixed in a 1:1 ratio with 0.2 M PB (Phosphate buffer), pH adjusted to 7.2-7.8*
Triton X-100	*Sigma-Aldrich, Chemie GmbH, 82024 Taufkirchen, G*
30 % Sucrose	*Sigma-Aldrich, Chemie GmbH, 82024 Taufkirchen, G*
Phosphate Buffered Saline (PBS) 10x, pH=7,2/7,4	*2,6 g NaH2PO4 · H2O 14,4g Na2 HPO4· 2H2O 87,5g NaCl (Merck) dH2O ad 1l*
TBS 10x (Tris buffered saline), pH=7,6	*61 g Tris base (121,14 g/mol), (Sigma-Aldrich) 90 g NaCl dH2O ad 1l*

Phosphate Buffer (PB) O,2 M	*27,598 g NaH2PO4· H2O,* *35,598 g Na2 HPO4· 2H2O* *dH2O ad 1l*
Gibco goat serum	*Invitrogen GmbH, Darmstadt, Germany*
DMSO	*Sigma-Aldrich® Chemie GmbH, 82024 Taufkirchen,*
Cryoprotective Solution: 25 % Glycerol (85%), 25 % Etyhlenglycol, 50 % PBSx1	*Custom made* *Chemicals from Sigma-Aldrich® Chemie GmbH, 82*
0.1 % Sodium Azide (NaN_3) in PBSx1	*Sigma-Aldrich, Chemie GmbH, 82024 Taufkirchen,*
Sodium Citrate Buffer	*10mM Sodium Citrate, pH 8.5*

3.1.2.2 Antibodies, vital dyes and tracers

Antibody	Source
Polyclonal rabbit anti-Iba1	*SynapticSystems #234013*
Polyclonal rat anti-CD3	*Serotec, MCA1477*
Polyclonal anit-HA	*GeneTex, #GTX115044*
Rabbit anti-spectrin	*Millipore*
Goat-anti-rabbit Alexa fluor® 594 antibody	*Invitrogen GmbH, Darmstadt, Germany*
Goat-anti-mouse Alexa fluor® 635 antibody	*Invitrogen GmbH, Darmstadt, Germany*
Goat-anti-rabbit Alexa fluor® 488 antibody	*Invitrogen GmbH, Darmstadt, Germany*
Neurotrace 435/455 blue fluorescent Nissl stain	*Invitrogen GmbH, Darmstadt, Germany*
Neurotrace 640/660 deep-red fluorescent Nissl stain	*Invitrogen GmbH, Darmstadt, Germany*
Goat-anti-rat Alexa fluor® 594 antibody	*Invitrogen GmbH, Darmstadt, Germany*
Goat-anti-rat Alexa fluor® 635 antibody	*Invitrogen GmbH, Darmstadt, Germany*

3.1.2.3 Tools and materials for histology

Description	Source
Microscope slides 76x26 mm	*Gerhard Menzel Glasbearbeitungswerk GmbH & Co. KG, Braunschweig, Germany*
Microscope cover slips 24x60 mm	*Gerhard Menzel Glasbearbeitungswerk GmbH & Co. KG, Braunschweig, Germany*
Parafilm	*Brand GmbH & Co. KG, Wertheim Germany*
Pipettes, pipette tips and tubes (2ml and 1,5 ml)	*Eppendorf AG, Hamburg, Germany*
12-well cell culture plates	*Becton, Dickinson and Company, Franklin Lakes (New Jersey), USA*
Tissue Tek Cryomold Standard, 25x20x5 mm	*Sakura Finetek Europe B.V., Alphen aan den Rijn, The Netherlands*
Tissue Tek Cryomold Biopsy, 10x10x5 mm	*Sakura Finetek Europe B.V., Alphen aan den Rijn, The Netherlands*
Tissue Tek optimal cutting temperature (O.C.T.)	*Sakura Finetek Europe B.V., Alphen aan den Rijn, The Netherlands*
Vectashield Mounting Medium	*Vector Laboratories, Inc., Burlingame (California), USA*
Paper filters (185 mm Ø circles)	*Whatman Schleicher & Schuell GmbH, Dassel, Germany*
50 ml centrifuge tubes	*Greiner Bio-One GmbH, Frickenhausen, Germany*

3.1.2.4 Technical devices

Description	Source
Leica CM1850 cryostat	*Leica Microsystems GmbH, Wetzlar, Germany*
Vibratome 1000Plus	*Intracel LTD, Shepreth, Royston, Great Britain*
Vortex-Genie 2	*Scientific Industries, Inc., Bohemia (New York), USA*

KERN EW 150-3M (scales)	*Kern & Sohn GmbH, Balingen-Frommern, Germany*
Laboratory pH meter inoLAB	*WTW Wissenschaftlich-Technische Werkstätten, Weilheim, Germany*
Magnetic stirring hotplate MR 3001K and stirring bars	*Heidolph Instruments GmbH & Co. KG, Schwabach, Germany*
Ismatec IP high precision multichannel pump (pump for perfusions)	*ISMATEC SA, Labortechnik – Analytik, Glattbrugg, Switzerland*
Olympus IX71inverted fluorescence microscope	*Olympus GmbH, Hamburg, Germany*

3.1.3 Imaging

3.1.3.1 Imaging devices

Description	Source
FV1000 confocal system mounted on an upright BX61 microscope, equipped with an y10/0.4 water immersion objective and x20/0.85 and x60/1.42 oil immersion objectives (confocal microscopy)	*Olympus GmbH, Hamburg, Germany*
Olympus FV1000 MPE multiphoton Microscope *X25/1,05 water immersion objective*	*Olympus GmbH, Hamburg, Germany*
Objectives: x4/0.13, x10/0.4 air objectives; x25/1.05 water immersion objective; x40/0.85, x60/1.42 oil immersion objectives	*Olympus GmbH, Hamburg, Germany*
Small animal ventilator	*Harvard Apparatus*
Intratracheal cannula (1.0 mm OD, 13 mm length)	*Harvard Apparatus*
Spinal clamping device (spinal adaptor for a stereotaxic frama)	*Narishige STS-A*
Gravity superfusion system containing in-line heater	*Warner Instruments*
vacuum system with suction tube	*Custom-built*
Stage for spinal clamping device	*Luigs & Neumann SM 5-9 stage and*

	controller unit
MaiTai eHP/HP titanium:sapphire laser	*Newport/Spectraphysics, Irvine, California, USA*

3.1.4 EAE induction

3.1.4.1 Reagents for immunization

Description	Source
Purified recombinant MOG (from E. Coli)	*Stock solution, produced by laboratory of Doron Merkler (Universität Göttingen, University of Geneva) and by laboratory of Martin Kerschensteiner*
Purified MOG peptide (N35-55)	*Schafer-N Copenhagen, Denmark*
Mycobacterium Tuberculosis H37 RA	*Sigma-Aldrich® Chemie GmbH, 82024 Taufkirchen, Germany*
Incomplete Freund's adjuvant (IFA)	*Sigma-Aldrich® Chemie GmbH, 82024 Taufkirchen, Germany*
Pertussis toxin from Bordetella pertussis, inactivated	*Sigma-Aldrich® Chemie GmbH, 82024 Taufkirchen, Germany*

3.1.4.2 Tools for immunization

Description	Source
10 ml syringes	*Hamilton*
Hypodermic Needles BD Microlance 3 23 Gauge (0,6 mm, blue) for subcutaneous emulsion immunization	*Becton, Dickinson and Company, Franklin Lakes (New Jersey), USA*

3.1.5 Software

3.1.5.1 Data analysis

Description	Source
Adobe Creative Suite (Photoshop, Illustrator)	*Adobe Systems, Inc., San Jose, California, USA*
ImageJ /FIJI	*General Public License http://rsbweb.nih.gov/ij/download.html*
Graphpad Prism	*GraphPad Software, La Jolla, California, USA*
Microsoft Office (Powerpoint, Excel, Word)	*Microsoft Corporation, Redmond, Washington, USA*

3.2 Experimental Animals

All animals were socially housed on 12-h light/dark cycle under controlled standard conditions in the animal facilities of the institution. The animals were kept in Eurostandard Type II long cages 365x207x140 mmH (Tecniplast, Hohenpeißenberg, Germany) stored in IVC rack system with a maximum of five mice per cage. Autoclaved food (regular food “Maus” from Ssniff, Soest, Germany) and autoclaved tap water were supplied ad libitum. All animal experiments were performed in accordance with regulations of the animal welfare act and protocols approved by the Regierung von Oberbayern (permit number 55.2-1-54-2532-64).

For the experiments adult female and male wild-type and several transgenic mice lines were used (between 6 – 12 weeks of age).

In particular, C57/Bl6 were purchased from Janvier Labs. B6.Tg(Thy1-CERTNL15)/Griesb were provided by Oliver Griesbeck (MPI for Neurobiology, Martinsried). They express the corresponding GECI protein CerTNL15 (Heim and Griesbeck, 2004; Heim et al., 2007) under the neuronal expression cassette Thy-1.2 on a C57Bl/6 background. This mouse line allowed the investigation of calcium dynamics within axons in healthy and EAE mice. Therefore the following transgenic mouse lines were crossed with B6.Tg(Thy1-CERTNL15)/Griesb and maintained on this genetic background, if not indicated otherwise.

To investigate the involvement of TrpM4 in axonal disintegration in EAE lesions, trpM4tm1.1Knt mice were used (first described by (Vennekens et al., 2007)). This mouse line was kindly provided by Manuel A. Friese and maintained on a C57Bl/6J background. The knockout is a result of a targeted genetic deletion of the exons 15 and 16 from the gene locus. For the calcium imaging experiments TrpM4-/- animals were crossed with CerTNL15 mice. As control group littermate mice heterozygous for TrpM4 were chosen.

B6.129X1-Sarm1tm1Aidi/Ker were used for the Sarm1-/- experiments. The knock-out of Sarm1 in this strain is a result of a targeted disruption of exon 3 through 6 of this gene. This mouse strain was first described by Kim et al (Kim et al., 2007) and we received this strain as a gift from Marc R. Freeman. As control CerTNL15 positive Sarm1+/- littermates were used. For the initial characterization experiments performed by Catherine Sorbara Sarm1-/- were crossed to B6.Cg-Tg(Thy1-YFP)16Jrs/J, to obtain mice with an axonal labeling.

ΔNLS R213AR215A Wld^S mice (Beirowski et al., 2009) were crossed to CerTNL15 and F1 mice positive for CerTNL15 and ΔNLS were used for experimental analysis. The mouse line was kindly provided and bred at the animal facilities of Thomas Misgeld (Institute of Neuroscience, TUM.

3.3 Methods

3.3.1 Induction of experimental autoimmune encephalomyelitis (EAE)

Mice with a C57J/Bl6 background were immunized as previously described (Abdul-Majid et al., 2000). Briefly, mice were injected with a total of 250 µL of an emulsion of 300 – 400 µg of purified recombinant myelin oligodendrocyte glycoprotein (MOG, N1-125, expressed in E. coli) in complete Freund's adjuvant with 5 – 10 mg/mL mycobacterium tuberculosis H37 Ra. The solutions were mixed very thoroughly to obtain a thick emulsion that does not disperse in water. Directly and 48 h after immunization the mice were given 300 – 400 ng of pertussis toxin (Ptx) intraperitoneally. Mice were weighed daily and the severity of behavioral and neurological deficits was observed. A standardized clinical EAE scoring system was used (see table 1). On average, 10 days after immunization the mice showed weight loss and the day after first clinical signs of EAE.

Score	Clinical symptoms
0	no detectable clinical signs
0.5	partial tail weakness
1	tail paralysis
1.5	gait instability or impaired righting ability
2	hind limb paresis
2.5	hind limb paresis with dragging of one foot
3	total hind limb paralysis
3.5	hind limb paralysis and fore limb paresis
4	hind limb and fore limb paralysis
5	death

Table 1. EAE clinical scoring scale.

3.3.2 Tissue processing and immunohistochemistry

Animals were lethally anesthetized with isoflurane and perfused transcardially with 25 mL 1xPBS/Heparin solution followed by 30 mL 4 % PFA in 0.1 M phosphate buffer for uniformly preservation of the tissue. After dissection, the tissue was post-fixed in 4 % PFA overnight at 4°C. The microdissected CNS was cryoprotected in 30 % sucrose in 1xPBS for 24 – 72 h, depending on the tissue, before the region of interest was embedded in Tissue-Tek optimal cutting temperature (O.C.T.) compound and frozen at – 20 °C. Before immunohistochemistry the tissue was sectioned using a cryostat.

3.3.2.1 Characterization of axonal morphology within EAE lesions

For the assessment of axonal morphology 50 µm thick longitudinal sections at L3/L4 were obtained and stained free-floating. Subsequently, the sections were rinsed three times with 1xPBS for 10 minutes at room temperature and incubated for blocking in 20 % goat serum in 1xPBS with 0.5 % TritonX-100 for 1 hour at room temperature. The nuclei were visualized with Nissl-staining Neurotrace NT640/660 (1:500) for 30 min at room temperature. The samples were mounted with Vectashield and covered with a coverslip glass sealed with nail polish.

3.3.2.2 Characterization of immune cell distribution within EAE lesions

For the CD3 and Iba1 staining 50 µm thick longitudinal sections at L3/L4 were stained free-floating. The sections were washed in 1xPBS three times for 10 min. For a sharper staining an antigen retrieval with sodium citrate was performed. Briefly, sections were incubated in pre-heated Sodium Citrate Buffer for 30 min at 85 °C. Then the sections were rinsed three times in 1xPBS/0.5 % TritonX-100, before they were blocked in 20 % goat serum in 1xPBS/0.5 % TritonX-100 for 1h at room temperature. After that, the sections were incubated at 4 °C overnight with the following primary antibodies: rat anti-CD3 (1:250, Invitrogen) and rabbit anti-Iba1 (1:250, Wako). After washing the sections three times with 1xPBS/0.5 % TritonX-100, the secondary antibodies anti-rat AlexaFluor594 (1: 500, Invitrogen), anti-rabbit AlexaFluor647 (1: 500, Invitrogen) and NT640/660 (1:500, Invitrogen) were applied for 4 h at room temperature. After mounting with Vectashield the sections were covered with a coverslip glass and sealed with nail polished.

3.3.3 Confocal microscopy

Fixed tissue samples previously stained were scanned on a FV1000 confocal system mounted on an upright BX61 microscope (Olympus). The system was equipped with a 10x/0.4 water immersion objective, 20x/0.85 and 60x/1.42 oil immersion objectives, and with standard filter sets. Recorded 12-bit Images were processed with ImageJ or Adobe Photoshop.

3.3.4 Surgery procedures

3.3.4.1 Dorsal hemisection injury

As a positive control for Wallerian-like degeneration, we used the dorsal hemisection injury model. Mice were anesthetized with an i.p. injection of MMF and given 15 µL of Metacam. The cranial spinal cord was exposed with a laminectomy at C4 level and the dorsal spinal cord was transected using a very fine pair of scissors (iridectomy scissors) as previously described (Lang et al., 2012; Lee and Lee, 2013). Muscle tissue was sewed together and the wound was closed with staples. After the surgery, the animals were kept on a heating pad until fully awake, rehydrated and treated with Metacam twice per day for 48 hours.

3.3.4.2 Osmotic pump implantation

For chronic treatment with Calpain Inhibitor 3, osmotic pumps were implanted subcutaneously in mice with EAE 1 day after onset. For the experiment, the 1007D model of Alzet osmotic pumps was chosen. The average pump rate is 12 µL per day and with a total capacity of 100 µL can be in use for more than 7 days.

In short, mice were anesthetized with MMF one day after onset of the clinical symptoms of EAE. To access the intervertebral space the caudal lumbar vertebral column was opened. A hole was pinched into the dura and the catheter was slowly inserted below the dura while pointing caudally to avoid trauma to the spinal cord. The catheter tube was fixed to the vertebral muscle tissue at two places to avoid a displacement. The osmotic pump was connected to the intraspinal catheter and placed into a skin pocket. The osmotic pumps were filled with 0.1 mL 2mM CI3 in 10 % DMSO in saline or vehicle solution (10 % DMSO in saline) and incubated over 12 hours prior to implantation in saline at 37 °C as recommended by the supplier. After the wound was closed, the mice were rehydrated with 1 mL of s.c. injected Ringer's solution, left for recovery on a heating pad and given 0.1 mL temgesic. After 5 days of treatment, the mice were

perfused transcardially with 4 % PFA. To evaluate the success of delivery, the pumps were weighed and the residual volume was measured.

3.3.5 2-Photon in vivo imaging

According to previously established protocols (Kerschensteiner et al., 2005; Misgeld et al., 2007; Romanelli et al., 2013) mice were intraperitoneally anaesthetized with MMF. After anaesthesia, the fur above the lumbar spinal cord, the right hindlimb and above the throat was shaved. To stabilize the breathing rate and to reduce breathing artefacts a tracheotomy was performed. Therefore, the mouse was fixed in a supine position and after a tracheotomy the tracheal tube of a breathing device is inserted. With a few stitches the tube was secured. Then the mouse was carefully turned around, fixed again and with a dorsal laminectomy the spinal cord was exposed. Two to 3 vertebrae were removed during the surgery. To clean and moist the spinal cord it was constantly rinsed with prewarmed aCSF. Afterwards the vertebral column was fixed using a spinal clamping device, which allows controlled movement in x,y and z. axis during imaging. To monitor for vital parameter a thigh sensor was clipped on the shaved hindlimb. To allow immersion of the objective a well consisting of 3 % Agarose/aCSF was built around the exposed spinal cord. The agarose well allowed to hold aCSF throughout the complete imaging session and to incubate the spinal cord with intravital dyes (Romanelli et al., 2013).

Only animals with a score higher than 2.5 were used for imaging to ensure to find proper lesions. Prior to imaging the clamped and exposed spinal cord was incubated with Neurotrace 640/660 (1:500) to visualize the density of nuclei to define a lesion. Several lesion sites were imaged repetitively every 2 hours to follow the axonal morphological changes. To ensure that the anesthesia is deep enough, the breathing rate and oxygenation was controlled constantly. When the depth of anesthesia dropped, the mouse was injected with additional 0.1 mL MMF. The images were acquired with a 25x/1.25 water immersion objective at 1024x1024 pixel resolution and with a pixel dwell time of 2 µs/pixel.

For the calpain inhibition experiments, the mice were treated with 0.1 mL 100 nM calpain inhibitor III (CI3) in 0.5 % DMSO or 0.1 mL vehicle solution (0.5 % DMSO) 30 min prior to imaging. During imaging the immersion fluid consisted of CI3 solution or vehicle solution in aCSF to ensure constant presence of the treatment during experiments. The solution renewed every 2 hours.

To control for phototoxicity, damage caused during surgery and dye toxicity the same procedure was performed with healthy animals. After several hours of imaging no morphological changes in the axons were observed.

3.3.6 Data evaluation and Statistics

For data processing and analysis Adobe Photoshop CS6 and FIJI (http://fiji.sc/Fiji) were used. Statistical analysis of the experimental data was performed with GraphPad Prism 7.01.

3.3.6.1 Axonal pathology after dorsal hemisections in Sarm1 and ΔNLS- Wld^S animals

To validate the neuroprotective properties of Sarm1 and ΔNLS- Wld^S transgene, the axonal morphology was evaluated 3 days after dorsal hemisection. Four to 6 images of the cervical dorsal spinal cord 200 – 600 µm cranially from the injury site were taken per animal. As an internal control for tissue damage due to the surgical procedure, images were taken as well from the opposite ventral part. No damage was observed in these areas. The first 50 axons dorsal to ventral were evaluated and classified into stage 0, 1 and 2 axons (according to (Nikić et al., 2011)). Three animals per group were analyzed.

3.3.6.2 In vivo analysis of calcium signals and dynamic analysis

As already described (Schumacher, 2016) the ratio of YFP/CFP signal was used to estimate the intra-axonal calcium concentration. In short, images of the first timepoint were opened using the Bioformats Importer plugin of ImageJ as two separate channels showing the CFP and FRET signals separately. In one of the two channels, ROI were selected within an identified axon and adjacent to that outside of that axons a background ROI was selected. The intensity ratio within one axon did not vary much, therefore only one ROI was drawn within an axon. The diameter was measured at three distinct sites of one axon. The same ROIs were transferred to the other channel to obtain the corresponding intensities. To calculate the intensity ratio the following formula was used (adapted from (Schumacher, 2016)):

$$Ratio = \frac{(YFP_{Int} - YFP_{BG})}{(CFP_{Int} - CFP_{BG})} - BF$$

With YFP representing fluorescence intensity of yellow fluorescent protein variants and CFP standing for fluorescence intensity of blue fluorescence protein variants. The bleedthrough factor (BF) is an experimentally measured value. Since this factor does not change the intensity

ratio itself and I was only interested in the qualitative changes of the intraaxonal changes, the BF correction was not applied.

For the lesion characterization *in vivo* for Sarm1 and ΔNLS-Wld^S experiments, the intensities and the respective background of the first 30 axons from dorsal surface of the spinal cord were measured and their morphology was noted, according to the stages previously introduced (Nikić et al., 2011).

In case of the TrpM4 experiment, calpain inhibition and analysis of the dynamic transitions, the fluorescence ratios and axonal morphologies were obtained from the first 80 axons from dorsal surface of the spinal cord. In case less than 80 axons were identified within one lesion, axons were further identified in another lesion of the same animal. After reaching 80 axons, only stage0 and stage1 axons were evaluated, in order to increase the size of the high calcium cohort for the further dynamic analysis.

Changes in intra-axonal calcium level and axonal morphology were traced 4 hours after the first imaging timepoint. Since I was interested in the fate of axons with increased intra-axonal calcium only those axons were followed over time. Axons were relocated in the second timepoint based on their position to peculiar anatomical structures like blood vessels. The dynamic rates were calculated as following:

$$r_{FR} = \frac{number\ of\ fragmentation\ events}{number\ of\ all\ \ observed\ high\ ca\ stage\ 1\ axons}$$

$$r_{SR} = \frac{number\ of\ swelling\ events}{number\ of\ all\ observed\ high\ ca\ stage\ 0\ axons}$$

$$r_{MR} = \frac{number\ of\ morphology\ recovery\ events}{number\ of\ all\ observed\ high\ ca\ stage\ 1\ axons}$$

$$r_{CD} = \frac{number\ of\ events\ of\ calcium\ level\ decreases}{number\ of\ all\ observed\ high\ ca\ stage\ 0\ and\ 1\ axons}$$

There are several transitions possible. Healthy appearing, high calcium axons could develop swellings. These transitions are reflected with the swelling rate. As fragmentation, we consider only the transition of high calcium stage 1 axons that fragment after 4 h. There are as well recovery processes detectable, as it was already seen in previous experiments (Nikić et al., 2011; Schumacher, 2016). As recovery, we consider all transitions that improved either the morphology or the calcium level of the observed axons. Since the mechanisms involved in calcium level decrease and deswelling are probably distinct from each other, we differentiated two different recovery rates: rate of decreased calcium (r_{CD}) and rate of morphology improvement (r_{MR}). An overview of all transition of interest are depicted in *Figure 6*.

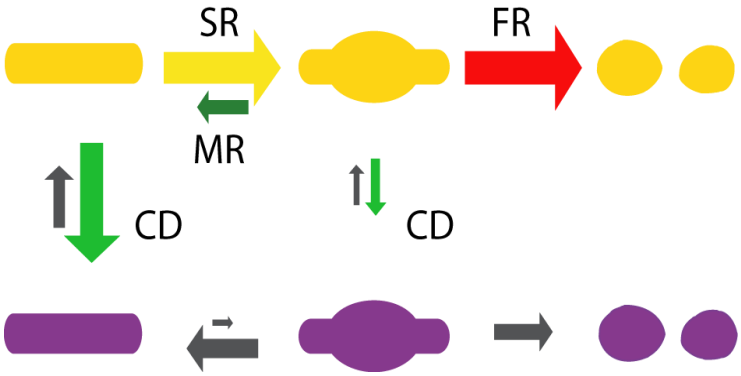

Figure 6. Overview of transition of interest.

Axons are classified by their morphology as normal appearing axons (stage 0), swelling (stage 1) or fragments (stage 2) or based on their $[Ca^{2+}]_{cyt}$ levels as high calcium (yellow) or low calcium axons (magenta). Possible transitions that high calcium populations undergo, are either fragmentation from $stage1^{high}$ to stage2 (FR=fragmentation rate), swelling from $stage0^{high}$ to $stage1^{high}$ (SR=swelling rate). A decrease in cytosolic calcium (CD=rate of calcium decrease) or a morphological recovery (MR=rate of morphological recovery) are considered as recovery processes. Adapted from (Schumacher et al., 2016).

To obtain reliable transition rates I introduced several evaluation criteria to optimize the analysis and ensure that at least 25 axons (stage 0 and stage 1) with increased intra-axonal calcium at timepoint 0 were available for the calculation of the transition rates.

3.3.6.3 Axonal morphology within EAE lesions in fixed tissue

The analysis of axonal stages in chronic fixed EAE tissue was performed on confocal images obtained with a 60x/objective. After identifying the lesion area based on infiltrating cells stained with Neurotrace a line of 500 µm length was drawn from the lesion border. Using the cell counter plugin of ImageJ axons crossing this line were classified according to their morphology into stages. Stage 0 axons are normal appearing, undisrupted axons, whereas stage 1 axons display at least one swelling. As soon as an axon shows a disruption it was classified as stage 2. When at least 3 fragments were lying in proximity to each other on a virtual line, there were as well counted to the stage 2 axons.

3.3.6.4 Evaluation of lesion load

Overview images of coronal spinal cord sections were taken with a 20x objective at the confocal microscope. Lesion area was defined based on the Neurotrace staining. Using the polygon selection tool of ImageJ the whole section, white matter and areas occupied by infiltrating cells within the grey matter were outlined. Area of white matter was calculated by subtracting the grey matter area from outline area. The lesion load is determined as the ratio of area occupied by infiltrating cells to white matter area. For the evaluation 2 – 3 sections were used per animal.

3.3.6.5 Evaluation of cell composition

For evaluation of immune cell composition, coronal spinal cord sections were stained with antibodies against CD3 and Iba1. The infiltrating cells within the CNS were visualized by Neurotrace staining. Two lesions of 3 section per animal were analyzed in a blinded fashion. For every lesion, the lesion area was measured and the numbers of CD3 positive and Iba1 positive cells within the lesion were counted. Lesion area was assessed based on Neurotrace staining in a maximum intensity z projection of the image that was obtained with a 60x objective on the confocal microscope. This area was furthermore used to identify the lesion.

For analysis of cell composition, the cell counter plugin in ImageJ was used. To reduce counting mistakes due to staining artefacts only the middle planes of a z-stack were used. To assess the numbers of microglia within a lesion, the NT and Iba1 positive cells were counted. Mature T cell were identified based on the positive CD3 staining. The cell composition within the lesion is shown as cell density, calculated as cell number normalized to the lesion area.

4 Results

4.1 In vivo imaging of axonal calcium levels and dynamics in vivo

In previous experiments my colleague Adrian-Minh Schumacher followed the fate of axons in healthy and EAE induced animals expressing the calcium sensor CerTNL15 in neurons. Due to the characteristics of the calcium sensor it is possible to measure the calcium concentration through ratiometric imaging. It was found that in healthy axon in non-EAE mice the intra-axonal calcium concentration is tightly controlled (*Figure 7*). In EAE lesions, more about one third (25.1 ± 6.8 %) of swollen axons (stage 1) show increased calcium levels. Interestingly, also normal appearing axons (stage 0) show increased intra-axonal calcium (8.3 ± 2.8 %).

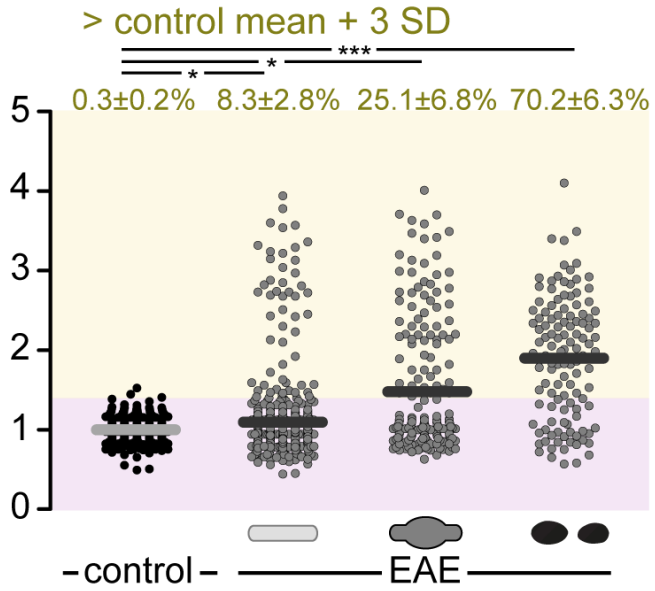

Figure 7. Axonal calcium levels in healthy axons and in axons in acute EAE lesions (Witte et al., submitted).

Distribution of cytosolic calcium levels of single axons in healthy and acute EAE mice, displayed by YFP/CFP channel ratios and normalized to the mean of control axons. Axons with intensity ratios +3 SD above the control mean (visualized as color-coded threshold) were defined as axons with elevated calcium. On the top: Percentages represent the number of axons with elevated $[Ca^{2+}]_{cyt}$,, shown as mean ± SEM, grouped in the different stages of degeneration (tested per animal in n=6 control and n=11 EAE mice, Kruskal-Wallis followed by one-sided Mann-Whitney U post-hoc tests). * p < 0.05 and *** p < 0.001.

To investigate whether calcium influences the probability of axons to degenerate, their changes in morphology and calcium levels in EAE lesions were followed over time. The observed transitions are summed up in *Figure 8*. Axons with higher calcium levels are more likely to swell (16 % vs. less than 1 %) and to fragment (19 % vs. 4 %), compared to axons with normal calcium levels. Recovery of axons from stage 1 was already observed in EAE lesions in earlier experiments (Nikić et al., 2011). Axons with lower calcium levels are more probable to recover than axons with high calcium levels (6 % vs. 3 %). These observations lead to the conclusion that calcium is likely to be involved in the degradation process of axons in acute EAE.

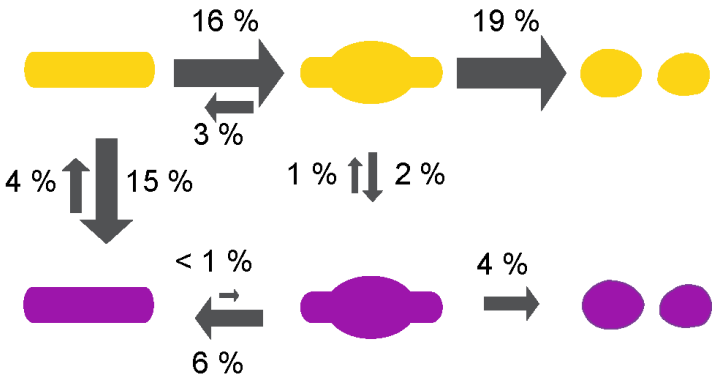

Figure 8. Diagram showing mean transition probabilities (per hour and axons).

Mean transition probabilities of axons between morphological changes per observed 'axon hour' in high $[Ca^{2+}]_{cyt}$ (yellow) and low $[Ca^{2+}]_{cyt}$ axons (magenta). Symbols represent FAD stages 0 (normal appearing), 1 (swollen) and 2 (fragmented). n=277 axons in 8 animals. Adapted from (Schumacher, 2016) and (Witte et al., 2018, submitted).

Before addressing this hypothesis with different transgenic lines or drug treatment, it was necessary to reproduce the results with control animals used in the following project, using the same surgical and imaging methods. I compared the axonal staging of 8 EAE animals used in the experiments that were performed by Adrian-Minh Schumacher (described above) with the distribution of axonal morphology of the EAE animals that I used as controls for this project (see *Figure 9A*). The axonal morphology was determined for a representable axon number within several lesions separately. The mean distributions across all lesions within one animal were displayed in the graph. There were no statistically significant differences observed using a chi-square test between the previous data set (stage 0: 64.18 ± 3.75 %, stage 1: 20.45 ± 3.36 %, stage 2: 15.45 ± 2.22 %) and the control data set that I obtained (stage 0: 59.89 ± 0.98 %, stage 1: 22.25 ± 1.57 %, stage 2: 17.85 ± 1.25 %).

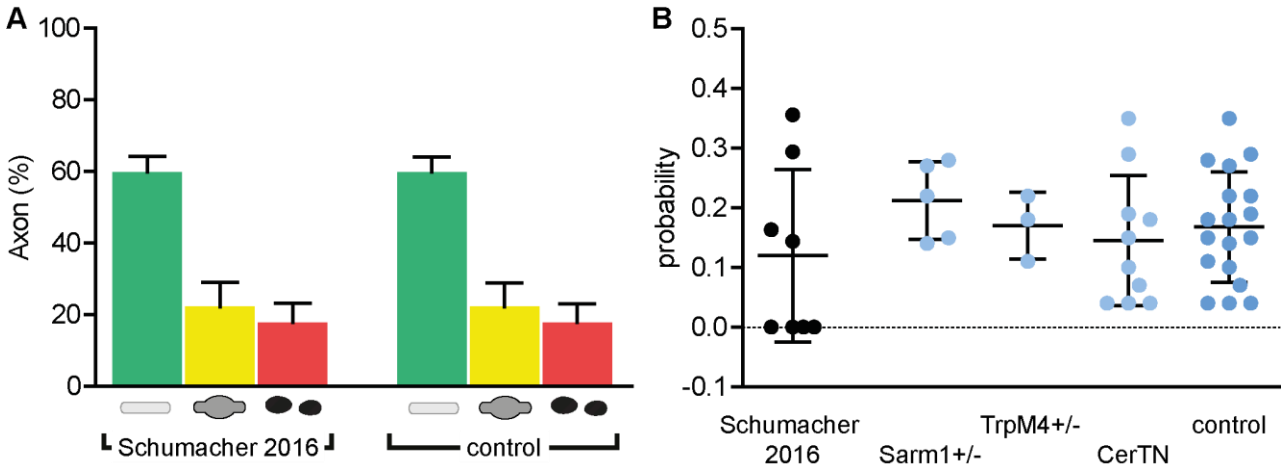

Figure 9. Previous experimental data on axonal morphology and fragmentation probabilities could be reproduced.

A) Comparison of the mean frequency (in % ± SEM) of axon stages in EAE lesions, as observed in previous experiments (n = 8, all CerTNL15) and in EAE animals used as control in this project (n = 17, n = 5 Sarm1+/- x CerTNL15, n = 3 TrpM4 +/- x CerTNL15 and n = 9 CerTNL15). There is no significant difference observable (chi-square test, p = 0.9807). B) Comparison of the fragmentation rates measured in previous experiments (n = 8, all CerTNL15) and measured in the control EAE animals used in this thesis (n = 18 control, n = 5 Sarm1+/- x CerTNL15, n = 3 TrpM4+/- x CerTNL15, and n = 10 CerTNL15). The cohort of all EAE control groups are pooled together as control. With a one-way ANOVA with adjusted p-value due to multiple comparisons there were no statistical significant differences between groups observable.

Next, I compared the fragmentation rates of axons with high calcium of each animal from the previous experiments and the control groups in my experiments, since in this thesis I am mainly focusing on the mechanisms that lead to axon degeneration in EAE (see *Figure 9B*). The transition rates have a large spread. The fragmentation rates observed by my colleague (0.120 ± 0.05) is not significant different from the fragmentation rates of all EAE animals that were used as control groups in the single experiments (0.168 ± 0.02). Comparing the single different transgenic lines with the previous results shows no significant difference as well (Sarm1+/-: 0.212 ± 0.03, TrpM4+/-: 0.170 ± 0.03, CerTNL15: 0.145 ± 0.03).

Herewith, I could reproduce the previous experimental data. Since F1 TrpM4+/- x CerTNL15 and Sarm1 +/- x CerTNL15 appear to be similar to F0 CerTNL15 animals, I can assume that the heterozygous deletion of Sarm1 and TrpM4 alleles in these mice has no observable influence and can be used in the following experiments as valid littermate control groups.

4.2 Wallerian-like degeneration pathways show no major contribution to neuroinflammatory axon degeneration *in vivo*

4.2.1 ΔNLS-Wld^S and Sarm1-/- protect against Wallerian degeneration

To have a readout for the calcium concentration we crossed the previously described lines of Sarm1-/- and ΔNLS-Wld^S with CerTNL15. For experiments the F1 generation that is positive for CerTNL15 as determined via PCR was used for experiments. As already mentioned, I used Sarm1+/- x CerTNL15 as control group for Sarm1-/- x CerTNL15. The control group for ΔNLS-Wld^S consisted of littermates negative for the ΔNLS-Wld^S gene, but positive for CerTNL15.

Before investigating the effect of these transgenic mouse lines in EAE, we performed a dorsal hemisection and assessed the extent of Wallerian degeneration to validate the protective capacity of Sarm1-/- and ΔNLS-Wld^S in the spinal axon population that we subsequently studied in EAE. The axonal morphology was assessed 3 mm rostral from the lesion site three days after the injury. Representative images of the dorsal hemisection lesion are shown in *Figure 10*.

The first 30 axons from the lesion border were classified by their morphology into fragmented and intact axons. Both healthy appearing and swollen axons were considered as intact axons. The results are displayed in *Figure 10*. In both control groups only 30 % remained intact, whereas most of the axons fragmented 3 days post injury (Sarm1+/-: intact – 32.11 ± 5.75, fragmented – 62.63 ± 36.48; CerTNL15: intact – 31.63 ± 3.90, fragmented: 68.5 ± 3.88). In the presence of the protective ΔNLS-Wld^S around 80 % of the axons survived the insult (ΔNLS: intact – 74.82 ± 1.948, fragmented – 25.06 ± 1.96). A similar result was observed in Sarm1-/- mice. 70 % of the axons remained intact (Sarm1-/-: intact – 70.46 ± 3.47, fragmented – 29.54 ± 3.47). The transgenic CerTNL15 mouse lines either lacking Sarm1 or overexpressing ΔNLS-Wld^S are therefore delaying Wallerian fragmentation in a spinal cord lesion model.

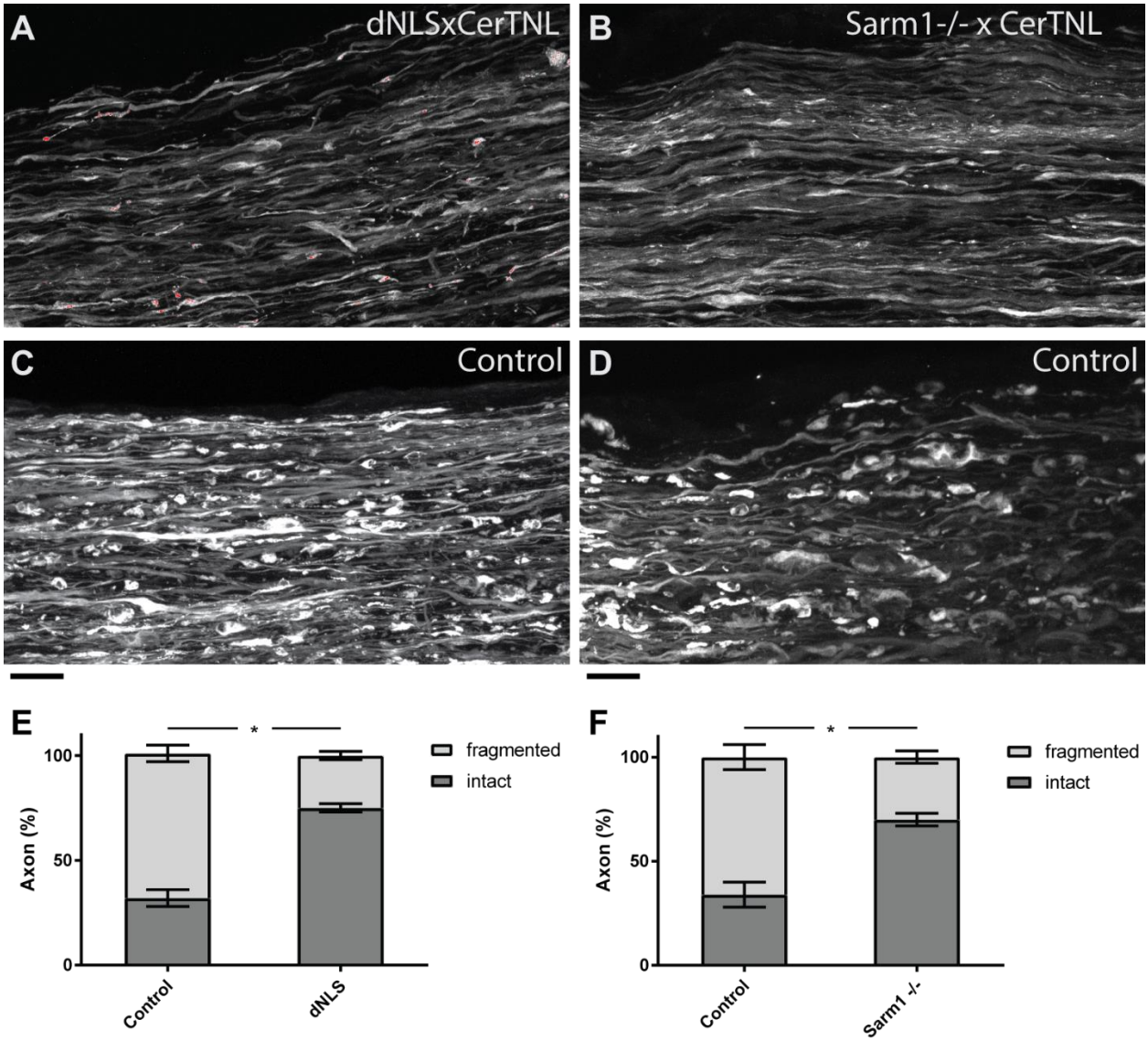

Figure 10. Positive control for Wallerian-like Degeneration

A – D) Representative confocal images of the cervical spinal cord of animals 3 days after dorsal hemisection. (A) ΔNLS-WldsxCerTNL15, B) Sarm1-/-xCerTNL15, C) CerTN D) Sarm1+/- x CerTNL15). The black scale bar represents 20 µm. E) Quantification of intact and fragmented axons 3 days after dorsal hemisection in ΔNLS-WldsxCerTNL15 and littermates CerTNL15 (mean ± S.D, n=3 for each group, one-way ANOVA with multiple comparisons p = 0.0456). F). Quantification of intact and fragmented axons 3 days after dorsal hemisections in Sarm1-/-xCerTNL15 animals and control littermates Sarm1+/-xCerTNL15 (mean ± S.D, n=3 for each group, one-way ANOVA with multiple comparisons p = 0.0237). Since all data groups passed the normality test according to Shapiro-Wilk the two-sided student's t test was used for statistical analysis, * p < 0.05.

4.2.2 ΔNLS-Wld^S and Sarm1 do not ameliorate clinical disease course of EAE

After I demonstrated that the used transgenic lines present indeed axonal protective features in a spinal cord injury model, I investigated whether the ΔNLS-Wld^S or Sarm1-/- modulate the pathogenesis of MOG-induced EAE.

After EAE induction mice were weight and scored daily. The clinical disease progression is visualized in the following diagrams.

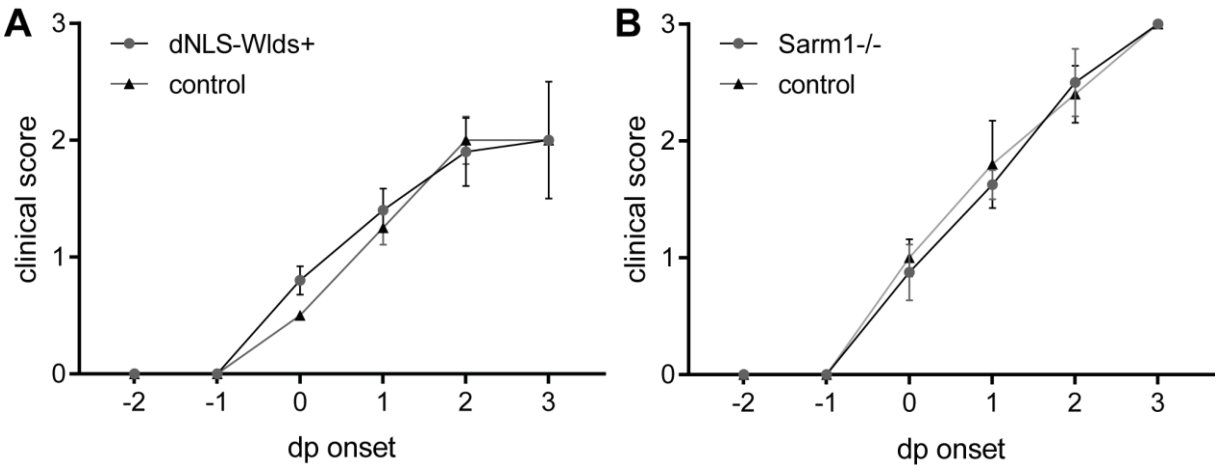

Figure 11. Acute clinical disease score of ΔNLS-Wld^S and Sarm1-/- mice

A) Clinical disease score assessed daily after immunization of ΔNLS-Wld^S (n = 15) and their wildtype littermates (n = 16), column p=0.5546. B) Clinical EAE score assessed daily after immunization of Sarm1-/- x Thy1YFP (n = 10) and littermates Sarm1+/- xThy1YFP mice (n = 10), p=0.9320. In both disease scores no significant difference was observable, as assessed by repeated measures two-way ANOVA.

ΔNLS-Wld^{S}xCerTNL15 mice did not show a significant difference in their disease onset and at acute EAE compared to their CerTNL15 positive littermates negative for ΔNLS.

There is as well no significant difference observable between Sarm1-/- and control mice, in the acute phase and in the chronic phase (data not shown). It has to be noted, that the animals in the Wld^S group appeared less sick than the Sarm1 animals. Both groups were bred and housed in a different environment, which might have had an influence in the disease severity.

4.2.3 Immune cell infiltration and axonal morphology is unchanged in chronic EAE lesions of Sarm1-/- mice

Although we did not observe any differences in the clinical progression of EAE, we tested for differences in the lesion load in the chronic phase and differences in axonal morphology in chronic lesions of Sarm1-/- group.

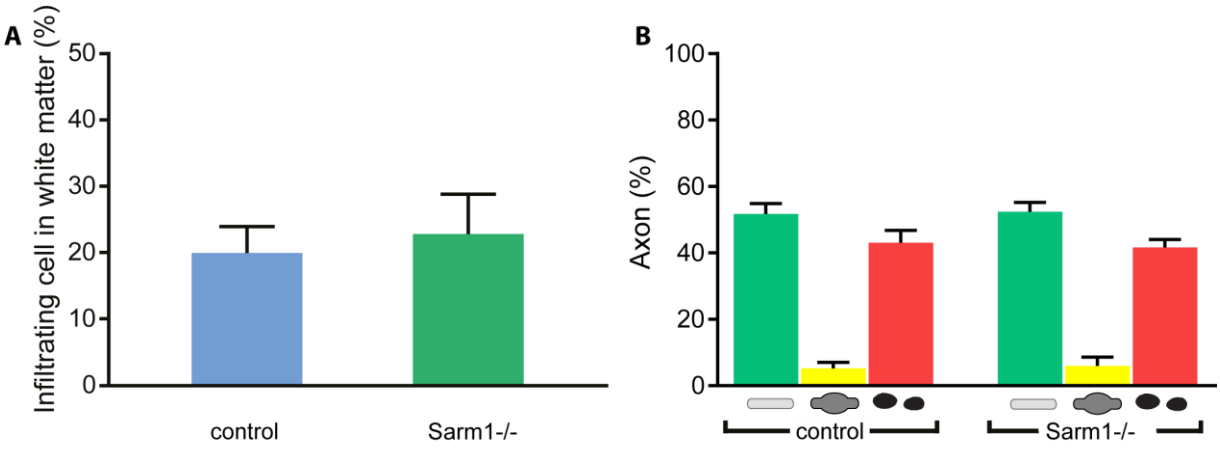

Figure 12. Infiltrations spread and axonal staging in chronic lesions.

A) Lesion load measured as area occupied by infiltrating cells in the white matter, displayed as percentage mean ± SEM (n = 5 Sarm1-/-; n = 5 Sarm1+/-, control). Since both data groups passed the normality test according to Shapiro-Wilk the two-sided, unpaired student's t test was used for statistical analysis. No statistical difference was observable, p=0.6967. B) Distribution of axonal morphology within older lesions 32 days after EAE induction (n = 11 Sarm1-/-, n = 9 Sarm1+/-). Data sets passed the normality test according Shaphiro-Wilk. There was no statistical difference observable using chi-square test (χ^2=0.6618, p=0.7183).

To assess the lesion load we measured the occupancy of infiltrating cells within the white matter in Sarm1-/- x Thy1YFP tissue and in the control groups Sarm1+/- x Thy1YFP that were sacrificed 32 days after EAE induction. As *Figure 12* shows there is no significant difference between the control (19.95 ± 4.02 %) and the Sarm1-/- group (22.84 ± 5.91 %).

The axonal distribution within chronic EAE lesions (32 days after EAE induction) was comparable between Sarm1-/- mice and their control group.

4.2.4 Axon degeneration stages are unaltered in acute EAE lesions in ΔNLS-Wld^S and Sarm1-/- mice

In the acute phase 2-3 days after onset of EAE symptoms, the disability of mice reaches its peak. I characterized the distribution of axonal damage stages in the lumbar spinal cord within acute lesions to be able to see if delaying Wallerian-like degeneration has an effect on axonal degeneration. *Figure 13* displays the results from this characterization.

In the Sarm1-/- group there is no difference in appearance of normal appearing (stage 0) axons (Sarm1-/-: 61.28 ± 1.77 % vs Sarm1+/-: 59.89 ± 1.43 %), swollen (stage 1) axons (Sarm1-/-: 20.71 ± 2.92 % vs Sarm1+/-: 22.25 ± 2.29 %) or fragmented (stage 2) axons (Sarm1-/-: 18.01 ± 2.43 % vs Sarm1+/-: 17.85 ± 1.82 %). The same is observed in the ΔNLS-Wld^S group (ΔNLS: 65.58 ± 2.31 % vs CerTNL15: 60.88 ± 2.71 % for stage 0 axons, ΔNLS: 22.16 ± 2.02 % vs CerTNL15: 23.42 ± 2.08 % for stage 1 axons and ΔNLS: 11.26 ± 1.80 % vs CerTNL15: 14.45 ± 1.71 % for stage 2 axons). This suggests that the presence of ΔNLS+ has not an axonprotective effect in acute EAE lesions, at least on the morphological level.

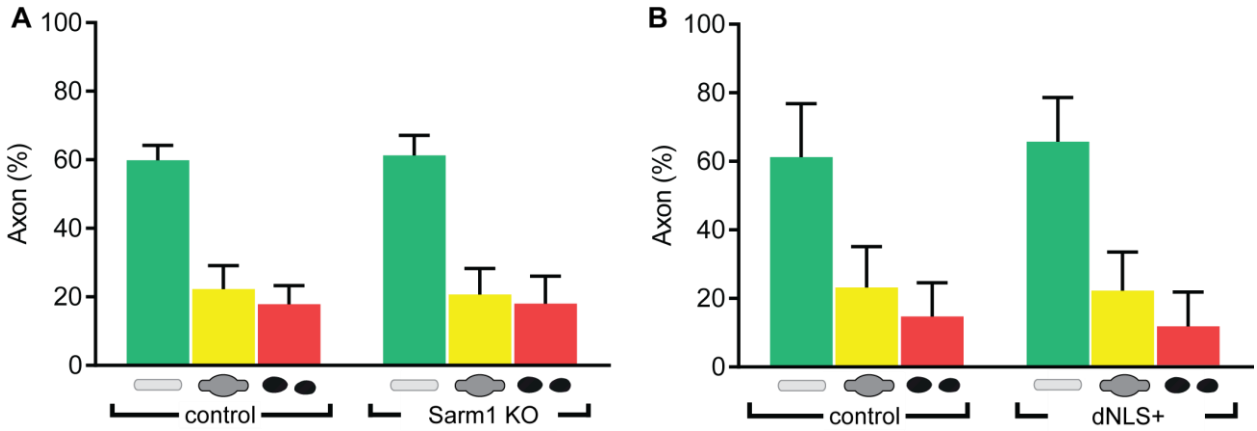

Figure 13. Axonal damage in acute EAE lesions in Sarm1-/- and ΔNLS-Wld^S animals.

A) Distribution of axonal damage stages at onset+2 or onset+3 (acute EAE) in Sarm1-/- x CerTNL15 (n = 10) and their littermate control Sarm1+/- x CerTNL15 (n = 8) (χ^2=0.7532, p=0.6826). B) Distribution of axonal morphology in axons in acute EAE lesions in ΔNLS x CerTNL15 (n = 9) and ΔNLS negative CerTNL15 (n = 7). The distribution of axon stages is not significantly different (chi-square test χ^2 = 0.162, p = 0.9222).

4.2.5 ΔNLS-Wld^S and Sarm1-/- do not alter intra-axonal calcium concentrations *in vivo*

To address, whether Wallerian-like degeneration could influence the calcium regulation within axons in EAE, I measured the YFP/CFP ratios of axons that I identified for axonal staging and grouped them according to their stages. As a robust detection of elevated calcium levels, I defined the cut-off value for YFP/CFP ratios based on the mean +3SD of the ratios measured in control animals. In previous experiments it was observed that around 16 % of the healthy appearing axons have increased intra-axonal calcium levels, even a higher percentage of swollen axons (about 50 %) show an increase in calcium. This I can observe as well in Sarm1 and ΔNLS groups. 10.02 ± 4.076 % stage 0 axons in Sarm1-/- mice and 17.9 ± 6.043 % stage 0 axons in Sarm1+/- mice have calcium levels above the cut-off (normalized to healthy control animals, population means ± SEM: Sarm1-/-: 1.01 ± 0.01 vs Sarm1+/-: 1.21 ± 0.01). One third (31.09 ± 7.439 % for Sarm1-/- and 36.91 ± 8.97 % for Sarm1+/-) of swollen axons in these mice are classified as calcium high axons (population means ± SEM: Sarm1-/-: 1.21 ± 0.03 vs Sarm1+/-: 1.38 ± 0.03). About two third (67.27 ± 7.53 % for Sarm1-/- and 69.35 ± 4.83 % for Sarm1+/-) of stage 2 axons have increased calcium levels (population means ± SEM: Sarm1-/-: 1.38 ± 0.04 vs Sarm1+/-: 1.68 ± 0.06). Using Shapiro-Wilk test I found that the data sets were not normally distributed. Therefore, I used the Mann-Whitney test with Bonferroni-Dunn post hoc adjustment of p-value to find that there is no significant difference observed in in healthy Sarm1-/- and Sarm1+/- animals regarding intra-axonal concentrations. Nevertheless, it needs to be noted that in EAE Sarm1-/- animals the intra-axonal levels are less increased as compared to EAE Sarm1+/- animals.

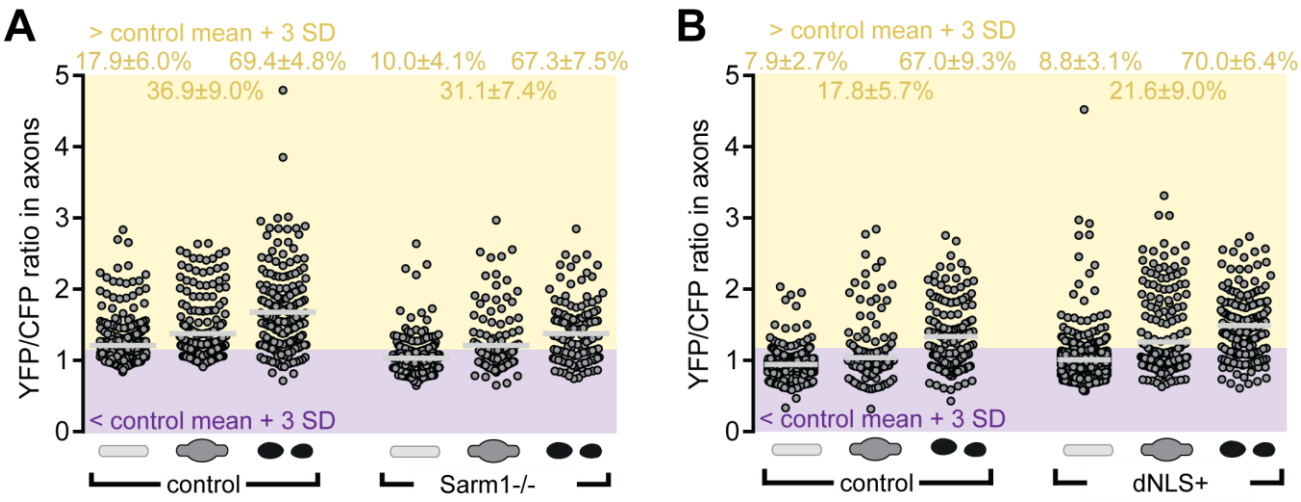

Figure 14: Distribution of calcium levels in axons in acute EAE lesions in Sarm1-/-and ΔNLS-Wld^S mice.

A) Distribution of intra-axonal calcium concentration measured as YFP/CFP ratio at beginning of 2PM imaging in Sarm1-/- and control Sarm1+/- mice (Sarm1-/- n = 4, Sarm1+/- n = 9). B) Distribution of cytosolic calcium concentration at beginning of 2PM imaging in ΔNLS+ and control mice (ΔNLS+ n = 9, ΔNLS- n = 7). No statistically significant difference was observed using Mann-Whitney U test following Bonferroni-Dunn post-hoc correction.

The distribution of intra-axonal calcium concentration in axons of ΔNLS+ animals behaves similar. The mean intra-axonal calcium concentration rises with the damage, but it is not significantly different between ΔNLS and control group after using Bonferroni-Dunn corrected Mann-Whitney test as normal distribution of data could not be confirmed using Shapiro-Wilk test: The mean cytosolic calcium levels are very similar between both groups: ΔNLS+: 1.0 ± 0.01, n = 864 vs CerTNL15: 0.97 ± 0.01, n = 674 for stage 0 axons; ΔNLS+: 1.28 ± 0.03, n = 244 vs CerTNL15: 1.07 ± 0.02, n = 228 for stage 1 axons and ΔNLS+: 1.51 ± 0.03, n = 171 vs CerTNL15: 1.36 ± 0.04, n = 165 for stage 2 axons. As well the fraction of calcium high axons is very comparably within lesions of ΔNLS+ and ΔNLS- animals. In ΔNLS+ mice 8.8 ± 3.1 % of stage 0 axons are classified as high calcium axons and about the same fraction (7.9 ± 2.7 %) of stage 0 axons have elevated calcium levels in the control group. 21.6 ± 9.0 % of stage 1 axons in ΔNLS+ mice and 17.8 ± 5.7 % of stage 1 axons in control mice are elevated in calcium, whereas again about two thirds of stage 2 axons are categorized as high calcium in both groups (ΔNLS+: 67.0 ± 9.3 % and ΔNLS-: 70.0 ± 6.4 %).

4.3 The effects of TrpM4-/- on EAE needs further investigation

4.3.1 TrpM4-/- has no effect on clinical disease course

To assess, whether genetical depletion of the TRPM4 channel alters clinical disease course of EAE, we monitored TrpM4-/- and their control group TrpM4+/- mice daily for 35 days after immunization. The clinical course of these mice is shown in figure 15. There is no significant difference observable between TrpM4-/- and control, neither in the acute phase directly after disease onset, nor in the chronic phase of the disease.

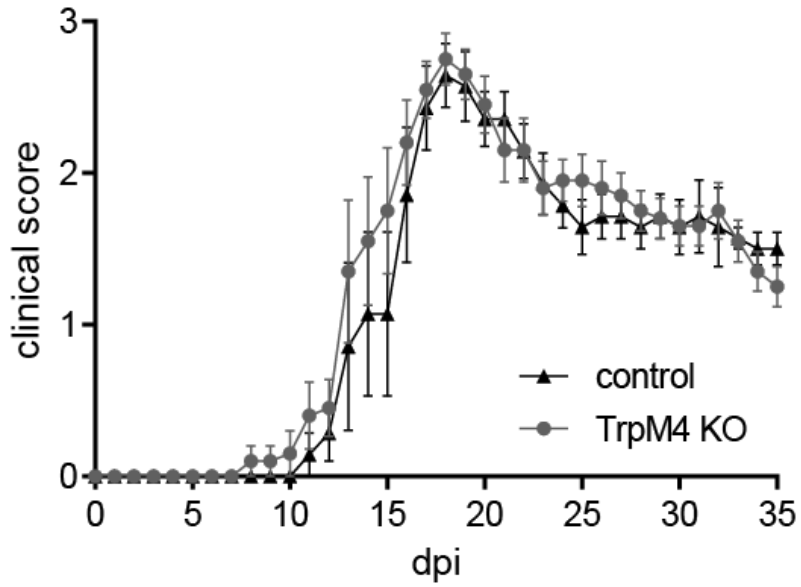

Figure 15. Clinical EAE progression in TrpM4-/- x CerTN and TrpM4+/- x CerTN mice.

The animals were scored daily from the day of immunization over 35 days. There is no significant difference observable between TrpM4-/- (n = 10) and their littermate controls (TrpM4+/-, n = 10), tested with a two-way ANOVA with a multiple measures p value adjustment, p=0.5196).

4.3.2 The influence of TrpM4 on axon degeneration in EAE requires further study

We used our *in vivo* imaging approach to assess axon damage stages and intra-axonal calcium levels in acute EAE lesions in TrpM4-/- animals. Again, only mice with a clinical score higher than 2 were selected. As already described previously, we characterized the axons within the EAE lesions regarding their morphology and calculated the calcium ratios. The results are displayed in *Figure 15*.

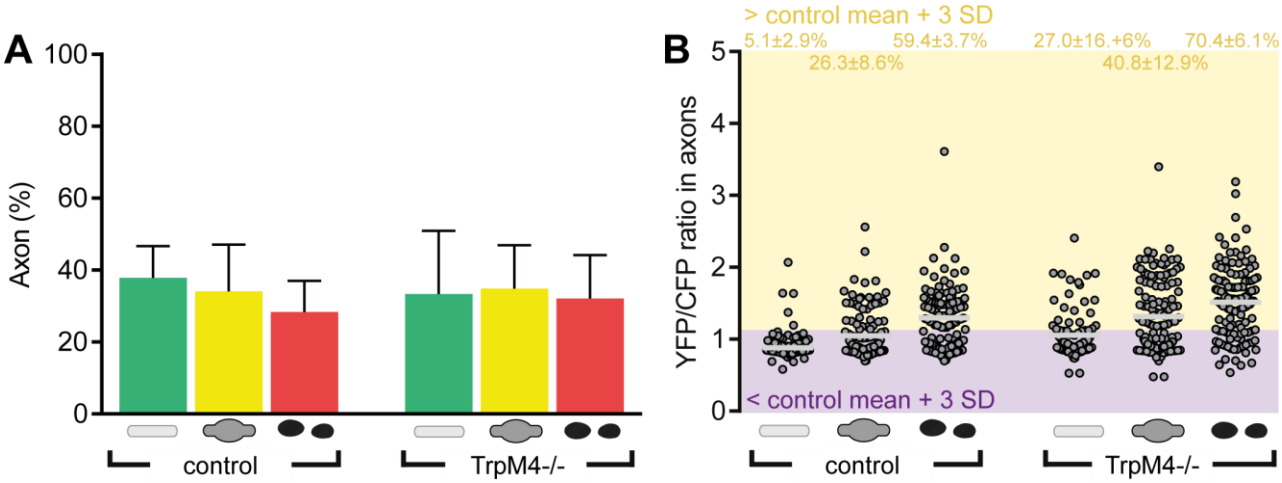

Figure 16. Axonal morphology and calcium distribution in TrpM4-/- and controls

A) Distribution of axonal stages within an animal in acute EAE in TrpM4+/- x CerTNL15 (n = 5) and TrpM4-/-xCerTNL15 (n = 5) animals. B) Distribution of intra-axonal calcium concentration within an acute EAE lesion in TrpM4+/- x CerTNL15 (n = 5) and TrpM4-/-xCerTNL15 (n = 5). Mann-Whitney test with Bonferroni-Dunn correction showed that the differences are not statistically significant.

The overall distribution of axonal morphology in both groups differs compared to previous data sets. Here I took a different approach and evaluated 80 axons in total for each animal. In case the 80 could not be reached in one lesion, it was filled up with axons from another lesion. The lack of the TrpM4 appears to have no influence on the axonal morphology in the EAE lesion. The distributions of intact (TrpM4-/-: 33.75 ± 6.9 % vs TrpM4+/-: 37.25 ± 5.6 %), swollen (TrpM4-/-: 35.25 ± 5.8 % vs TrpM4+/-: 33.5 ± 5.4 %) or fragmented axons (TrpM4-/-: 31 ± 6.1 % vs TrpM4+/-: 29.25 ± 3.0 %) are similar, independent if TrpM4 is present or not.

The intraaxonal calcium levels, on the other hand, are elevated in the TrpM4-/- group throughout all stages, but this observation is statistically not significant (Bonferroni-Dunn corrected Mann Whitney test as normal distribution could not be confirmed using Shapiro-Wilk test). The means (mean ± SEM) of intra-axonal calcium concentration for the control TrpM4+/- animals are 0.90 ± 0.01 (stage 0), 1.06 ± 0.03 (stage 1) and 1.31 ± 0.04 (stage 2). In TrpM4-/- animals I measured the following means: stage 0 – 1.07 ± 0.05, stage 1 – 1.33 ± 0.06 and stage

2 – 1.53 ± 0.04 (mean ± SEM.). All means are normalized to the intra-axonal concentration measured in healthy TrpM4+/- or TrpM4-/- animals.

In addition, we were interested in the influence of TrpM4 on the fragmentation and swelling rates. Therefore, we followed axons and their fate over 4 hours of imaging, as described in section 3.3.6.2. The calculated transition rates are summarized in *Figure 16*. Since applying the strict evaluation criteria would leave us with only low animal numbers, I show here animals in which I could follow at least 15 high calcium axons in the 4 hour time window, being confronted with increased variability in the data sets.

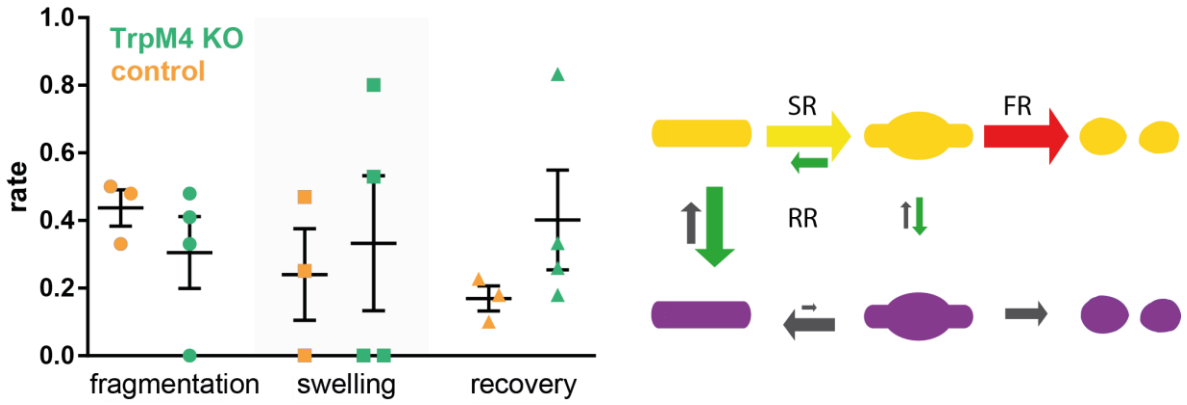

Figure 17. Axonal dynamics over 4 h in EAE TrpM4 animals and their control

Overview of calculated transition rates during 4 hours of imaging, displayed as events/hour (TrpM4-/- n = 4, TrpM4+/- n = 3). Since data values are normally distributed (Shapiro-Wilk) two-sided, unpaired student's t test was used to assess statistical differences between groups.

Both fragmentation rates for TrpM4-/- (0.31 ± 0.11) and TrpM4+/- (0.43 ± 0.05) are in the same range. The same is true for the swelling rate (TrpM4-/-: 0.33 0.20 vs TrpM4+/-: 0.24 ± 0.14). Although, there is a tendency for higher recovery rates in the TrpM4-/- group (0.40 ± 0.15) compared to the TrpM4+/- group (0.17 ± 0.04), this difference is not statistically significant (unpaired two-tailed t test, p = 0.2464). These are only preliminary data. Unfortunately, we were dependent on harsh evaluation criteria to obtain reliable dynamic rates and therefore, our group sizes were reduced to only 2 animals for each group. Furthermore, I pooled all possible recovery processes together, because of the low numbers of transitions I could observe during imaging. Therefore, more experimental data need to be added to be able to draw conclusions.

4.4 Inhibition of calpain ameliorates neurodegeneration in EAE lesions

4.4.1 Inhibition of calpain results in decreased fragmentation rates in acute EAE

In neurodegenerative disease, calpain is found to be overexpressed and several studies have used calpain inhibition to improve disease outcome after EAE induction (Fà et al., 2016; Guyton et al., 2005; Hassen et al., 2006; Kling et al., 2017; Machado et al., 2015; Nixon et al., 1994). Williams et al. showed that using calpain inhibitor III rescues the axons from fragmentation after traumatic injury (Williams et al., 2014). To test whether calpain inhibition exhibits a beneficial effect on axon survival in acute EAE, we treated mice with a score of 2.5 and higher during imaging with a calpain inhibitor. The exact treatment procedure is described in chapter 3.3.5.

Beforehand, we characterized the EAE lesion of the groups that were treated with either CI3 or vehicle regarding their axonal stage distribution and calcium levels (as previously described). As *Figure 18(A)* and *18(B)* indicate, lesions were comparable between groups before treatment start concerning calcium levels and axonal damage.

The axonal staging is based on the first 80 axons that were found in lesions in an animal before treatment. Stage 0 axons appeared in the vehicle group (42.36 ± 2.0 %) with the same frequency as in the CI3 treated group (44.63 ± 2.7 %). There is as well no significant difference observable in the distribution of swollen axons (vehicle: 31.94 ± 3.1 % vs CI3: 33.13 ± 2.8 %). The distribution of fragmented axons is similar in vehicle (25.69 ± 2.3 %) and in CI3 group (22.25 ± 1.7 %).

Both groups are very comparable regarding the density of infiltrating cells that were visualized within the imaged lesion area in vivo with Neurotrace. Although the CI3 group tends to have higher cell densities, there is no significant difference between vehicle treated group (2527 ± 248 nuclei/mm²) and CI3 treated group (3171 ± 290 nuclei/mm²).

I measured the YFP/CFP ratios of these axons in untreated lesions and grouped them according to their axonal stage. The mean calcium levels of normal appearing axons in both groups is comparable (vehicle: 1.02 ± 0.01, 304 axons vs CI3: 1.09 ± 0.01, 400 axons). The average calcium level is increased in swollen axons in both groups (vehicle: 1.20 ± 0.03, 228 axons vs CI3: 1.24 ± 0.03, 286 axons). The calcium concentrations of fragmented axons are comparable as well (vehicle: 1.47 ± 0.04, 180 axons vs CI3: 1.38 ± 0,03, 194 axons). I could not detect a significant difference with Bonferroni-Dunn corrected Mann-Whitney U test between CI3 treated and vehicle treated group regarding the percentage of detected fraction of calcium high axons. There were 27.39 ± 7.86 % of stage 0, calcium high axons in CI3 treated mice, whereas in vehicle treated mice I detected 17.07 ± 5.07 % of stage 0, high calcium axons. Even a higher percentage of high calcium axons were observed in swollen axons: for the CI3 group

about half of the axons were increased in intracellular calcium (50.77 ± 6.93), for the vehicle group 43.21 ± 5.40 %. Two third of stage 2 axons showed increased cytosolic calcium (CI3 group: 72.47 ± 5.13 %; vehicle group: 64.85 ± 7.08 %).

The transitions were determined as determined in previous sections and are depicted in *Figure 18)*. The transition rates are based on images obtain from lesions during treatment Although the recovery (vehicle: 0.21 ± 0.04 vs CI3: 0.30 ± 0.04) and the swelling rates (vehicle: 0.25 ± 0.05 vs CI3: 0.23 ± 0.05) were not affected by the CI3 treatment, the fragmentation rate of the CI3 treated groups was significantly reduced (0.25 ± 0.04) compared to the control group (0.40 ± 0.07). The fragmentation rate of the control group (0.48 ± 0.05), on the other hand, lied in the same range as the calculated fragmentation rates of the control populations used in the previous experiments, namely TrpM4+/- and Sarm1+/- (see *Figure 9(B)*).

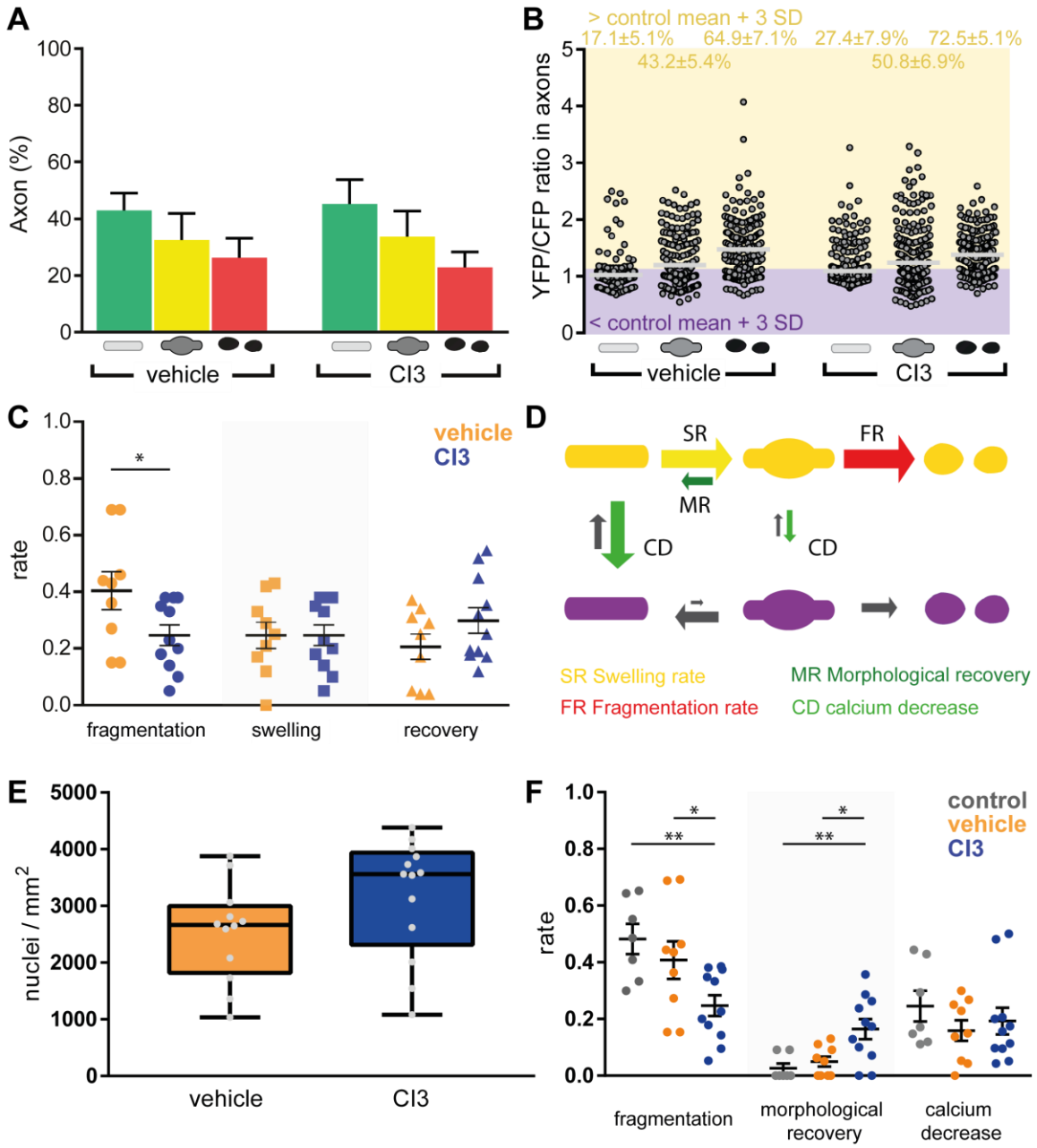

Figure 18. Overview of acute Calpain inhibition.

A+B) Group Equivalence before treatment start: A) Distribution of axonal stages in acute EAE lesions in vivo of vehicle (n = 9) and CI3 treated animals (n = 11) before treatment. Using chi-square test no statistical difference could be observed. B) Distribution of intra-axonal calcium concentration before treatment (vehicle n = 9, CI3 n = 11). No statistical difference between groups could be observed using Bonferroni-Dunn corrected Mann-Whitney U test.

C-F) After treatment: C) Overview of calculated transition rates during 4 hours of imaging and treatment, displayed as events/hour (vehicle n = 9, CI3 n = 11). Since data values are normally distributed (Shapiro-Wilk) two-sided unpaired student's t test was used to assess statistical differences between groups. * $p < 0.05$. D) Overview of possible transitions. Of particular interest are the transitions of axons with high cytosolic calcium: swelling (SR) and fragmentation (FR). Recovery events can be differentiated in morphological recovery (MR) or calcium decrease (CD). E) Densities of infiltrating cells within the imaged lesion site in vivo of vehicle (n = 9) and CI3 treated animals (n = 11) at first imaging time point. F) The dynamic rates of vehicle and the CI3 treated groups were compared to the calculated rates of the control animals used in the previous experiments (TrpM4Het and Sarm1Het). After a Shapiro-Wilk test it can be assumed that all data sets are normally distributed. For statistical analysis we used two-way ANOVA. * $p < 0.05$, ** $p < 0.005$.

Interestingly, the decrease in fragmentation events in presence of CI3 was reflected in the increase of morphological recovery (see *Figure 18(F)*). As mentioned above, there are several recovery processes possible. The sole morphological recovery of swollen axons to normal appearing axons without a change in intra-axonal calcium concentration was increased significantly under CI3 treatment (CI3-MR: 0.16 ± 0.04), whereas it remained low in the vehicle treated groups (veh-MR: 0.05 ± 0.02), similar like the morphological dynamic rates of the control population (control-MR: 0.03 ± 0.02). The rate of calcium decrease was in contrast not affected by the treatment. The rates of calcium decrease of CI3 treated group (CI3-CD: 0.19 ± 0.05) and vehicle treated group (veh-CD: 0.16 ± 0.04) were in the same range as of the control populations (control-CD: 0.25 ± 0.05).

4.4.2 Composition of infiltrating immunes cells in calpain inhibitor treated animal in acute EAE is unchanged

Since calpain was inhibited with a pharmaceutical drug, we cannot exclude that the drug also has effects on the infiltrating immune cells that could lead to secondary neuroprotection. To address this question, we used the dorsal segments of the lumbar spinal cord that was used for imaging and investigated those for lesion load and composition of infiltrating immune cells.

The lesion load was determined as percentage of area within the white matter that is infiltrated with Neurotrace positive cells. In *Figure 19(B)* the values are represented as the mean ± SEM. There is not a significant difference detectable between the CI3 treated (38.33 ± 5.82 %) and the vehicle treated group (30.43 ± 4.31 %).

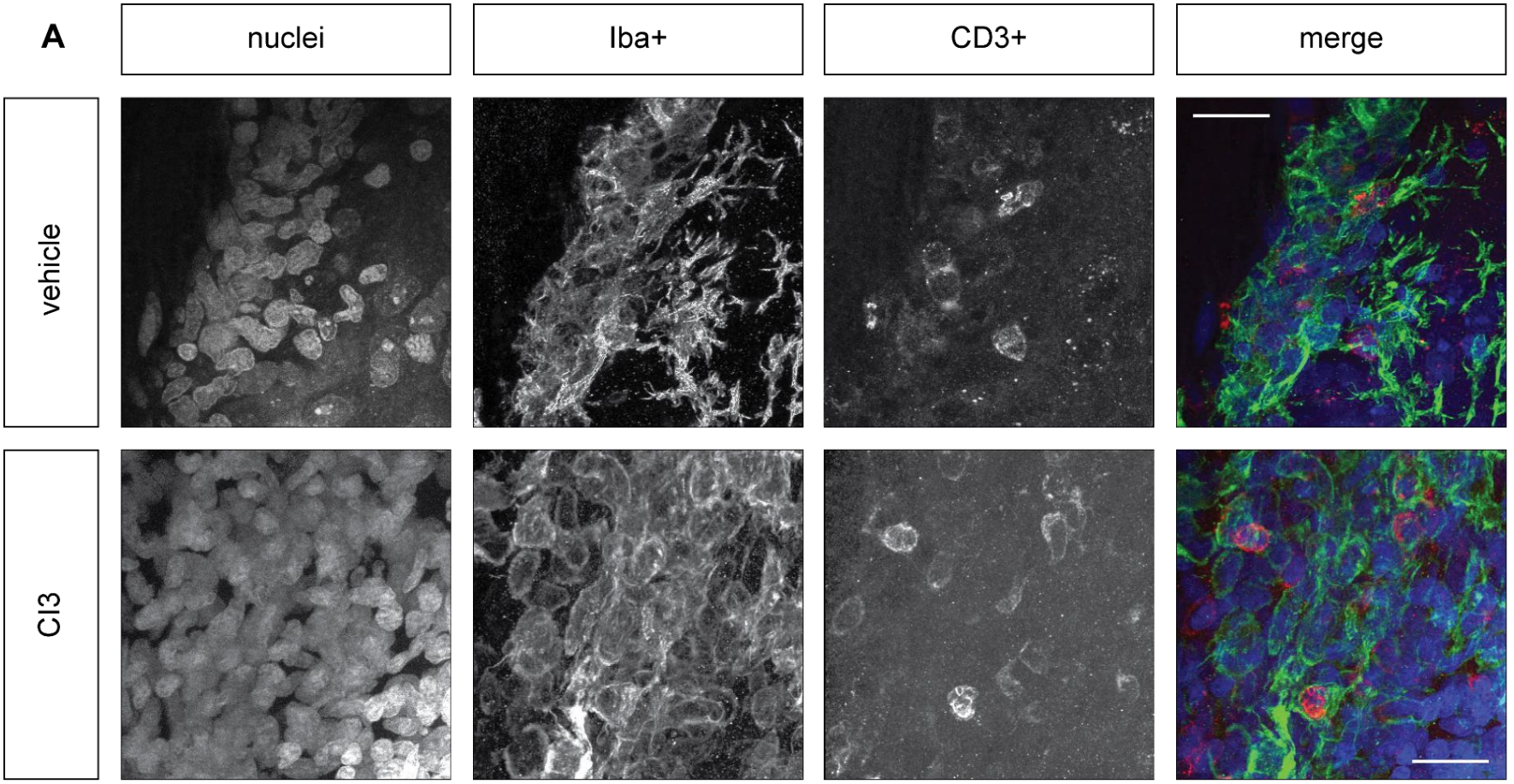
A
nuclei
Iba+
CD3+
merge
vehicle
CI3

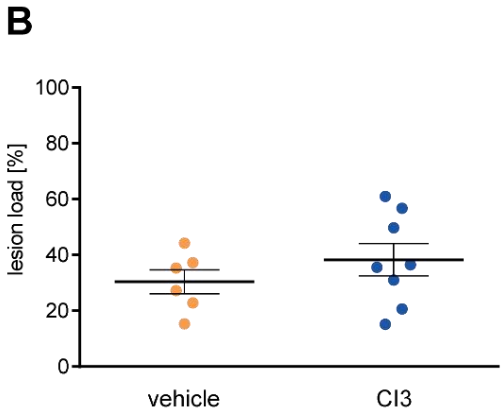
B
lesion load [%]
100
80
60
40
20
0
vehicle
CI3

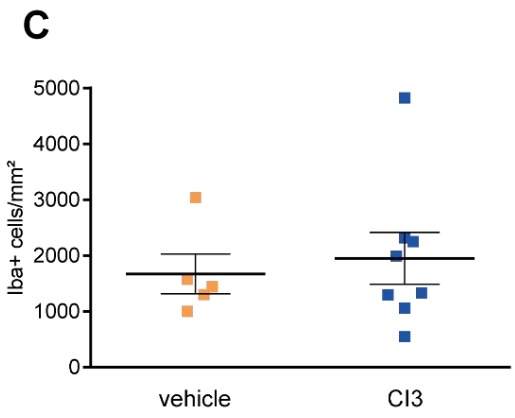
C
Iba+ cells/mm²
5000
4000
3000
2000
1000
0
vehicle
CI3

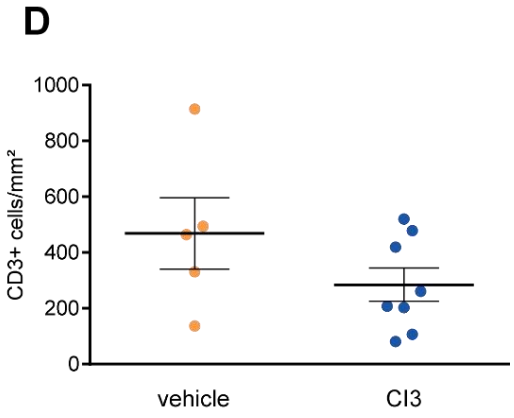
D
CD3+ cells/mm²
1000
800
600
400
200
0
vehicle
CI3

Figure 19 (previous page). Distribution of CD3+ and Iba+ cells within acute EAE lesions in animals acutely treated with Calpain inhibitor

A) Representative images of nuclei infiltration (stained with Neurotrace640/669), T cells (CD3+ staining) and microglia (Iba1+ staining) within acute lesions of imaged animals that were treated either with CI3 or with vehicle. B) Lesion load as fraction of area occupied by infiltrating cells within the white matter (vehicle: n = 6, CI3: n = 8). C) Density of Iba positive cell within an EAE lesion in number/mm^2 (vehicle: n = 5, CI3: n = 8). D) Density of CD3 positive cells within an EAE lesion in number/mm^2 (vehicle: n = 5, CI3: n = 8). No statistical difference was detected using two-sided student's t test after confirming normal distribution using Shapiro-Wilk test.

Through immunohistochemistry we analyzed the infiltration density of CD3 positive T cells and Iba1 positive microglia within the lesions. The results from the quantification are summarized in *Figure 19(C)* and *19(D)*. The mean density of Iba1 positive cells in vehicle treated animals is 1671 ± 356 cells/mm^2, comparable to the mean density of Iba1 positive cells observed in CI3 treated animals (1949 ± 464 cells/mm^2). The density of CD3 positive cells in vehicle treated animals (468 ± 128 cells/mm^2) is not significantly different from the density observed in CI3 treated animals (285 ± 59 cells/mm^2). Since there was no significant difference visible, it is likely that calpain inhibition does not affect the fragmentation rate via immunomodulatory mechanisms. After applying Shapiro-Wilk test it can be assumed that all data sets are normally distributed. Therefore, I applied the two-sided unpaired student's t test for statistical analysis.

4.4.3 Long term treatment with calpain inhibitor does not ameliorate disease progression

To determine if a long-term treatment with CI3 would ameliorate the clinical disease progression, we implanted osmotic pumps that allowed a continuous treatment for 7d intrathecally. C57/Bl6 mice were immunized with MOG and their disease development was observed daily. Mice that showed their first clinical symptoms (onset of EAE) were randomly assigned a pump filled either with CI3 or vehicle. The pump was implanted one day after onset and left one week for treatment. The overall clinical course is shown in *Figure 20(B)*.

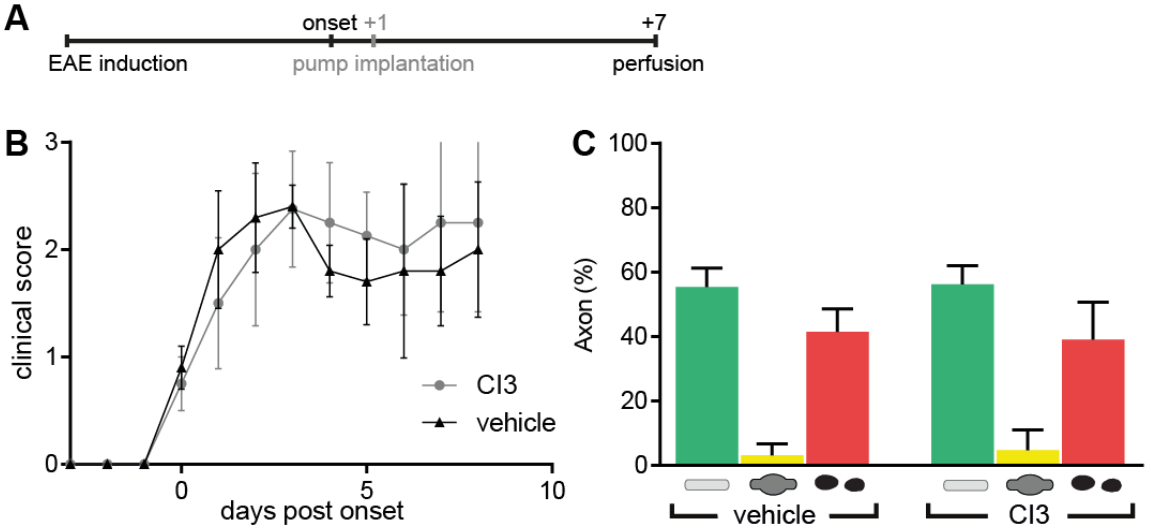

Figure 20. Long-term treatment with calpain inhibitor: EAE disease course and axonal morphology

A) Experimental timeline. One day after EAE onset animals were implanted randomly with either with vehicle or CI3 filled osmotic pumps. B) Clinical disease course is not influenced by long-term treatment with CI3 (vehicle: n = 4, CI3: n = 5; 2way ANOVA, p=0.7815). C) Distribution of axonal stages within EAE lesions 7 days after treatment (vehicle: n = 4, CI3: n = 5).

Since we were not able to observe a reduced disease severity due to treatment with CI3, we investigated the EAE lesions from these mice for axonal damage within lesion. The results are displayed in *Figure 20(C)*. Although we observed an effect of calpain inhibition in acute EAE in vivo, there were no changes detectable after long term treatment with CI3 with an osmotic pump. The distribution of normal appearing axons in the vehicle group (55.39 ± 2.62 %) is very similar as observed in the CI3 treated group (56.19 ± 2.92 %). I observed in both groups similar numbers of swollen axons (vehicle: 3.13 ± 1.61 % vs. CI3: 4.74 ± 3.15 %) and fragmented axons (vehicle: 39.07 ± 5.81 % vs. CI3: 41.47 ± 3.21 %). No statistical significant difference could be detected using chi-square test (χ^2=0.303, p=0.8594).

5 Discussion

5.1 Key findings

Axonal degeneration critically determines the long-term consequences of neuroinflammatory lesions. In previous works, it was already shown that *in vivo* imaging is an excellent tool to study axonal degeneration during neuroinflammation (Kerschensteiner et al., 2005; Nikić et al., 2011; Sorbara et al., 2012). These studies revealed that axons in experimental and human neuroinflammatory lesions undergo focal axonal degeneration and identified the intraaxonal accumulation of calcium as a key determinant of axonal fate. In this study, I examined by *in vivo* 2 photon imaging how dysregulated calcium levels could trigger axonal dysfunction and subsequent fragmentation. I identified a potential therapeutic target within this neurodegenerative mechanism. Based on the results that I obtained in this thesis the following conclusions can be drawn:

- Wallerian degeneration-like pathway appears not to be involved in the axonal fragmentation process in acute EAE lesions. Neither the lack of Sarm1 nor the presence of the Wld^S protein could prevent focal axonal degeneration in EAE lesions, although they did effectively limit Wallerian degeneration after axon transection in the same axon population. As a result, neither genetic manipulation affected the acute or chronic course of EAE.
- Axonal fragmentation can be reduced *in vivo* in acute EAE by inhibition of calpain, a calcium activated non-lysosomal protease. This treatment did not affect immune cell infiltration in the studied acute EAE lesions. This suggests that calpain inhibition could act as an axonprotective mechanism in neuroinflammatory lesions. Although we have yet to identify a suitable therapeutic application protocol that results in long term axonal protection.

5.2 Using *in vivo* imaging to study the mechanisms involved in axonal degeneration in an animal model of MS

In this work, I collected data for the most part by using a two-photon laser scanning microscope in living transgenic mouse lines that expressed a FRET-based calcium sensor in a large subset of their neurons. *In vivo* multiphoton imaging has been succeeding as an experimental paradigm, with its advantages of imaging in a living organism under mostly intact and physiological conditions. Using multiphoton imaging, we gain insights in dynamic processes in deeper layers of the CNS. However, there are the risks of non-linear toxicity and tissue damage by linear heating. These potential problems can be reduced by adjusting laser power, imaging duration and repeats.

In our lab, we established the calcium measurement with Thy1-CerTNL15 transgenic mouse strain that showed a stable expression of the sensor CerTNL15 driven in a large subset of neurons already around birth (Heim et al., 2007). The two fluorophores Cerulean and Citrine are linked through a sequence of fast chicken skeletal muscle troponin C, that allows FRET after a conformational change induced by calcium binding. The skeletal muscle protein Troponin was chosen because no other function is known besides being involved in skeletal muscle contraction. With this choice of linker, the sensor does not interfere with endogenous cell mechanisms and the sensor itself is not uncontrollably modified by cellular interaction, thereby minimizing the risk of false positive intensity change (Direnberger et al., 2012). My colleague Minh Schumacher could exclude that the sensors function was diminished by pH change that occurs in tissue acidosis or by direct oxidation via ROS/RNS; both are common in immune-mediated neurodegenerative models (Schumacher, 2016).

CerTNL15 is reported to be expressed brightly and homogeneously throughout the whole neuron as well as its axons and dendrites (Heim et al., 2007). We were able to trace single axons along distances >100 µm and over time for several hours and identify their morphological changes during degeneration. Nevertheless, due to resolution limits, there is still remaining doubt if axons that we identify as fragmented are actually disassembled, or if the observed swollen bodies are still undetectably connected. This could be resolved with e.g. EM. With suitable control groups, I could minimize the measurement errors due to differences in anesthesia and vital functions, surgical trauma and microscope setup. CerTN responds linearly to cytosolic calcium concentration within physiologically relevant ranges. Therefore, it is a suitable sensor for measuring calcium levels. To increase validity of calcium readouts and as established in previous experiments, I decided to determine a cut-off to robustly distinguish physiological calcium levels from pathologically increased ones in a binary fashion. This cut-off value is based on the mean YFP/CFP intensity ratio obtained from axons of healthy CerTNL15

mice, added the three-fold standard deviation. Because CerTNL15 naturally competes for calcium binding, it inherently is also a calcium buffer. However, in our experimental paradigm, its buffering capacity is neglectable, since we observe up to 4-fold intensity ratio changes that persist over time in axons. Using the cut-off and the previously described classification of axon morphology (Nikić et al., 2011) I was able to reproduce the previous observations on axonal populations, calcium levels and transition rates using the similar methods.

One major drawback of assessing dynamic transitions *in vivo* is the low sample size that we were able to collect due to my specific question. The efficiency of this experimental approach has been proven not to be optimal. To reduce variance in the differentially active neuroinflammatory lesions, I decided to use strict inclusion criteria and only evaluate mice, in which I could track at least 25 intact axons with pathologically increased calcium levels over the entire imaging period for reliable statistical analysis. Nevertheless, in some cases the variance in the calculated transition rates was large. In case of TrpM4, Sarm1 and ΔNLS groups, not enough animals passed the criteria, leaving us with inconclusive results. In case of the calpain group we could include enough animals for statistical analysis and could observe a significant reduction in fragmentation rate, despite large variance.

In comparison to previous studies on neurodegeneration in EAE, I could resolve the fate of single axons within acute EAE lesions in various conditions, e.g. genetic manipulation or under calpain inhibitor treatment in real-time. Using *in vivo* 2-photon microscopy allows us to gain further insights into the mechanisms of neurodegeneration in EAE, since we are able to study dynamic behavior of single axons regarding their morphology and cytosolic calcium concentrations.

5.3 Wallerian degeneration-like mechanisms are likely not involved in axonal fragmentation in acute EAE

I investigated the role of Wallerian-like degeneration elements in EAE lesions through well-known transgenic models that delay WD. Both Sarm1 and Wld^S affect the classical WD pathway. However, the exact connection between these two mediators is not fully understood. These molecules have in common that both of them influence the NAD biosynthesis and it is proposed that they carry out their protection through reducing the NAD depletion in injured axons.

In the past, several studies investigated the effect of Wld^S in MOG peptide induced EAE. Two studies with Wld^S mice observed a modest delay of EAE onset and a modest attenuation of neurological disability accompanied by reduced demyelination and axonal loss (Chitnis et al., 2007; Kaneko et al., 2006), without altering immune infiltration. This study found that Wld^S exerts its neuroprotective effect either through decreasing the numbers of activated macrophage/microglia (Chitnis et al., 2007) or through maintaining neuronal NAD levels that can be simulated by administration of the NAD biosynthesis precursor NAM (Kaneko et al., 2006). On the other hand, in a more recent study (Singh et al., 2017) no striking differences were observable in EAE severity after MOG-induced EAE in Wld^S mice. This study observed a moderate decrease in Wallerian degeneration identified through immunoreactivity against NPY-Y1R serum in the acute stages of EAE and through increase of NAD levels in spinal cords of Wld^S animals with EAE compared to WT. In line with the results of my study, the degree of inflammation and demyelination was comparable throughout the EAE disease stages. The net axonal loss was similar in the chronic EAE in both groups. In our study, we used an even stronger Wld^S mutant that is lacking the nuclear localization sequence (ΔNLS) and thereby retargeting the mutant protein from the nucleus to the cytosol. Transgenic mice overexpressing ΔNLS-Wld^S show an even more robust delay of Wallerian degeneration after a nerve lesion (Beirowski et al., 2009). Axon preservation in ΔNLS-Wld^S lasts for up to 7 weeks after lesion, whereas in mice overexpressing the nuclear version Wld^S in same quantities the axons are preserved only up to 4 weeks.

If axonal degeneration in EAE was, even if only partially, driven by a Wallerian-like degenerating pathway, ΔNLS-Wld^S mice should exhibit an even stronger protection from axonal loss and present with an increased attenuation of disease pathology. However, the ΔNLS-Wld^S mice in our EAE experiments neither showed a delayed disease onset nor a reduction in their clinical disability. Furthermore, in the acute phase of the disease we could not observe a difference in the numbers of swollen or fragmented axons within the active lesion. Wld^S is a gain-of-function mutation and its exact protective mechanism is still elusive. There are reports that Wld^S, besides

substituting Nmnat2, possesses increased calcium buffering capacity. We could however not observe any changes in intra-axonal calcium concentration in ΔNLS-Wld^S mice, suggesting that WLD pathways show no influence on calcium in neuroinflammatory axon degeneration, neither "upstream" nor "downstream" of calcium elevation.

In contrast to Wld^S, Sarm1 is not formed by spontaneous mutation and its deletion shows even a more persistent axonal protection than Wld^S (Gilley et al., 2017). In our study, mice of the Sarm1 groups had a tendency to higher overall disease severity compared to the ΔNLS-Wld^S groups, but lack of Sarm1 did not attenuate the clinical symptoms. Examining lesion load, axon pathology and calcium levels, I was not able to observe a significant difference.

In the past years, new players were identified that play a role in Wallerian-like or WLD^S-sensitive axon disassembly. Thanks to mutagenesis screens and injury assays, a novel mediator of axon death was found in drosophila (Neukomm et al., 2017). The appropriately named Axundead (axed) mutant saves axons from degeneration after activation of dSarm signalling, loss of Nmnat, axotomy and all three combined. Thereby axed lies downstream of dSarm. It is noteworthy, that axed mutant axons retain their circuit functionality after axotomy, indicating a long-term functional preservation. Based on the strong conservation of dSarm/Sarm1 pathway it is likely that a mammalian homolog for axed will be soon identified. According to our results with Sarm1-/-, axed is however probably not a good candidate for intervention therapies in neuroinflammatory conditions, since we did not find any evidence for a critical role of the Sarm1 pathway.

In summary, these results suggest that delaying Wallerian degeneration-like mechanisms does not halt axonal fragmentation in acute EAE. However, Wallerian degeneration might be involved in secondary degenerative processes. It is supposed that the clinical course of multiple sclerosis runs through several phases, every phase sensitive to different influences. In the initial phase, inflammation is the dominant factor (Hasseldam and Johansen, 2010), which is responsible for relapses in MS. Axonal degeneration conditioned by the amount of prior disease activity drives persistent neurological disability in the later, chronic phases, even in absence of active inflammation (Coles et al., 1999). Although there is axon damage already present in early phases of MS (Dziedzic et al., 2010; Filippi et al., 2003), it appears that another mechanism distinct from WD drives this axonal loss. Wallerian-like degeneration might however be rather involved in a process with much slower kinetics, which could apply in the progressive variants of MS, thereby contributing to the increasing permanent disability.

5.4 Effect of TrpM4 deficiency in acute EAE require further study

In my study, loss of TrpM4 showed no effect on disease severity as it was described in a previous study of TrpM4-/- in EAE (Schattling et al., 2012). Here, TrpM4+/- x CerTNL15 were used as the control group to the knockout mice. As I showed that TrpM4+/- x CerTNL15 animals behave like wildtype (WT) CerTNL15 mice in several features, the different outcome cannot be explained by the different choice of control group. However, the reduction of disease severity is more prominent in the later chronic phase of EAE in the study of Schattling et al.. Additional experiments could reveal if the lack of TrpM4 has neuroprotective influence on later timepoints.

In this study, my interest focused on the effect of TrpM4-/- in the acute phase of disease, in which Schattling et al. could not detect any difference between TrpM4-/- and WT group. In their study they recorded TrpM4-dependent cation currents in hippocampal-derived cells. A potential difference between WT and TrpM4-/- cells was only detectable after previous glutamate incubation. Assuming no glutamate-induced excitotoxicity is involved in the acute phase of EAE, then the lack of TrpM4 could exert its neuroprotective effect in a different setting which might be more glutamate-dependent, as in the later chronic phase, in which Schattling et al. indeed found an ameliorating effect of TrpM4-/-. One explanation why I observed a different clinical EAE progression in TrpM4-/- mice might be that rather astrocytic TrpM4 is influencing EAE than axonal TrpM4. TrpM4 expression is increased in active-demyelinating white matter brain lesions of MS patients (Schattling et al., 2012) which lead to the conclusion that axonal TrpM4 overexpression might lead to axonal damage in EAE. Since the animals used in Schattling and in this thesis are global knock outs the TrpM4 deficiency is not limited to the axons but extents also to other cell types like astrocytes and immune cells. Recent findings revealed that TrpM4 and Sur1 are *de novo* upregulated in injury and disease especially in astrocytes and form heteromeric channels (Makar et al., 2015). The sulfonamide glibenclamide, which is widely used in Type II diabetes treatment, acts through inhibition of Sur1. Both subunits, Sur1 and TrpM4, are required for the manifestation of the pathological effects by forming a heteromer consisting of the regulatory subunit Sur1 and the pore-forming subunit TrpM4 (Woo et al., 2013). In another study (Gerzanich et al., 2017), the authors found that astrocytes are the predominant cell type that upregulates the heteromeric channel TrpM4-Sur1 in both chronic EAE and MS lesions. The ablation of Abcc8, which encodes the TrpM4 channel, decreases the amount of multiple pro-inflammatory and pathogenic mediators that are secreted by astrocytes in lesions. These findings support our observation that TrpM4 deficiency had no influence on the fragmentation rate in axons in acute EAE lesions. Since TrpM4 is known to be involved in edema development (Simard et al., 2009; Walcott et al., 2012), it is surprising that we did not observe a reduction in the swelling rate in TrpM4-/-. There might be compensatory mechanisms

involved that at least in part replace the function of TrpM4 channels or TrpM4 overexpression after injury is rather associated with astrocytes than axons like the study of Gorse et al. shows (Gorse et al., 2018). However, our data on the influence of TrpM4-/- is still preliminary, and more experimental data needs to be conducted to be able to verify these observations. Moreover, to strengthen the significance of our experimental data a reasonable control experiment (like the dorsal hemisection of the spinal cord as model of spinal cord injury to test the neuroprotective effects of Sarm1-/- and ΔNLS-Wld^S) has to be developed that demonstrates the neuroprotective potential of TrpM4-/- as it was shown in previous studies (Cho et al., 2014; Leiva-Salcedo et al., 2017; Makar et al., 2015; Schattling et al., 2012).

5.5 Calpain inhibition reduces axonal fragmentation in acute EAE in vivo

Through inhibition of calpain via Calpain Inhibitor III we could significantly reduce the fragmentation rate *in vivo* in acute EAE lesions. By examining the immune cell composition, we could exclude an effect of the drug on immune cell infiltration. To validate calpain inhibitor treatment, we treated mice immunized with recombinant MOG over 7 days either with calpain inhibitor III or with vehicle. Although we were not able to reduce disease symptoms or improve axonal morphology with this long-term treatment, calpain is highly likely to be involved in the fragmentation processes in active EAE lesions.

Calpain inhibitor III has limited solubility in DMSO and therefore the resulting treatment concentration via the osmotic pump might be below the effective concentration, as its release from the pump is limited to a set flow rate. Other studies using the same calpain inhibitor showed that this drug given i.p. is an effective long-term neuroprotectant for axonal injury (Ai et al., 2007). Hassen et al. confirmed the ability of calpain inhibitor for long-term neuroprotection. They treated mice i.p. prior to and after EAE onset with another calpain inhibitor, CYLA that is able to cross the BBB and they observed a reduction of disease severity regarding inflammation, demyelination and axonal injury in both treatment groups (Hassen et al., 2008). In our treatment paradigm during *in vivo* imaging sessions, a higher total concentration of the drug could be reached by bath incubation, which might explain the significant amelioration of axon fragmentation that we could detect in these experiments. Calpain inhibitor III is used as treatment option in many different injury or neurodegeneration models (Ai et al., 2007; Crocker et al., 2003; Kawamura et al., 2005; Kunz et al., 2004; Ono et al., 2016; Samantaray et al., 2013; Thompson et al., 2010). We chose this type of calpain inhibitor based on the positive treatment outcome on axons in a contusion model (Williams et al., 2014).

Calpain inhibitor III mostly targets calpain, in contrast to other compounds that inhibit caspases and other proteases. Nevertheless, cathepsin B is a side target of calpain inhibitor III (Siklos et al., 2015). By using a pharmaceutical inhibition, we cannot exclude that the observed effects are results from inhibition of other molecules.

Moreover, calpain is a very potent protease that is involved in several pathways (for review, see (Goll et al., 2003)). Its cleavage products are involved even in competing mechanisms. For instance, calpain activation can inhibit apoptosis by cleaving members of the caspase family thereby blocking caspase-3 activation (Chua et al., 2000), but under other conditions it cleaves pro-caspase 3, thereby triggering programmed cell death (Cheng et al., 2018). Calpain activation is involved throughout the development of the CNS (Arthur et al., 2000) and recent work suggests that calpains are important for adult neurogenesis as well (Machado et al.,

2015). It can be even discussed that synaptic plasticity and neurodegeneration share common signaling pathways including histone acetylation and deacetylation and mTOR signaling (Baudry and Bi, 2016). The controlled activation of calpain under physiological conditions is e.g. involved in synaptic function and memory formation (Liu et al., 2008). In pruning, regrowth, but also in cell death calpain has the same substrates: structural and scaffolding proteins, enzymes and receptors. Among others, the extent of calpain activation is determining which process is executed (Gan-Or and Rouleau, 2016). Several isoforms of calpain exist that exhibit partly even opposite functions. For example, calpain-1 is rather associated with induction of LTP, whereas calpain-2 is involved in limiting this LTP and is involved in neurodegeneration (Baudry and Bi, 2016; Wang et al., 2013). These examples lead to the conclusion that calpain can be only a potential therapeutic target if its inhibition is specific and coordinated in time and location. To achieve this, several questions need to be addressed first. Calpain-2 appears to be a good candidate (Baudry and Bi, 2016; Seinfeld et al., 2016; Wang et al., 2018a, 2018b), but other calpain isoforms might be still identified.

A few studies show that calpain expression was increased in activated T cells (Nicole et al., 2013), and its inhibition in MBP-specific T cells attenuated their encephalitogenicity in RR-EAE mice after transplantation (Guyton et al., 2009). To increase the validity of our finding that neuroprotection via CI3 is inherent to neurons, the calpain inhibition should be more specifically targeted. This can be achieved by viral overexpression of the endogenous calpain inhibitor calpastatin. In an optical nerve crush model, the neuroprotective potential of calpastatin overexpression was shown (Yang et al., 2013). The viral construct contains a CMV promotor which targets expression injected in the CNS not only to neurons, but also to other cell types like astrocytes. To overcome this unspecificity, several ways are possible: either through injection of the construct in DRGs, or by replacing the CMV promotor with a hSyn that drives expression specifically to neurons.

Supposing that inhibition of calpain within the neurons indeed restricts degeneration, the mechanism driving axonal degeneration in acute EAE lesions remains elusive. Since with calpain many destructive pathways converge, it might be still an optimal target for neuroprotection (see *Figure 21*). Wallerian-like degeneration and TrpM4-mediated excitotoxicity, that both are described in this thesis, involve at some point the activation of the neuronal death executor, calpain. There are many studies that show that calpain inhibition attenuates axonal damage in different disease models like AD (Rao et al., 2008, 2014), PD (Diepenbroek et al., 2014), ALS (Rao et al., 2016), traumatic brain injury (Ma et al., 2012; Schoch et al., 2012), ON (Hoffmann et al., 2013) and MS (Hassen et al., 2006, 2008). Although it is not clear what initiated the axonal disassembly, by inhibiting a downstream executor we are able to prevent further degeneration.

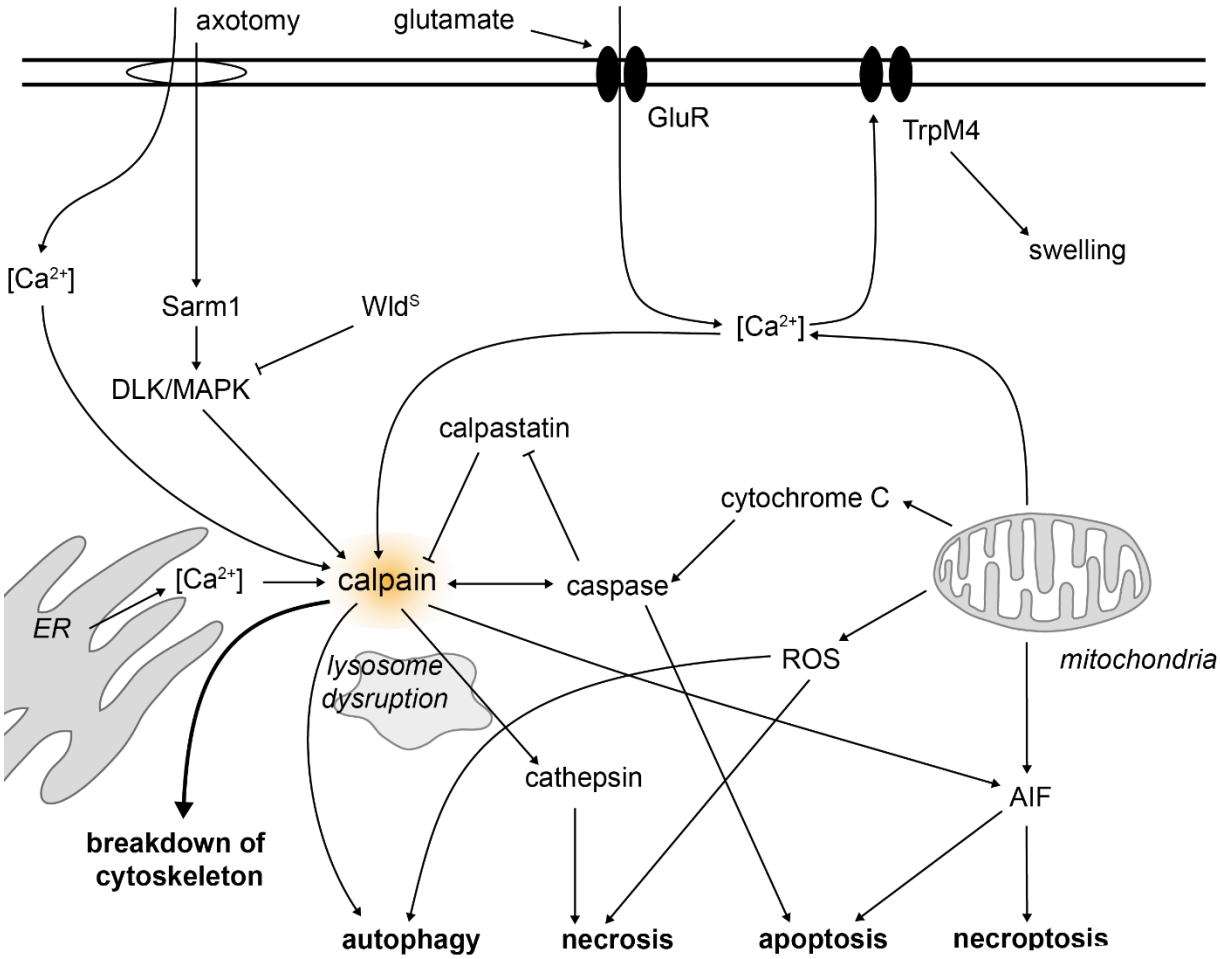

Figure 21: Schematic overview of possible calpain-dependent neurodegeneration pathways.

Depicted are some of the possible, both physiological and pathological cell death pathways (autophagy, necrosis, apoptosis) and necroptosis and pathways that lead to axonal damage (axotomy, excitotoxicity). All of them involve in the later stages an increase in intracellular calcium and the overactivation of calpain which if not inhibited lead to the excessive proteolysis of cytoskeletal proteins. Inhibition of calpain by activation of the endogenous inhibitor calpastatin or pharmacological intervention potentially is axonprotective since it prevents the uncontrolled breakdown of the cytoskeleton.

5.6 Relevance for MS

In the recent decades, the focus of MS research shifted to understanding the neurodegenerative arm of the disease. As discussed earlier, the current available DMT mostly aim to positively influence the disease outcome by modifying the immunological component, they have only limited effect on the preservation of neuronal structure and function, and thereby on the long-term outcome (Graetz et al., 2018). Instead of only focusing solely on the inflammatory processes, treatment strategies might be more promising, that target the neurodegenerative processes as well. Potential neuroprotective agents should either promote the endogenous repair mechanisms, target survival pathways or inhibit the neurodegenerative cascade, but for development of a suitable treatment, the processes underlying the axonal loss in EAE and MS need to be understood. Using 2 photon imaging and transgenic mouse lines FAD could be identified in lesions in EAE, an established animal model for MS (Nikić et al., 2011) and pathological increased intra-axonal calcium correlated with higher risk of axonal fragmentation. Since axonal abnormalities resembling FAD were found in MS biopsies as well, it can be assumed that calcium dysregulation is involved in MS as well. One possible point of action for neuroprotection is to decrease ion imbalance (specifically Ca^{2+}) within axons by blockage of ion channels. Voltage-gated and acid-sensing ion channels (ASICs) are discussed among others to contribute to ion dysregulation observed in EAE and MS (Ingwersen et al., 2018; Ortega-Ramírez et al., 2017). Despite investigating several ion channels, a clear candidate could not be isolated so far. Another neuroprotective approach is rescuing neurons and their processes from oxidative stress by scavenging ROS and RNS with antioxidative reagents (van der Goes et al., 1998; Ghafourifar et al., 2008; Nikić et al., 2011).

Based on the previous findings, my work further investigated which possible destructive mechanisms are activated by the increased calcium levels. Calpain seems a promising therapeutic target for neuroprotective strategies. In several murine models of neurodegeneration, the inhibition of calpain with synthetic inhibitor peptides (SNJ-1945 used in MS model (Trager et al., 2014) and cortical impact traumatic brain injury (Bains et al., 2013); MDL-28170 used in spinal cord injury model (Brocard et al., 2016); Calpeptin used in EAE model (Das et al., 2013; Guyton et al., 2010)) or via overexpression of the endogenous calpastatin (Diepenbroek et al., 2014; Schoch et al., 2012; Ma et al., 2012; Rao et al., 2014, 2016; Yang et al., 2013) was found to successfully attenuate degeneration. However, a long-term treatment with calpain inhibitor using intrathecal osmotic pumps showed that the delivery of intervention is a critical point that needs in itself further development.

In contrast to other neuroprotective approaches, calpain as a target has a major advantage. Different neurodegenerative processes like excitotoxicity, apoptosis, necrosis and others lead to

the overactivation of calpain as the executor of axonal disintegration. Targeting calpain might present a promising strategy to delay neuronal death, axonal fragmentation or to promote recovery processes without the full understanding of the disease causes, which needs further investigations and better disease models.

5.7 Concluding remarks

Since MS was for the first time recognized as disease entity back in the 19th century, the disease remains enigmatic, particularly because it manifests in many different forms. No person diagnosed with MS will have the same clinical course, which makes it even harder to grasp the nature of this disease. Over the years, there have been several debates about the primary cause: traditionally MS was seen as an autoimmune disease of the CNS in which aberrant immune cell enter the CNS through a broken BBB and turn against their own body and attack CNS components like the insulating myelin. Myelin loss and aggressive interaction of activated immune cells leads to neurodegeneration (outside-in model). Other clinical observations lead to the competing inside-out model: Primary degeneration and/or oligodendrocyte death initiate autoimmune and inflammatory response through release of antigenic proteins and lipids. There is evidence supporting both models, but since the solely use of DMT does not halt disability progression in most of MS patients, the development of additional neuroprotective strategies is in any case necessary. Therefore, MS research in the past years shifted partly to investigate the neurodegenerative part of the disease.

In my thesis I investigate several mechanisms of axon destruction that are presumed to be involved in neurodegeneration in MS. Since my work is a follow up of my colleagues Ivana Nikic and Minh Schumacher it was first necessary to show that I can reproduce their findings with the methods they established. In the first part of my work, I show that I could successfully reproduce the observation of calcium dysregulation in early axonal stages within active EAE lesions. By following the fate of these axons over a longer period, I was able to obtain similar transition rates. Additionally, by reproducing the previous findings I could show that the control animals for the transgenic experiments are behaving similar to the WT-CerTNL15, thereby justifying the use of heterozygous TrpM4 and Sarm1 as control mice.

I showed that both, Sarm1-/- and the Wld^S mutant, which are known to delay significantly Wallerian-like degeneration after spinal cord injury, are not able to significantly halt focal axonal degeneration in acute EAE lesions. This does not exclude that the Wallerian degeneration-like pathways are involved in later phases or in sites distant to the actual lesions as a form of secondary degeneration.

Finally, I demonstrated that pharmacological inhibition of calpain reduces fragmentation rates in acute EAE. As a converging point for several distinct degenerative mechanisms, calpain inhibition would overcome our current lack of understanding the exact cause of neurodegeneration in MS. Furthermore, a more effective targeting strategy than the intrathecal delivery need to be developed for long-term protection. Better treatment strategies that target

neuroprotection and remyelination besides immunomodulation promise MS patients and their families to fundamentally improve quality of life and reduce their constant anxiety of what this unpredictable disease might bring them.

6 References

Ai, J., Liu, E., Wang, J., Chen, Y., Yu, J., and Baker, A.J. (2007). Calpain inhibitor MDL-28170 reduces the functional and structural deterioration of corpus callosum following fluid percussion injury. Journal of Neurotrauma *24*, 960–978.

Amor, S., Peferoen, L.A., Vogel, D.Y., Breur, M., van der Valk, P., Baker, D., and van Noort, J.M. (2014). Inflammation in neurodegenerative diseases--an update. Immunology *142*, 151–166.

Arthur, S.J., Elce, J.S., Hegadorn, C., Williams, K., and Greer, P.A. (2000). Disruption of the Murine Calpain Small Subunit Gene, Capn4: Calpain Is Essential for Embryonic Development but Not for Cell Growth and Division. Molecular and Cellular Biology *20*, 4474–4481.

Avery, M.A., Sheehan, A.E., Kerr, K.S., Wang, J., and Freeman, M.R. (2009). WldS requires Nmnat1 enzymatic activity and N16–VCP interactions to suppress Wallerian degeneration. The Journal of Cell Biology *184*, 501–513.

Babetto, E., Beirowski, B., Russler, E.V., Milbrandt, J., and DiAntonio, A. (2013). The Phr1 Ubiquitin Ligase Promotes Injury-Induced Axon Self-Destruction. Cell Reports *3*, 1422–1429.

Bains, M., Cebak, J.E., Gilmer, L.K., Barnes, C.C., Thompson, S.N., Geddes, J.W., and Hall, E.D. (2013). Pharmacological analysis of the cortical neuronal cytoskeletal protective efficacy of the calpain inhibitor SNJ-1945 in a mouse traumatic brain injury model. Journal of Neurochemistry *125*, 125–132.

Baudry, M., and Bi, X. (2016). Calpain-1 and Calpain-2: The Yin and Yang of Synaptic Plasticity and Neurodegeneration. Trends in Neurosciences *39*, 235–245.

Beirowski, B., Babetto, E., Gilley, J., Mazzola, F., Conforti, L., Janeckova, L., Magni, G., Ribchester, R.R., and Coleman, M.P. (2009). Non-Nuclear WldS Determines Its Neuroprotective Efficacy for Axons and Synapses In Vivo. The Journal of Neuroscience *29*, 653–668.

Bettelli, E., Pagany, M., Weiner, H.L., Linington, C., Sobel, R.A., and Kuchroo, V.K. (2003). Myelin Oligodendrocyte Glycoprotein–specific T Cell Receptor Transgenic Mice Develop Spontaneous Autoimmune Optic Neuritis. The Journal of Experimental Medicine *197*, 1073–1081.

Billiau, A. and Matthys, P. (2001). Modes of action of Freund's adjuvants in experimental models of autoimmune diseases. Journal of Leukocyte Biology *70*.

Bitsch, A., Schuchardt, J., Bunkowski, S., Kuhlmann, T., and Brück, W. (2000). Acute axonal injury in multiple sclerosisCorrelation with demyelination and inflammation. Brain *123*, 1174–1183.

Bjartmar, C., Kinkel, R., Kidd, G., Rudick, R., and Trapp, B. (2001). Axonal loss in normal-appearing white matter in a patient with acute MS. Neurology *57*, 1248–1252.

Breckwoldt, M.O., Pfister, F.M., Bradley, P.M., Marinković, P., Williams, P.R., Brill, M.S., Plomer, B., Schmalz, A., Clair, D.K., Naumann, R., Griesbeck, O., Schwarzländer, M.; Godinho, L., Bareyre, F., Dick, T., Kerschensteiner, M., Misgeld, T. (2014). Multiparametric optical analysis of mitochondrial redox signals during neuronal physiology and pathology in vivo. Nature Medicine *20*, 555–560.

Brocard, C., Plantier, V., Boulenguez, P., Liabeuf, S., Bouhadfane, M., Viallat-Lieutaud, A., Vinay, L., and Brocard, F. (2016). Cleavage of Na(+) channels by calpain increases persistent Na(+) current and promotes spasticity after spinal cord injury. Nature Medicine *22*, 404–411.

Burnard, S., Lechner-Scott, J., and Scott, R.J. (2017). EBV and MS: Major cause, minor contribution or red-herring? Multiple Sclerosis and Related Disorders *16*, 24–30.

Campbell, A.K. (2014). Intracellular Calcium.

Chen, C.-Y., Lin, C.-W., Chang, C.-Y., Jiang, S.-T., and Hsueh, Y.-P. (2011). Sarm1, a negative regulator of innate immunity, interacts with syndecan-2 and regulates neuronal morphology. The Journal of Cell Biology *193*, 769–784.

Cheng, S.-Y.Y., Wang, S.-C.C., Lei, M., Wang, Z., and Xiong, K. (2018). Regulatory role of calpain in neuronal death. Neural Regeneration Research *13*, 556–562.

Chitnis, T., Imitola, J., Wang, Y., Elyaman, W., Chawla, P., Sharuk, M., Raddassi, K., Bronson, R.T., and Khoury, S.J. (2007). Elevated neuronal expression of CD200 protects Wlds mice from inflammation-mediated neurodegeneration. The American Journal of Pathology *170*, 1695–1712.

Cho, C.-H.H., Kim, E., Lee, Y.-S.S., Yarishkin, O., Yoo, J.C., Park, J.-Y.Y., Hong, S.-G.G., and Hwang, E.M. (2014). Depletion of 14-3-3γ reduces the surface expression of Transient Receptor Potential Melastatin 4b (TRPM4b) channels and attenuates TRPM4b-mediated glutamate-induced neuronal cell death. Molecular Brain *7*, 52.

Chua, B., Guo, K., and Li, P. (2000). Direct cleavage by the calcium-activated protease calpain can lead to inactivation of caspases. The Journal of Biological Chemistry *275*, 5131–5135.

Chuang, C.-F., and Bargmann, C.I. (2005). A Toll-interleukin 1 repeat protein at the synapse specifies asymmetric odorant receptor expression via ASK1 MAPKKK signaling. Genes & Development *19*, 270–281.

Cianfoni, A., Niku, S., and Imbesi, S. (2007). Metabolite findings in tumefactive demyelinating lesions utilizing short echo time proton magnetic resonance spectroscopy. AJNR. American Journal of Neuroradiology *28*, 272–277.

Coleman, M.P., Conforti, L., Buckmaster, A.E., Tarlton, A., Ewing, R.M., Brown, M.C., Lyon, M.F., and Perry, H.V. (1998). An 85-kb tandem triplication in the slow Wallerian degeneration (Wlds) mouse. Proceedings of the National Academy of Sciences *95*, 9985–9990.

Coles, A., Wing, M., and of…, M.P. (1999). Monoclonal antibody treatment exposes three mechanisms underlying the clinical course of multiple sclerosis.

Comi, G., Martinelli, V., Rodegher, M., Moiola, L., Bajenaru, O., Carra, A., Elovaara, I., Fazekas, F., Hartung, H., Hillert, J., Komoly, S., Lubetzki, C., Montalban, X, Myhr, K. M., Ravnborg, M., Rieckmann, P., Wynn, D., Young, C., Filippi, M and PreCISe for the study group (2009). Effect of glatiramer acetate on conversion to clinically definite multiple sclerosis in patients with clinically isolated syndrome (PreCISe study): a randomised, double-blind, placebo-controlled trial. Lancet (London, England) *374*, 1503–1511.

Confavreux, C., and Vukusic, S. (2006). Age at disability milestones in multiple sclerosis. Brain *129*, 595–605.

Conforti, L, Wilbrey, A., Morreale, G., Janeckova, L., Beirowski, B., Adalbert, R., Mazzola, F., Stefano, M., Hartley, R., Babetto, E., Smith, T., Gilley, J., Billington, R. A., Genazzani, A. A., Ribchester, R. R., Magni, G. and Coleman, M. (2009). Wld S protein requires Nmnat activity and

a short N-terminal sequence to protect axons in mice. The Journal of Cell Biology *184*, 491–500.

Cong, J., Goll, D., Peterson, A., and Kapprell, H. (1989). The role of autolysis in activity of the Ca2+-dependent proteinases (mu-calpain and m-calpain). The Journal of Biological Chemistry *264*, 10096–10103.

Cottin, P., Vidalenc, P., and Ducastaing, A. (1981). Ca2+-dependent association between a Ca2+-activated neutral proteinase (CaANP) and its specific inhibitor. FEBS Letters *136*, 221–224.

Crocker, S.J., Smith, P.D., Jackson-Lewis, V., Lamba, W.R., Hayley, S.P., Grimm, E., Callaghan, S.M., Slack, R.S., Melloni, E., Przedborski, S., Robertson, G.-S., Anisman, H., Merali, Z., Park, D.-S. (2003). Inhibition of calpains prevents neuronal and behavioral deficits in an MPTP mouse model of Parkinson's disease. The Journal of Neuroscience: The Official Journal of the Society for Neuroscience *23*, 4081–4091.

Dal, C.M., Kim, B., Miller, S., and Melvold, R. (1996). Theiler's Murine Encephalomyelitis Virus (TMEV)-Induced Demyelination: A Model for Human Multiple Sclerosis. Methods (San Diego, Calif.) *10*, 453–461.

Das, A., Guyton, M., Butler, J.T., Ray, S.K., and Banik, N.L. (2008). Activation of calpain and caspase pathways in demyelination and neurodegeneration in animal model of multiple sclerosis. CNS & Neurological Disorders Drug Targets *7*, 313–320.

Das, A., Guyton, M., Smith, A., Wallace, G., well, M.L., Matzelle, D.D., Ray, S.K., and Banik, N.L. (2013). Calpain inhibitor attenuated optic nerve damage in acute optic neuritis in rats. Journal of Neurochemistry *124*, 133–146.

Degelman, M.L., and Herman, K.M. (2017). Smoking and multiple sclerosis: A systematic review and meta-analysis using the Bradford Hill criteria for causation. Multiple Sclerosis and Related Disorders *17*, 207–216.

DeLuca, H., and Plum, L. (2016). UVB radiation, vitamin D and multiple sclerosis. Photochemical & Photobiological Sciences *16*, 411–415.

Denk, W., Strickler, J., and Webb, W. (1990). Two-photon laser scanning fluorescence microscopy. Science (New York, N.Y.) *248*, 73–76.

Dheen, T.S., Kaur, C., and Ling, E.-A. (2007). Microglial Activation and its Implications in the Brain Diseases. Current Medicinal Chemistry *14*, 1189–1197.

Diepenbroek, M., Casadei, N., Esmer, H., Saido, T.C., Takano, J., Kahle, P.J., Nixon, R.A., Rao, M.V., Melki, R., Pieri, L., Helling, S., Marcus, K., Krueger, R., Masliah, E., Riess, O., Nuber, S. (2014). Overexpression of the calpain-specific inhibitor calpastatin reduces human alpha-Synuclein processing, aggregation and synaptic impairment in [A30P]αSyn transgenic mice. Human Molecular Genetics *23*, 3975–3989.

Direnberger, S., Mues, M., Micale, V., Wotjak, C.T., Dietzel, S., Schubert, M., Scharr, A., Hassan, S., Wahl-Schott, C., Biel, M., Krishnamoorthy, G., Griesbeck, O. (2012). Biocompatibility of a genetically encoded calcium indicator in a transgenic mouse model. Nature Communications *3*, 1031.

Disanto, G., Barro, C., Benkert, P., Naegelin, Y., Schädelin, S., Giardiello, A., Zecca, C., Blennow, K., Zetterberg, H., Leppert, D., Kappos, L., Gobbi, C., Kuhle, J. and the Swiss Multiple Sclerosis Cohort Study Group (2017). Serum Neurofilament light: A biomarker of neuronal damage in multiple sclerosis. Annals of Neurology *81*, 857–870.

Dutta, R., and Trapp, B.D. (2007). Pathogenesis of axonal and neuronal damage in multiple sclerosis. Neurology *68*, S22-31; discussion S43-54.

Dutta, R., McDonough, J., Yin, X., Peterson, J., Chang, A., Torres, T., Gudz, T., Macklin, W.B., Lewis, D.A., Fox, R.J., Rudick, R., Mirnics, K., Trapp, B. (2006). Mitochondrial dysfunction as a cause of axonal degeneration in multiple sclerosis patients. Annals of Neurology *59*, 478–489.

Dziedzic, T., Metz, I., Dallenga, T., König, F., Müller, S., Stadelmann, C., and Brück, W. (2010). Wallerian Degeneration: A Major Component of Early Axonal Pathology in Multiple Sclerosis. Brain Pathology *20*, 976–985.

Fà, M., Zhang, H., Staniszewski, A., Saeed, F., Shen, L.W., Schiefer, I.T., Siklos, M.I., Tapadar, S., Litosh, V.A., Libien, J., Petukhov, P.A., Teich, A.F., Thatcher G., Arancio O. (2016). Novel Selective Calpain 1 Inhibitors as Potential Therapeutics in Alzheimer's Disease. Journal of Alzheimer's Disease: JAD *49*, 707–721.

Filippi, M., Bozzali, M., Rovaris, M., Gonen, O., Kesavadas, C., Ghezzi, A., Martinelli, V., Grossman, R., Scotti, G., Comi, G., Falini, A. (2003). Evidence for widespread axonal damage at the earliest clinical stage of multiple sclerosis. Brain: A Journal of Neurology *126*, 433–437.

Finkelsztejn, A. (2014). Multiple Sclerosis: Overview of Disease-Modifying Agents. Perspectives in Medicinal Chemistry *6*, 65–72.

Fisniku, L., Brex, P., Altmann, D., Miszkiel, K., Benton, C., Lanyon, R., Thompson, A., and Miller, D. (2008). Disability and T2 MRI lesions: a 20-year follow-up of patients with relapse onset of multiple sclerosis. Brain *131*, 808–817.

Flachenecker, P., Kobelt, G., Berg, J., Capsa, D., Gannedahl, M., and Platform, E. (2017). New insights into the burden and costs of multiple sclerosis in Europe: Results for Germany. Multiple Sclerosis (Houndmills, Basingstoke, England) *23*, 78–90.

Flachenecker, P., Stuke, K., Elias, W., Freidel, M., Haas, J., Pitschnau-Michel, D., Schimrigk, S., Zettl, U.K., and Rieckmann, P. (2008). Multiple sclerosis registry in Germany: Results of the extension phase 2005/2006. Deutsches Ärzteblatt International *105*, 113–119.

Fletcher, J., Lalor, S., Sweeney, C., Tubridy, N., and Mills, K. (2010). T cells in multiple sclerosis and experimental autoimmune encephalomyelitis. Clinical & Experimental Immunology *162*, 1–11.

Gale, C.R., and Martyn, C.N. (1995). Migrant studies in multiple sclerosis. *47*, 425–448.

Gan-Or, Z., and Rouleau, G.A. (2016). Calpain 1 in neurodegeneration: a therapeutic target? The Lancet Neurology *15*, 1118.

Gerdts, J., Summers, D.W., Sasaki, Y., DiAntonio, A., and Milbrandt, J. (2013). Sarm1-Mediated Axon Degeneration Requires Both SAM and TIR Interactions. The Journal of Neuroscience *33*, 13569–13580.

Gerzanich, V., Makar, T.K., Guda, P.R., Kwon, M.S., Stokum, J.A., Woo, S.K., Ivanova, S., Ivanov, A., Mehta, R.I., Morris, A.B., Bryan J., Bever, C.T., Simard, J. M. (2017). Salutary effects of glibenclamide during the chronic phase of murine experimental autoimmune encephalomyelitis. Journal of Neuroinflammation *14*, 177.

Gerzanich, V., Woo, K.S., Vennekens, R., Tsymbalyuk, O., Ivanova, S., Ivanov, A., Geng, Z., Chen, Z., Nilius, B., Flockerzi, V., Freichel, M., Simard, M.J. (2009). De novo expression of Trpm4 initiates secondary hemorrhage in spinal cord injury. Nature Medicine *15*, 185–191.

Ghafourifar, P., Mousavizadeh, K., Parihar, M.S., Nazarewicz, R.R., Parihar, A., and Zenebe, W.J. (2008). Mitochondria in multiple sclerosis. Frontiers in Bioscience: A Journal and Virtual Library *13*, 3116–3126.

Gilley, J., Ribchester, R.R., and Coleman, M.P. (2017). Sarm1 Deletion, but Not WldS, Confers Lifelong Rescue in a Mouse Model of Severe Axonopathy. Cell Reports *21*, 10–16.

Gold, R. (2014). Diagnose und Therapie der Multiplen Sklerose. Leitlinien Für Diagnostik Und Therapie in Der Neurologie.

Goll, D.E., Thompson, V., Li, H., Wei, W., and Cong, J. (2003). The calpain system. Physiological Reviews *83*, 731–801.

Goll, D.E., Thompson, V.F., Taylor, R.G., and Zalewska, T. (1992). Is calpain activity regulated by membranes and autolysis or by calcium and calpastatin? BioEssays *14*, 549–556.

Gorse, K., Lantzy, M.K., Lee, E.D., and Lafrenaye, A.D. (2018). Trpm4 induces astrocyte swelling but not death after diffuse traumatic brain injury. Journal of Neurotrauma.

Graetz, C., Groppa, S., Zipp, F., and Siller, N. (2018). Preservation of neuronal function as measured by clinical and MRI endpoints in relapsing-remitting multiple sclerosis: how effective are current treatment strategies? Expert Review of Neurotherapeutics *18*, 203–219.

Guo, J., She, J., Zeng, W., Chen, Q., Bai, X., and Jiang, Y. (2017). Structures of the calcium-activated, non-selective cation channel TRPM4. Nature.

Guyton, K.M., Wingrave, M.J., Yallapragada, A.V., Wilford, G.G., bnick, E.A., Matzelle, D.D., Tyor, W.R., Ray, S.K., and Banik, N.L. (2005). Upregulation of calpain correlates with increased neurodegeneration in acute experimental auto-immune encephalomyelitis. Journal of Neuroscience Research *81*, 53–61.

Guyton, M., bnick, E.A., Ray, S.K., and Banik, N.L. (2005). A role for calpain in optic neuritis. Annals of the New York Academy of Sciences *1053*, 48–54.

Guyton, M., Das, A., Samantaray, S., Wallace, G.C., Butler, J.T., Ray, S.K., and Banik, N.L. (2010). Calpeptin attenuated inflammation, cell death, and axonal damage in animal model of multiple sclerosis. Journal of Neuroscience Research *88*, 2398–2408.

Guyton, M.K., Brahmachari, S., Das, A., Samantaray, S., Inoue, J., Azuma, M., Ray, S.K., and Banik, N.L. (2009). Inhibition of calpain attenuates encephalitogenicity of MBP-specific T cells. Journal of Neurochemistry *110*, 1895–1907.

Haines, J.D., Inglese, M., and Casaccia, P. (2011). Axonal Damage in Multiple Sclerosis. Mount Sinai Journal of Medicine: A Journal of Translational and Personalized Medicine *78*, 231–243.

Hasseldam, H., and Johansen, F.F. (2010). Neuroprotection without Immunomodulation Is Not Sufficient to Reduce First Relapse Severity in Experimental Autoimmune Encephalomyelitis. Neuroimmunomodulation *17*, 252–264.

Hassen, G., Feliberti, J., Kesner, L., Stracher, A., and Mokhtarian, F. (2006). A novel calpain inhibitor for the treatment of acute experimental autoimmune encephalomyelitis. Journal of Neuroimmunology *180*, 135–146.

Hassen, G., Feliberti, J., Kesner, L., Stracher, A., and Mokhtarian, F. (2008). Prevention of axonal injury using calpain inhibitor in chronic progressive experimental autoimmune encephalomyelitis. Brain Research *1236*, 206–215.

Hauser, S.L., Waubant, E., Arnold, D.L., Vollmer, T., Antel, J., Fox, R.J., Bar-Or, A., Panzara, M., Sarkar, N., Agarwal, S., Langer-Gould, A., Craig, H. S. (2008). B-cell depletion with rituximab in relapsing-remitting multiple sclerosis. The New England Journal of Medicine *358*, 676–688.

Healy, B., and Liguori, M. (2012). Multiple Sclerosis: Diagnosis and Therapy. Wiley 163–180.

Heim, N., Garaschuk, O., Friedrich, M.W., Mank, M., Milos, R.I., Kovalchuk, Y., Konnerth, A., and Griesbeck, O. (2007). Improved calcium imaging in transgenic mice expressing a troponin C–based biosensor. Nature Methods *4*, 127–129.

Helmchen, F., and Waters, J. (2002). Ca2+ imaging in the mammalian brain in vivo. European Journal of Pharmacology *447*, 119–129.

Hoffmann, D.B., Williams, S.K., Jovana, B., Müller, A., Stadelmann, C., Naidoo, V., Bahr, B.A., Diem, R., and Fairless, R. (2013). Calcium Influx and Calpain Activation Mediate Preclinical Retinal Neurodegeneration in Autoimmune Optic Neuritis. Journal of Neuropathology & Experimental Neurology *72*, 745–757.

Hollenbach, J.A., and Oksenberg, J.R. (2015). The immunogenetics of multiple sclerosis: a comprehensive review. Journal of Autoimmunity *64*, 13–25.

Hopt, A., and Neher, E. (2001). Highly Nonlinear Photodamage in Two-Photon Fluorescence Microscopy. Biophysical Journal *80*, 2029–2036.

Imam, S.A., Guyton, M.K., Haque, A., Vandenbark, A., Tyor, W.R., Ray, S.K., and Banik, N.L. (2007). Increased calpain correlates with Th1 cytokine profile in PBMCs from MS patients. Journal of Neuroimmunology *190*, 139–145.

Ingwersen, J., Santi, L., Wingerath, B., Graf, J., Koop, B., Schneider, R., Hecker, C., Schröter, F., Bayer, M., Engelke, A., Dietrich, M., Albrecht, P., Hartung, H.-P. P., Annunziata, P., Aktas, O., Prozorovski, T. (2018). Nimodipine confers clinical improvement in two models of experimental autoimmune encephalomyelitis. Journal of Neurochemistry.

Inman, D.M., and Harun-Or-Rashid, M. (2017). Metabolic Vulnerability in the Neurodegenerative Disease Glaucoma. Frontiers in Neuroscience *11*, 146.

Jares-Erijman, E.A., and Jovin, T.M. (2003). FRET imaging. Nature Biotechnology *21*, 1387–1395.

Kabat, E., Wolf, A., and Bezer, A. (1947). The rapid production of acute disseminated encephalomyelitis in rhesus monkeys by injection of heterologous and homologous brain tissue with adjuvants. The Journal of Experimental Medicine *85*, 117–130.

Kaneko, S., Wang, J., Kaneko, M., Yiu, G., Hurrell, J.M., Chitnis, T., Khoury, S.J., and He, Z. (2006). Protecting Axonal Degeneration by Increasing Nicotinamide Adenine Dinucleotide Levels in Experimental Autoimmune Encephalomyelitis Models. The Journal of Neuroscience *26*, 9794–9804.

Kapoor, R., Davies, M., Blaker, P.A., Hall, S.M., and Smith, K.J. (2003). Blockers of sodium and calcium entry protect axons from nitric oxide-mediated degeneration. Annals of Neurology *53*, 174–180.

Kawakami, N., Bartholomäus, I., Pesic, M., and Mues, M. (2012). An autoimmunity odyssey: how autoreactive T cells infiltrate into the CNS. Immunological Reviews *248*, 140–155.

Kawamura, M., Nakajima, W., Ishida, A., Ohmura, A., Miura, S., and Takada, G. (2005). Calpain inhibitor MDL 28170 protects hypoxic–ischemic brain injury in neonatal rats by inhibition of both apoptosis and necrosis. Brain Research *1037*, 59–69.

Kerschensteiner, M., Schwab, M.E., Lichtman, J.W., and Misgeld, T. (2005). In vivo imaging of axonal degeneration and regeneration in the injured spinal cord. Nature Medicine *11*, 572–577.

Kim, Y., Zhou, P., Qian, L., Chuang, J.-Z., Lee, J., Li, C., Iadecola, C., Nathan, C., and Ding, A. (2007). MyD88-5 links mitochondria, microtubules, and JNK3 in neurons and regulates neuronal survival. The Journal of Experimental Medicine *204*, 2063–2074.

Kitay, B.M., McCormack, R., Wang, Y., Tsoulfas, P., and Zhai, G.R. (2013). Mislocalization of neuronal mitochondria reveals regulation of Wallerian degeneration and NMNAT/WLDS-mediated axon protection independent of axonal mitochondria. Human Molecular Genetics *22*, 1601–1614.

Kleele, T., Marinković, P., Williams, P.R., Stern, S., Weigand, E.E., Engerer, P., Naumann, R., Hartmann, J., Karl, R.M., Bradke, F., Bishop, D., Herms, J., Konnerth, A., Kerschensteiner, M., Godinho, L and Misgeld, T. (2014). An assay to image neuronal microtubule dynamics in mice. Nature Communications *5*, 4827.

Kling, A., Jantos, K., Mack, H., Hornberger, W., Drescher, K., Nimmrich, V., Relo, A., Wicke, K., Hutchins, C.W., Lao, Y., Marsh, K. and Moeller, A. (2017). Discovery of Novel and Highly Selective Inhibitors of Calpain for the Treatment of Alzheimer's Disease: 2-(3-Phenyl-1H-pyrazol-1-yl)-nicotinamides. Journal of Medicinal Chemistry *60*, 7123–7138.

König, K. (2006). Handbook Of Biological Confocal Microscopy.

Kornek, B., Storch, M.K., Weissert, R., Wallstroem, E., Stefferl, A., Olsson, T., Linington, C., Schmidbauer, M., and Lassmann, H. (2000). Multiple Sclerosis and Chronic Autoimmune Encephalomyelitis A Comparative Quantitative Study of Axonal Injury in Active, Inactive, and Remyelinated Lesions. The American Journal of Pathology *157*, 267–276.

Kremenchutzky, M., Rice, G., Baskerville, J., Wingerchuk, D., and Ebers, G. (2006). The natural history of multiple sclerosis: a geographically based study 9: Observations on the progressive phase of the disease. Brain *129*, 584–594.

Krishnamoorthy, G., Saxena, A., Mars, L.T., Domingues, H.S., Mentele, R., Ben-Nun, A., Lassmann, H., Dornmair, K., Kurschus, F.C., Liblau, R.S. and Weckerle, H. (2009). Myelin-specific T cells also recognize neuronal autoantigen in a transgenic mouse model of multiple sclerosis. Nature Medicine *15*, 626–632.

Kunz, S., Niederberger, E., Ehnert, C., Coste, O., Pfenninger, A., Kruip, J., Wendrich, T.M., Schmidtko, A., Tegeder, I., and Geisslinger, G. (2004). The calpain inhibitor MDL 28170 prevents inflammation-induced neurofilament light chain breakdown in the spinal cord and reduces thermal hyperalgesia. Pain *110*, 409–418.

Lassmann, H. (2003). Axonal injury in multiple sclerosis. Journal of Neurology, Neurosurgery, and Psychiatry *74*, 695–697.

Lassmann, H., Brück, W., and Lucchinetti, C. (2001). Heterogeneity of multiple sclerosis pathogenesis: implications for diagnosis and therapy. Trends in Molecular Medicine *7*, 115–121.

Lassmann, H., Brück, W., and Lucchinetti, C.F. (2007). The Immunopathology of Multiple Sclerosis: An Overview. Brain Pathology *17*, 210–218.

Launay, P., Cheng, H., vatsan, S., Penner, R., Fleig, A., and Kinet, J.-P. (2004). TRPM4 Regulates Calcium Oscillations After T Cell Activation. Science *306*, 1374–1377.

Lehmann-Horn, K., Kinzel, S., and Weber, M.S. (2017). Deciphering the Role of B Cells in Multiple Sclerosis-Towards Specific Targeting of Pathogenic Function. International Journal of Molecular Sciences *18*.

Leiva-Salcedo, E., Riquelme, D., Cerda, O., and Stutzin, A. (2017). TRPM4 activation by chemically- and oxygen deprivation-induced ischemia and reperfusion triggers neuronal death. Channels (Austin, Tex.) *11*, 624–635.

Leloup, L., Shao, H., Bae, Y., Deasy, B., Stolz, D., Roy, P., and Wells, A. (2010). m-calpain Activation Is Regulated by Its Membrane Localization and by Its Binding to Phosphatidylinositol 4,5-Bisphosphate. Journal of Biological Chemistry *285*, 33549–33566.

Levite, M. (2017). Glutamate, T cells and multiple sclerosis. Journal of Neural Transmission (Vienna, Austria: 1996) *124*, 775–798.

Liu, H., Zein, L., Kruse, M., Guinamard, R., Beckmann, A., Bozio, A., Kurtbay, G., Mégarbané, A., Ohmert, I., Blaysat, G., Villain, E., Pongs, O. and Bouvagnet, P. (2010). Gain-of-Function Mutations in TRPM4 Cause Autosomal Dominant Isolated Cardiac Conduction Disease. Circulation: Cardiovascular Genetics *3*, 374–385.

Liu, J., Liu, M., and Signal., K. (2008). Calpain in the CNS: from synaptic function to neurotoxicity.

Lovas, G., Szilágyi, N., Majtényi, K., Palkovits, M., and Komoly, S. (2000). Axonal changes in chronic demyelinated cervical spinal cord plaques. Brain *123*, 308–317.

Lovett-Racke, A.E. (2017). Contribution of EAE to understanding and treating multiple sclerosis. Journal of Neuroimmunology *304*, 40–42.

Ma, M., Shofer, F.S., and Neumar, R.W. (2012). Calpastatin Overexpression Protects Axonal Transport in an In Vivo Model of Traumatic Axonal Injury. Journal of Neurotrauma *29*, 2555–2563.

Machado, V.M., Morte, M.I., Carreira, B.P., Azevedo, M.M., Takano, J., Iwata, N., Saido, T.C., Asmussen, H., Horwitz, A.R., Carvalho, C.M. and Araújo, I. M. M., (2015). Involvement of calpains in adult neurogenesis: implications for stroke. Frontiers in Cellular Neuroscience *9*, 22.

Mack, T., Reiner, M., Beirowski, B., Mi, W., Emanuelli, M., Wagner, D., Thomson, D., Gillingwater, T., Court, F., Conforti, L., Fernando, F. S., Tarlton, A., Andressen, C., Addicks, K., Magni, G., Ribchester, R. R., Perry, V. H. and Coleman, M. P. (2001). Wallerian degeneration of injured axons and synapses is delayed by a Ube4b/Nmnat chimeric gene. Nature Neuroscience *4*, 1199–1206.

Mahad, D., Ziabreva, I., Campbell, G., Lax, N., and Brain, W.K. (2009). Mitochondrial changes within axons in multiple sclerosis.

Makar, T.K., Gerzanich, V., Nimmagadda, V., Jain, R., Lam, K., Mubariz, F., Trisler, D., Ivanova, S., Woo, S., Kwon, M., Bryan, J., Bever, C. T. and Simard, J. M. (2015). Silencing of Abcc8 or inhibition of newly upregulated Sur1-Trpm4 reduce inflammation and disease progression in experimental autoimmune encephalomyelitis. Journal of Neuroinflammation *12*, 210.

Mathey, E.K., Derfuss, T., Storch, M.K., Williams, K.R., Hales, K., Woolley, D.R., Al-Hayani, A., Davies, S.N., Rasband, M.N., Olsson, T., Moldenhauer, A., Velhin, S., Hohlfeld, R., Meinl, E.

and Linington, C. (2007). Neurofascin as a novel target for autoantibody-mediated axonal injury. The Journal of Experimental Medicine *204*, 2363–2372.

Medaer, R. (1979) Does the history of multiple sclerosis go back as far as the 14th century? Acta Neurologica Scandinavica *60*, 189-192.

Miller, D.H., Chard, D.T., and Ciccarelli, O. (2012). Clinically isolated syndromes. The Lancet. Neurology *11*, 157–169.

Milo, R., and Miller, A. (2014). Revised diagnostic criteria of multiple sclerosis. Autoimmunity Reviews *13*, 518–524.

Misgeld, T., Kerschensteiner, M., Bareyre, F.M., Burgess, R.W., and Lichtman, J.W. (2007). Imaging axonal transport of mitochondria in vivo. Nature Methods *4*, 559–561.

Miyawaki, A., Llopis, J., Heim, R., McCaffery, J., Adams, J., Ikura, M., and Tsien, R. (1997). Fluorescent indicators for Ca2+ based on green fluorescent proteins and calmodulin. Nature *388*, 882–887.

Momeni, H.R. (2011). Role of calpain in apoptosis. Cell Journal *13*, 65–72.

Montalban, X., Hauser, S.L., Kappos, L., Arnold, D.L., Bar-Or, A., Comi, G., de Seze, J., Giovannoni, G., Hartung, H.-P.P., Hemmer, B., Lublin, F., Rammohan, K. W., Selmaj, K., Traboulsee, A., Sauter, A., Masterman, D., Fontoura, P., Belachew, S., Garren, H., Mairon, N., Chin, P. and Wolinsky, J. S. (2017). Ocrelizumab versus Placebo in Primary Progressive Multiple Sclerosis. The New England Journal of Medicine *376*, 209–220.

Neukomm, L.J., Burdett, T.C., Seeds, A., Hampel, S., Coutinho-Budd, J.C., Farley, J.E., Wong, J., Karadeniz, Y.B., Osterloh, J.M., Sheehan, A.E. and Freeman, M. R. (2017). Axon Death Pathways Converge on Axundead to Promote Functional and Structural Axon Disassembly. Neuron *95*, 78-91.e5.

Nicole, T., Jonathan, B.T., Azizul, H., Swapan, R.K., Craig, B., and Naren, B.L. (2013). The Involvement of Calpain in CD4+ T Helper Cell Bias in Multple Sclerosis. Journal of Clinical & Cellular Immunology *4*, 1000153.

Nikić, I., Merkler, D., Sorbara, C., Brinkoetter, M., Kreutzfeldt, M., Bareyre, F.M., Brück, W., Bishop, D., Misgeld, T., and Kerschensteiner, M. (2011). A reversible form of axon damage in experimental autoimmune encephalomyelitis and multiple sclerosis. Nature Medicine *17*, 495–499.

Nixon, R., Saito, K. -I., Grynspan, F., Griffin, W., Katayama, S., Honda, T., Mohan, P., Shea, T., and Beermann, M. (1994). Calcium-Activated Neutral Proteinase (Calpain) System in Aging and Alzheimer's Diseasea. Annals of the New York Academy of Sciences *747*.

Novo, A., and Batista, S. (2017). Obesity and Brain Function. Advances in Neurobiology *19*, 191–210.

Okuda, D., Mowry, E., Beheshtian, A., Waubant, E., Baranzini, S., Goodin, D., Hauser, S., and Pelletier, D. (2009). Incidental MRI anomalies suggestive of multiple sclerosis: the radiologically isolated syndrome. Neurology *72*, 800–805.

Ono, Y., Saido, T.C., and Sorimachi, H. (2016). Calpain research for drug discovery: challenges and potential. Nature Reviews. Drug Discovery *15*, 854–876.

Orrenius, S., Gogvadze, V., and Zhivotovsky, B. (2015). Calcium and mitochondria in the regulation of cell death. Biochemical and Biophysical Research Communications *460*, 72–81.

Ortega-Ramírez, A., Vega, R., and Soto, E. (2017). Acid-Sensing Ion Channels as Potential Therapeutic Targets in Neurodegeneration and Neuroinflammation. Mediators of Inflammation *2017*, 3728096.

Osterloh, J.M., Yang, J., Rooney, T.M., Fox, N.A., Adalbert, R., Powell, E.H., Sheehan, A.E., Avery, M.A., Hackett, R., Logan, M.A., MacDonald, J. M., Ziegenfuss, J. S., Milde, S., Hou, Y.-J. J., Nathan, C., Ding, A., Brown, R. H., Conforti, L., Coleman, M., Tessier-Lavigne, M., Züchner, S. and Freeman, M. R. (2012). dSarm/Sarm1 Is Required for Activation of an Injury-Induced Axon Death Pathway. Science *337*, 481–484.

Otsuka, Y., and Goll, D. (1987). Purification of the Ca2+-dependent proteinase inhibitor from bovine cardiac muscle and its interaction with the millimolar Ca2+-dependent proteinase. The Journal of Biological Chemistry *262*, 5839–5851.

Panneerselvam, P., Singh, L., Ho, B., Chen, J., and Ding, J. (2012). Targeting of pro-apoptotic TLR adaptor SARM to mitochondria: definition of the critical region and residues in the signal sequence. Biochemical Journal *442*, 263–271.

Perry, V., Brown, M., and Lunn, E. (1991). Very Slow Retrograde and Wallerian Degeneration in the CNS of C57BL/Ola Mice. European Journal of Neuroscience *3*, 102–105.

Pontremoli, S., Viotti, P.L., Michetti, M., Sparatore, B., Salamino, F., and Melloni, E. (1990). Identification of an endogenous activator of calpain in rat skeletal muscle. Biochemical and Biophysical Research Communications *171*, 569–574.

Rao, M.V., Campbell, J., Palaniappan, A., Kumar, A., and Nixon, R.A. (2016). Calpastatin inhibits motor neuron death and increases survival of hSOD1(G93A) mice. Journal of Neurochemistry *137*, 253–265.

Rao, M.V., McBrayer, M.K., Campbell, J., Kumar, A., Hashim, A., Sershen, H., Stavrides, P.H., Ohno, M., Hutton, M., and Nixon, R.A. (2014). Specific calpain inhibition by calpastatin prevents tauopathy and neurodegeneration and restores normal lifespan in tau P301L mice. The Journal of Neuroscience: The Official Journal of the Society for Neuroscience *34*, 9222–9234.

Rao, M.V., Mohan, P.S., Peterhoff, C.M., Yang, D.-S.S., Schmidt, S.D., Stavrides, P.H., Campbell, J., Chen, Y., Jiang, Y., Paskevich, P.A., Cataldo, A. M., Haroutunian, V. and Nixon, R. A. (2008). Marked calpastatin (CAST) depletion in Alzheimer's disease accelerates cytoskeleton disruption and neurodegeneration: neuroprotection by CAST overexpression. The Journal of Neuroscience: The Official Journal of the Society for Neuroscience *28*, 12241–12254.

Ribbons, K., McElduff, P., Boz, C., Trojano, M., Izquierdo, G., Duquette, P., Girard, M., Grand'Maison, F., Hupperts, R., Grammond, P., Oreja-Guevara, C., Petersen, T., Bergamaschi, R., Giuliani, G., Barnett, M., van Pesch, V., Amato, M.-P., Iuliano, G., Fiol, M., Slee, M., Verheul, F., Cristiano, E., Fernandez-Bolanos, R., Saladino, M.-L., Rio, M., Cabrera-Gomez, J., Butzkueven, H., van Munster, E., Braber-Moerland, L., Spitaleri, D., Lugaresi, Al, Shaygannejad, V., gray, O., Deri, N., Alroughani, R., and Lechner-Scott, J. (2015). Male Sex Is Independently Associated with Faster Disability Accumulation in Relapse-Onset MS but Not in Primary Progressive MS. PLOS ONE *10*, e0122686.

Rivers, T., Sprunt, D., and Berry, G. (1933). Observations on attempts to produce acute disseminated encephalomyelitis in monkeys. The Journal of Experimental Medicine *58*, 39–53.

Romanelli, E., Merkler, D., Mezydlo, A., Weil, M.-T.T., Weber, M.S., Nikić, I., Potz, S., Meinl, E., Matznick, F.E., Kreutzfeldt, M., Ghanem, Al. Conzelmann, K.-K. K., Metz, I., Brück, W., Routh, M., Simons, M., Bishop, D., Misgeld, T. and Kerschensteiner, M. (2016). Myelinosome formation

represents an early stage of oligodendrocyte damage in multiple sclerosis and its animal model. Nature Communications *7*, 13275.

Romanelli, E., Sorbara, C.D., Nikić, I., Dagkalis, A., Misgeld, T., and Kerschensteiner, M. (2013). Cellular, subcellular and functional in vivo labeling of the spinal cord using vital dyes. Nature Protocols *8*, 481–490.

Rose, T., Goltstein, P.M., Portugues, R., and Griesbeck, O. (2014). Putting a finishing touch on GECIs. Frontiers in Molecular Neuroscience *7*, 88.

Sajadi, A., Schneider, B.L., and Aebischer, P. (2004). Wlds-Mediated Protection of Dopaminergic Fibers in an Animal Model of Parkinson Disease. Current Biology *14*, 326–330.

Samantaray, S., Knaryan, V.H., Shields, D.C., and Banik, N.L. (2013). Critical role of calpain in spinal cord degeneration in Parkinson's disease. Journal of Neurochemistry *127*, 880–890.

Sarchielli, P., Greco, L., Floridi, A., Floridi, A., and Gallai, V. (2003). Excitatory Amino Acids and Multiple Sclerosis. Archives of Neurology *60*, 1082.

Sasaki, Y., Vohra, B.P., Lund, F.E., and Milbrandt, J. (2009). Nicotinamide Mononucleotide Adenylyl Transferase-Mediated Axonal Protection Requires Enzymatic Activity But Not Increased Levels of Neuronal Nicotinamide Adenine Dinucleotide. The Journal of Neuroscience *29*, 5525–5535.

Scalfari, A., Neuhaus, A., Degenhardt, A., Rice, G.P., Muraro, P.A., Daumer, M., and Ebers, G.C. (2010). The natural history of multiple sclerosis, a geographically based study 10: relapses and long-term disability. Brain *133*, 1914–1929.

Schaecher, K., Rocchini, A., Dinkins, J., Matzelle, D.., and Banik, N.. (2002). Calpain expression and infiltration of activated T cells in experimental allergic encephalomyelitis over time: increased calpain activity begins with onset of disease. Journal of Neuroimmunology *129*, 1–9.

Schattling, B., Steinbach, K., Thies, E., Kruse, M., Menigoz, A., Ufer, F., Flockerzi, V., Brück, W., Pongs, O., Vennekens, R., Kneussel, M., Freichel, M., Merkler, D. and Friese, M. A. (2012). TRPM4 cation channel mediates axonal and neuronal degeneration in experimental autoimmune encephalomyelitis and multiple sclerosis. Nature Medicine *18*, 1805–1811.

Schoch, K., von Reyn, C.R., Bian, J., Telling, G.C., Meaney, D.F., and Saatman, K.E. (2013). Brain injury-induced proteolysis is reduced in a novel calpastatin-overexpressing transgenic mouse. Journal of Neurochemistry *125*, 909–920.

Schoch, K.M., Evans, H.N., Brelsfoard, J.M., Madathil, S.K., Takano, J., Saido, T.C., and Saatman, K.E. (2012). Calpastatin overexpression limits calpain-mediated proteolysis and behavioral deficits following traumatic brain injury. Experimental Neurology *236*, 371–382.

Schumacher (2016). The role of calcium in axonal degeneration in an animal model of multiple sclerosis.

Seinfeld, J., Baudry, N., Xu, X., Bi, X., and Baudry, M. (2016). Differential Activation of Calpain-1 and Calpain-2 following Kainate-Induced Seizure Activity in Rats and Mice. ENeuro *3*.

Shi, Y., Feng, Y., Kang, J., Liu, C., Li, Z., Li, D., Cao, W., Qiu, J., Guo, Z., Bi, E., Zang, L., Lu, C., Zhang, J. Z. and Pei, G. (2007). Critical regulation of CD4+ T cell survival and autoimmunity by beta-arrestin 1. Nature Immunology *8*, 817–824.

Shrestha, B., Jiang, X., Ge, S., Paul, D., Chianchiano, P., and Pachter, J.S. (2017). Spatiotemporal resolution of spinal meningeal and parenchymal inflammation during experimental autoimmune encephalomyelitis. Neurobiology of Disease *108*, 159–172.

Siklos, M., BenAissa, M., and Thatcher, G.R. (2015). Cysteine proteases as therapeutic targets: does selectivity matter? A systematic review of calpain and cathepsin inhibitors. Acta Pharmaceutica Sinica. B *5*, 506–519.

Simard, Geng, Z., Woo, S., Ivanova, S., Tosun, C., Melnichenko, L., and Gerzanich, V. (2009). Glibenclamide reduces inflammation, vasogenic edema, and caspase-3 activation after subarachnoid hemorrhage. Journal of Cerebral Blood Flow and Metabolism: Official Journal of the International Society of Cerebral Blood Flow and Metabolism *29*, 317–330.

Simard, J., and Gerzanich, V. (2018). TRPM4 and the Emperor. Channels (Austin, Tex.) *12*, 174–175.

Simon, J., Kinkel, R., Jacobs, L., Bub, L., and Simonian, N. (2000). A Wallerian degeneration pattern in patients at risk for MS. Neurology *54*, 1155–1160.

Simon, R., Wade, R., DeLarco, J., and Baker, M. (1969). WALLERIAN DEGENERATION: A SEQUENTIAL PROCESS. Journal of Neurochemistry *16*, 1435–1438.

Singh, S., Dallenga, T., Winkler, A., Roemer, S., Maruschak, B., Siebert, H., Brück, W., and Stadelmann, C. (2017). Relationship of acute axonal damage, Wallerian degeneration, and clinical disability in multiple sclerosis. Journal of Neuroinflammation *14*, 57.

Sloane, J., Hinman, J., Lubonia, M., Hollander, W., and Abraham, C. (2003). Age-dependent myelin degeneration and proteolysis of oligodendrocyte proteins is associated with the activation of calpain-1 in the rhesus monkey. Journal of Neurochemistry *84*, 157–168.

Sorbara, C., Misgeld, T., and Kerschensteiner, M. (2012). In vivo imaging of the diseased nervous system: an update. Current Pharmaceutical Design *18*, 4465–4470.

Sorbara, C., Wagner, N., Ladwig, A., Nikić, I., Merkler, D., Kleele, T., Marinković, P., Naumann, R., Godinho, L., Bareyre, F., Bishop, D., Misgeld, T. and Kerschensteiner, M. (2014). Pervasive Axonal Transport Deficits in Multiple Sclerosis Models. Neuron *84*, 1183–1190.

Squier, M.K., Miller, A.C., Malkinson, A.M., and Cohen, J.J. (1994). Calpain activation in apoptosis. Journal of Cellular Physiology *159*, 229–237.

Storace, D.A., Braubach, O.R., Jin, L., Cohen, L.B., and Sung, U. (2015). Monitoring Brain Activity with Protein Voltage and Calcium Sensors. Scientific Reports *5*, 10212.

Stroissnigg, H., Trančíková, A., Descovich, L., Fuhrmann, J., Kutschera, W., Kostan, J., Meixner, A., Nothias, F., and Propst, F. (2007). S-nitrosylation of microtubule-associated protein 1B mediates nitric-oxide-induced axon retraction. Nature Cell Biology *9*, 1035–1045.

Tao, R., Zhao, Y., Chu, H., Wang, A., Zhu, J., Chen, X., Zou, Y., Shi, M., Liu, R., Su, N., Du, J., Zhou, H.-M., Zhu, L. Qian, X., Liu, H., Loscalzo, J. and Yang, Y. (2017). Genetically encoded fluorescent sensors reveal dynamic regulation of NADPH metabolism. Nature Methods *14*, 720–728.

Terry, R.L., Ifergan, I., and Miller, S.D. (2016). Experimental Autoimmune Encephalomyelitis in Mice. Methods in Molecular Biology (Clifton, N.J.) *1304*, 145–160.

Thompson, A.J., Banwell, B.L., Barkhof, F., Carroll, W.M., Coetzee, T., Comi, G., Correale, J., Fazekas, F., Filippi, M., Freedman, M.S., Fujihara, K., Galetta, S. L., Hartung, H., Kappos, L., Lublin, F. D., Marrie, R., Miller, A. E., Miller, D. H. Montalban, X., Mowry, E. M., Sorensen, P., Tintoré, M.; Traboulsee, A. L., Trojano, M., Uitdehaag, B. M.J., Vukusic, S., Woubant, E., Weinshenker, B. G. Reingold, S. C. and Cohen, J. A. (2017). Diagnosis of multiple sclerosis: 2017 revisions of the McDonald criteria. The Lancet Neurology.

Thompson, S.N., Carrico, K.M., Mustafa, A.G., Bains, M., and Hall, E.D. (2010). A pharmacological analysis of the neuroprotective efficacy of the brain- and cell-permeable calpain inhibitor MDL-28170 in the mouse controlled cortical impact traumatic brain injury model. Journal of Neurotrauma *27*, 2233–2243.

Tosun, C., Kurland, D.B., Mehta, R., Castellani, R.J., deJong, J.L., Kwon, M.S., Woo, S.K., Gerzanich, V., and Jmard (2013). Inhibition of the Sur1-Trpm4 channel reduces neuroinflammation and cognitive impairment in subarachnoid hemorrhage. Stroke *44*, 3522–3528.

Trager, N., Smith, A., Iv, G., Azuma, M., Inoue, J., Beeson, C., Haque, A., and Banik, N.L. (2014). Effects of a novel orally administered calpain inhibitor SNJ-1945 on immunomodulation and neurodegeneration in a murine model of multiple sclerosis. Journal of Neurochemistry *130*, 268–279.

Trapp, B.D., Peterson, J., Ransohoff, R.M., Rudick, R., Mörk, S., and Bö, L. (1998). Axonal Transection in the Lesions of Multiple Sclerosis. The New England Journal of Medicine *338*, 278–285.

Trojano, M., Paolicelli, D., Bellacosa, A., and Cataldo, S. (2003). The transition from relapsing-remitting MS to irreversible disability: clinical evaluation. Neurological Sciences *24*, S268-70.

Tullio, R., Averna, M., Stifanese, R., Parr, T., Bardsley, R.G., Pontremoli, S., and Melloni, E. (2007). Multiple rat brain calpastatin forms are produced by distinct starting points and alternative splicing of the N-terminal exons. Archives of Biochemistry and Biophysics *465*, 148–156.

van der Goes, A., Brouwer, J., Hoekstra, K., Roos, D., van den Berg, T., and Dijkstra, C. (1998). Reactive oxygen species are required for the phagocytosis of myelin by macrophages. Journal of Neuroimmunology *92*, 67–75.

van Noort, J.M., Baker, D., and Amor, S. (2012). Mechanisms in the Development of Multiple Sclerosis Lesions: Reconciling Autoimmune and Neurodegenerative Factors. CNS & Neurological Disorders - Drug Targets *11*, 556–569.

Viglietta, V., Baecher-Allan, C., Weiner, H.L., and Hafler, D.A. (2004). Loss of functional suppression by CD4+CD25+ regulatory T cells in patients with multiple sclerosis. The Journal of Experimental Medicine *199*, 971–979.

Walcott, B.P., Kahle, K.T., and Jmard (2012). Novel treatment targets for cerebral edema. Neurotherapeutics: The Journal of the American Society for Experimental NeuroTherapeutics *9*, 65–72.

Walker, L.J., Summers, D.W., Sasaki, Y., Brace, E., Milbrandt, J., and DiAntonio, A. (2017). MAPK signaling promotes axonal degeneration by speeding the turnover of the axonal maintenance factor NMNAT2. ELife *6*, e22540.

Waller, A. (1850). Experiments on the Section of the Glossopharyngeal and Hypoglossal Nerves of the Frog, and Observations of the Alterations Produced Thereby in the Structure of Their Primitive Fibres. Philosophical Transactions of the Royal Society of London *140*, 423–429.

Wang, J.T., Medress, Z.A., and Barres, B.A. (2012). Axon degeneration: Molecular mechanisms of a self-destruction pathway. The Journal of Cell Biology *196*, 7–18.

Wang, Y., Bi, X., and Baudry, M. (2018a). Calpain-2 as a therapeutic target for acute neuronal injury. Expert Opinion on Therapeutic Targets *22*, 19–29.

Wang, Y., Briz, V., Chishti, A., Bi, X., and Baudry, M. (2013). Distinct Roles for μ-Calpain and m-Calpain in Synaptic NMDAR-Mediated Neuroprotection and Extrasynaptic NMDAR-Mediated Neurodegeneration. The Journal of Neuroscience *33*, 18880–18892.

Wang, Y., Liu, Y., Lopez, D., Lee, M., Dayal, S., Hurtado, A., Bi, X., and Baudry, M. (2018b). Protection against TBI-Induced Neuronal Death with Post-Treatment with a Selective Calpain-2 Inhibitor in Mice. Journal of Neurotrauma *35*, 105–117.

Werner, P., Pitt, D., and Raine, C. (2001). Multiple sclerosis: altered glutamate homeostasis in lesions correlates with oligodendrocyte and axonal damage. Annals of Neurology *50*, 169–180.

Williams, P.R., Marincu, B.-N.N., Sorbara, C.D., Mahler, C.F., humacher, A.-M., Griesbeck, O., Kerschensteiner, M., and Misgeld, T. (2014). A recoverable state of axon injury persists for hours after spinal cord contusion in vivo. Nature Communications *5*, 5683.

Witte, M.E., Geurts, J., de Vries, H.E., van der Valk, P., and van Horssen, J. (2010). Mitochondrial dysfunction: A potential link between neuroinflammation and neurodegeneration? Mitochondrion *10*, 411–418.

Woo, S.K., Kwon, M.S., Ivanov, A., Gerzanich, V., and Jmard (2013). The sulfonylurea receptor 1 (Sur1)-transient receptor potential melastatin 4 (Trpm4) channel. The Journal of Biological Chemistry *288*, 3655–3667.

Wright, A.K., Wishart, T.M., Ingham, C.A., and Gillingwater, T.H. (2010). Synaptic Protection in the Brain of WldS Mice Occurs Independently of Age but Is Sensitive to Gene-Dose. PLoS ONE *5*, e15108.

Xiong, X., Hao, Y., Sun, K., Li, J., Li, X., Mishra, B., Soppina, P., Wu, C., Hume, R.I., and Collins, C.A. (2012). The Highwire Ubiquitin Ligase Promotes Axonal Degeneration by Tuning Levels of Nmnat Protein. PLoS Biology *10*, e1001440.

Yahata, N., Yuasa, S., and Araki, T. (2009). Nicotinamide mononucleotide adenylyltransferase expression in mitochondrial matrix delays Wallerian degeneration. The Journal of Neuroscience: The Official Journal of the Society for Neuroscience *29*, 6276–6284.

Yang, J., Weimer, R.M., Kallop, D., Olsen, O., Wu, Z., Renier, N., Uryu, K., and Tessier-Lavigne, M. (2013). Regulation of Axon Degeneration after Injury and in Development by the Endogenous Calpain Inhibitor Calpastatin. Neuron *80*, 1175–1189

Yang, J., Wu, Z., Renier, N., Simon, D., Uryu, K., and Cell, P.D. (2015). Pathological axonal death through a MAPK cascade that triggers a local energy deficit.

Zamvil, S., Nelson, P., Trotter, J., Mitchell, D., Knobler, R., Fritz, R., and Steinman, L. (1985). T-cell clones specific for myelin basic protein induce chronic relapsing paralysis and demyelination. Nature *317*, 355–358.

Zimmerman, U.P., Boring, L., Pak, Uj., Mukerjee, N., and Wang, K.K. (2000). The Calpain Small Subunit Gene Is Essential: Its Inactivation Results in Embryonic Lethality. IUBMB Life *50*, 63–68.

Websites:

National MS Society, “Types of MS”, unter: https://www.nationalmssociety.org/What-is-MS/Types-of-MS (aufgerufen am 3.05.2018).

9 Declaration (Eidesstattliche Versicherung/Affidavit)

Hiermit versichere ich an Eides statt, dass ich die vorliegende Dissertation *„In vivo analysis of calcium-initiated axon degeneration in an animal model of MS*“ selbständig angefertigt habe, mich außer der angegebenen keiner weiteren Hilfsmittel bedient und alle Erkenntnisse, die aus dem Schrifttum ganz oder annähernd übernommen sind, als solche kenntlich gemacht und nach ihrer Herkunft unter Bezeichnung der Fundstelle einzeln nachgewiesen habe.

I hereby confirm that the dissertation “*In vivo analysis of calcium-initiated axon degeneration in an animal model of MS*” is the result of my own work and that I have only used sources or materials listed and specified in the dissertation.

München, 24.05.2018

Munich, 24.05.2018

Marta M. Wesolowski

10 Acknowledgments

Nearly 5 years ago I began my journey for the PhD. A lot of things happened and changed during this long period. I am grateful for all these days and (way too many) nights, that I spend in the lab. Although I am happy that this chapter of my life gets to an end, I still have this passion for neuroscience that drove me into this direction.

Firstly, I would like to express my sincere gratitude to my supervisor Martin Kerschensteiner for hosting me in his lab, providing me with wide ranging scientific input and support throughout my PhD study, for his patience, motivation and immense knowledge. I think science is best done in conversation. And in Martins lab there were plenty of possibilities to exchange ideas and find solutions. In cases I was puzzled what to do next, I could always count on talking to my colleague Adrian-Minh Schumacher. Therefore, many many thanks for your support. As a busy resident doctor, you nevertheless always found some time for me for discussions.

Besides my advisor, I would like to thank the rest of my thesis committee: Prof. Thomas Misgeld, who joined in some of the project meetings and who allowed me to conduct part of my project in his lab, and Dr. Oliver Griesbeck, for their insightful comments and encouragement, but also for the hard question which incented me to widen my research from various perspectives.

Many thanks especially to my friends Elisa, Anne and Cathy who introduced me to all methods that were necessary for my project. And many thanks to Anja, Berni, Dana and Bianca. Without your work nothing would have been possible.

I am also very thankful to the Graduate School of Systemic Neurosciences for providing this amazing framework and opportunities to connect to fellow scientists through excursions and social activities.

I was lucky to be part of such an amazing lab. I really enjoyed the atmosphere in the Kerschensteiner and Bareyre lab. Thank you all for your support over the years. It nearly felt like a second home. I will for sure miss the *Small Lab* excursions into the mountains or the strawberry picking to improve our “bad” ;) work environment. Thank you, Anja and Kris, for the fun times that we had – in but also outside the lab!

Last but not least, I want to thank Zoltan Simon and my family and friends, especially Claudia Bijok, for their emotional and professional support in good and in bad times. I am also very grateful for my dance group Regös. Nagyon köszönöm hogy voltatok olyan jo barataim! You made my PhD to a valuable, formative chapter in my life that I would not want to have missed.